COMPARISONS OF IMPLICIT AND EXPLICIT TIME INTEGRATION METHODS IN FINITE ELEMENT ANALYSIS FOR LINEAR ELASTIC MATERIAL AND QUASI-BRITTLE MATERIAL IN DYNAMIC PROBLEMS

A thesis submitted to the Delft University of Technology to fulfill
the requirements for the degree of

Master of Science in Structural Engineering (Structural Mechanics)

by

Boyuan Yang

October 2019

The work in this thesis was made in the:

DIANA FEA   &
Faculty of Civil Engineering and
Geosciences
Delft University of Technology

ABSTRACT

In finite element analysis, nonlinear time-history analysis is a realistic and accurate analysis type for dynamic or seismic analysis due to its solutions contain wealthy data and complete response time-history. The most commonly used method, probably the only practical procedure, in nonlinear time-history analysis is the direct time integration method. It solves the governing equations of the system in time domain incrementally. In general, every direct time integration method could be classified as either an implicit method or an explicit method. Each category has its advantages and disadvantages in different aspects, e.g., stability, accuracy and computational costs. Understanding the differences between the two categories in both theoretical and practical aspects is very important for engineers to make the best analysis strategy for a specific dynamic or seismic analysis.

In this treatise, the fundamental theory of the direct time integration methods and several well-known methods will be reviewed. Many published comparisons, either in theoretical or practical level, will be briefly covered. Then, the most popular method in each category, i.e., implicit Newmark method and explicit central difference method, will be introduced and used in transient analyses and results comparisons. In total, five cases studies are included in this thesis, including three cases with linear elastic materials and two cases with quasi-brittle masonry material. These five cases are studied to answer the main research questions of this research:

> *What differences can be observed in comparisons of solutions obtained from implicit and explicit methods for linear elastic material in transient analysis and for quasi-brittle material under seismic load? Also, how are the performances of both methods with respect to the stability and accuracy aspects?*

The finite element models of all cases are built up in DIANA FEA 10.3, and transient analyses with both implicit and explicit methods are performed as well.

The first three cases with linear elastic materials include a simply supported beam under a harmonic point load, a double cantilever beam under point transient load ,and a simply supported thin plate under transient distributed load. The remaining two cases with quasi-brittle masonry material are the seismic analyses of a masonry wall model and a full-scaled URM house model (finally simplified), and they are referred from the experimental tests conducted by Graziotti et al. [2016] and modified in this thesis. Different analyses schemes are set for each case in order to investigate the influence of the adopted time step in each method. Finally, the comparisons are made between implicit and explicit method solutions concerning displacement responses for linear elastic material, and additionally cracks patterns and capacity curves for masonry material.

Based on the comparisons, the conclusions can be drawn to answer the main research questions.

For linear elastic materials

- The results show that both methods generally could accurately reproduce the displacement responses with proper time step. Few differences are observed in the displacement or stress responses of high frequency contents. The implicit method was strongly influenced by the adopted time step to ensure the accuracy of the high frequency vibration responses. Though the implicit method is unconditionally stable, a large time step could make high frequency information lost in the solution.

- The explicit method once satisfies the stability condition (called CFL stability condition), which means the time step used for the algorithm to proceed is smaller than the minimum natural period of all elements (called critical time step), the high frequency responses will always be accurately calculated, with regardless of large output time intervals. Moreover, the accuracy and stability could both be guaranteed once the CFL condition is satisfied, which means further decrement in time step is not necessary in the explicit method. However, since the critical time step is usually very small, rather long computation time is needed.

For quasi–brittle masonry material

- The comparisons show that the implicit and explicit solutions generally have a good agreement with each other in terms of displacement response, hysteresis curves, and crack patterns. The critical time step, determined by CFL based on the linear elastic phase of structure, could guarantee the accuracy and also stability for the material, which has a softening behavior, e.g., quasi-brittle masonry material. Similarly, no further reduction for critical time step is needed.

- The implicit method shows some difficulties to reach the convergence, as a result, there are some chaotic results in hysteresis curves of displacement versus base shear. Non-converged or hardly converged iteration procedures in implicit method could lead to inaccurate predictions of nonlinear behaviors.

- The explicit method has good results with smooth transitions in hysteresis curves, which benefit from no iteration involving. This advantage of the explicit method could be more significant when highly nonlinear behaviors are involved in the analysis. However, the disadvantage is that the explicit method needs a very small time step. For a complex model, the critical time step will be extremely reduced due to irregular-shaped mesh and connections with volumes close to zero.

- Mass scaling technique could be used to speed up the explicit method by adding artificial mass on specific elements to increase the available critical time step for the whole FE model. However, great caution is needed to use this technique. Generally speaking, the ratio between added mass and total mass should smaller than 10%. Slightly larger values could be allowed only with a detailed check of positions and properties of the elements with added mass.

According to the conclusions, the explicit method should be preferable in either one or several of the following situations:

- Short duration transient analysis, e.g., impact loading analysis.

- The high frequency vibrations are of interest, e.g., seismic analysis of high-rise buildings.

- Highly nonlinear behaviors are included in the model, which may cause enormous difficulties for convergence of the iteration process, e.g., severe cracking, local failure or crushing.

- The target structure has a regular geometry and a well-meshed FE model.

For other situations, the implicit method should be recommended due to its relatively large time step and unconditional stability.

ACKNOWLEDGEMENTS

CONTENTS

LIST OF FIGURES

LIST OF TABLES

1 | INTRODUCTION

1.1 MOTIVATION

The finite element method (FEM) is the most popular and efficient tool in engineering research and industrial simulation. For dynamic problems, especially the nonlinear dynamic time-history analysis, the direct time integration is the most commonly used and may be the only practical procedure to solve the governing equations of the finite element assemblage. There are several methods available for direct time integration procedure. In general, these methods could be classed as either implicit or explicit, and they both solve the dynamic governing equations in time domain incrementally.

The implicit methods are commonly unconditionally stable, which means no restriction in the time increment for the analysis. However, the solution to a set of equations involves iteration until the convergence norm is satisfied.

The explicit methods are usually conditionally stable, so the time increment needs to be small enough, specifically smaller than a critical time step, to ensure the solution will not blow up. However, the explicit methods could solve the equations directly and determine the solution at the end of each time increment without iteration.

The computational cost, stability, and many other properties of implicit and explicit methods are different. To save the computational effort and ensure the reliability of solutions, it is important to understand the advantages and disadvantages of these methods and evaluate their performances for particular problems. For this purpose, many comparisons have been made by either studying the fundamental theories or analyzing specific problems. However, most of the reported practical works are focusing on the quasi-static nonlinear problems, such as metal forming (Soltani et al. [1994], Choi et al. [2002]), solid mechanics (Harewood and McHugh [2007]), or the dynamic contact problems with linear elastic material property(Sun et al. [2000]). Seldom comparisons have been found about nonlinear material for dynamic problems or about the real structural dynamic response.

All these considerations form the motivation of making further comparisons of implicit and explicit methods for dynamic responses of structures with linear elastic material under transient load conditions and the seismic responses of structures with quasi-brittle material, i.e., masonry.

1.2 RESEARCH QUESTIONS AND SCOPE

Due to the reasons mentioned above, it is helpful to make comparisons of implicit and explicit methods in dynamic or transient analysis for both linear and nonlinear cases, then evaluated the performances and results of them.

The comparisons and evaluations are achieved by performing dynamic time-history analysis using both implicit and explicit methods for the same finite element model. The dynamic time-history analysis could provide a wealth of data that includes complete response of displacements, stresses, strains, or crack patterns for the model at each time step. According to this, the main research question could be raised as:

> *What differences can be observed in comparisons of solutions obtained from implicit and explicit methods for linear elastic material in transient analysis and for quasi-brittle material under seismic load? Also, how are the performances of both methods with respect to the stability and accuracy aspects?*

To approach the main research question, the following sub-questions can be formulated:

For linear elastic materials,

A) *What differences in displacement responses could be observed between the two methods?*

B) *What is the influence of different time steps to the displacement solutions in implicit and explicit methods?*

For quasi-brittle materials,

C) *What are the differences in nonlinear behaviors of the model between implicit and explicit solutions?*

D) *How do the adopted time step and the critical time step of explicit method influence the stability and accuracy of solutions?*

Since in direct time integration, the governing equations will be solved in the time domain, the most crucial parameter is the time step used for the integration scheme. Therefore, the main scope of this thesis will be the influences of the adopted time step on stability and accuracy of solutions.

1.3   APPROACH

To make comparisons and answer the research questions, five dynamic cases are selected, including three cases with linear elastic materials and two cases with quasi-brittle masonry material. The first three linear elastic materials cases are:

1) The steady-state response of a simply-supported beam to a point, sinusoidal in time force.

2) The response of a double cantilever elastic beam to a transient point force.

3) The response of a simply-supported thin plate to an out-of-plane transient distributed force (Maguire et al. [1993]).

Two masonry material cases include:

1) The response of a masonry wall subjected to in-plane cyclic load (Graziotti et al. [2016]) and in-plane seismic load.

2) The response of a full-scale masonry house on shaking table tests (Graziotti et al. [2016]).

All the numerical models and analyses are carried out in the finite element software DIANA FEA 10.3. It provides both implicit Newmark method and explicit central difference method, and also takes into account the transient effect of the dynamic load. For masonry material cases, DIANA FEA 10.3 offers engineering masonry material model to simulate the nonlinear behavior of the masonry structure. To answer the research questions, comparisons will be made mainly in aspects of displacement response for linear cases, and for masonry material cases, extra aspects of crack patterns and capacity curves will also be considered.

1.4 SYNOPSIS

This thesis has 6 chapters. Chapter 1 gives an introduction to this research work, including the motivation and research questions. Next, chapter 2 presents the literature review of the relevant studies about the definition and classification of direct time integration schemes and some well-known methods. Attention was also paid on some reports about comparisons of implicit and explicit methods in particular problems, as well as the recent development of the direct time integration methods. Then, the methodology is introduced in chapter 3, including the adopted implicit and explicit methods in this thesis, and also a brief overview of important features of them in the DIANA FEA 10.3.

The cases studies start with building finite element models for five studied cases in chapter 4. The outlines of transient analysis schemes for each case are also presented in detail in this chapter. Chapter 5 shows the results of all analyses; the comparisons and discussions are made to answer the research questions. Finally, conclusions are drawn, and the recommendations for future research are given in chapter 6.

2 | LITERATURE REVIEW

2.1 OVERVIEW

This chapter will cover the literature review of the direct time integration methods in nonlinear dynamic time history analysis. First, some general definitions of nonlinear dynamic time-history analysis and classifications of the direct time integration methods are reviewed. Second, few well-know and widely used direct time integration methods in finite element analysis are introduced. Attention is paid to some published comparisons between the performances of these methods for certain problems. Moreover, recent development of direct time integration methods are presented as well.

2.2 NONLINEAR DYNAMIC TIME–HISTORY ANALYSIS

2.2.1 Definition

Nonlinear analysis capability was firstly needed in the aerospace industry few decades ago, due to the demand of using new configuration components and increasing use of brittle material (Felippa and Park [1979]). The continuous developments of the nonlinear analysis benefit a lot from the progress in solution techniques in finite element codes as well as the growing computational capacity of the software. These developments brought the nonlinear analysis into other applications, such as civil engineering. The "nonlinear" refers to the structural model that has nonlinear force-displacement relationships or geometrical nonlinearities or even both. In seismic analysis, The nonlinear analysis allows designers to more closely follow the response of the structure under seismic loading until the ultimate or collapse limit states (Mourad and Sabah [2015]).

The dynamic analysis has very significant advantage compared to the static analysis, because the former one takes into account the inertial effect. Neglecting such effect may leads to conservative results. Also, for the structure under impact load, the inertial effect is the deterministic factor to generate the real response of the structure. However, the dynamic analysis is more expensive. In fact, with the increasing computational capacity, the nonlinear static analysis could be finally embedded in the nonlinear dynamic analysis (Felippa and Park [1979]).

In nonlinear dynamic time-history analysis, the external load is considered to generate a complete response history for any place on the structure. The results of the nonlinear time-history analysis will be a wealth of the data, that includes the complete response of displacements, stresses or strains in time-history for the any point of interest on the structure. Especially in seismic analysis, this complete response is an obvious advantage of nonlinear dynamic time-history analysis when compared to another important type of seismic analysis, nonlinear pushover analysis. For instance, the latter one usually provides the force-displacement capacity curves, such as maximum base shear for a given maximum target displacement of the earthquake signal. However, the time history information has been lost, such as the time needed to reach the maximum base shear under certain seismic input and possibility of that maximum base shear might be reached multiple times under different value of top displacement (Mourad and Sabah [2015]). Hence, the

nonlinear dynamic time-history analysis could be seen as the most realistic and accurate analysis method to study the structures under seismic loading (Lagaros et al. [2015]).

2.2.2 Classification of direct time integration methods

For nonlinear dynamic time-history analysis, the only practical solution procedure is direct time integration. Direct time integration is directly integrating the equation of motions (EOMs) of the system in time domain without any transformation of the EOMs into different form. The essence of direct time integration is that the EOMs are satisfied instead of at any time t, they are only satisfied at discrete time intervals Δt apart. Therefore, all solution techniques employed in static analysis can probably also be used in direct time integration (Bathe [1982]).

In finite element analysis, the direct time integration algorithms could be generally classified into two categories: implicit time integration methods and explicit time integration methods. The classification is based on using the equilibrium conditions at different time to solve the EOMs of the system to get solution at time $t + \Delta t$. The implicit methods using the EOMs at time $t + \Delta t$ while the explicit methods using ones at time t to get the target solution at time $t + \Delta t$. Based on this property, they can also be distinguished by that the implicit methods will solve the matrix system of the EOMs one or more times per step to advance the solution, and the explicit methods may be advanced without storing a matrix or solving a system of equations (Hughes et al. [1979]). Implicit methods generally have unconditionally stability, which means no time step restriction to attain stability. Explicit methods, on the other hand, always require very small time step to ensure the stability of the algorithms. However, due to the fact the there is no need to solve the matrix system, the explicit methods take less computational cost per time step than the implicit methods. In general, the choice of the direct time integration methods really depends on the type of problem. There is no optimal approach for all cases (Belytschko [1976]).

2.3 WIDELY USED DIRECT TIME INTEGRATION METHODS

To apply the direct time integration methods, the governing equations of the system need to be derived first. In principle, the basic idea and procedures of direct time integration is the same for governing equations of linear and nonlinear systems, so it is convenient to start with equations of equilibrium governing the linear system. The well-known governing equations in finite elements analysis could be written as Equation 2.1.

$$\mathbf{M\ddot{U}} + \mathbf{C\dot{U}} + \mathbf{KU} = \mathbf{R} \tag{2.1}$$

where $\mathbf{M}$, $\mathbf{C}$ and $\mathbf{K}$ are the mass, damping, and stiffness matrices; $\mathbf{R}$ is the external load vector; $\mathbf{U}$, $\mathbf{\dot{U}}$ and $\mathbf{\ddot{U}}$ are the displacement, velocity and acceleration vectors of the finite element assemblage. In principle, the only difference between dynamic analysis and static analysis is the former one takes into account the effect of inertia force and damping force, which are the first term and second term in Equation 2.1 respectively.

The generalized derivation of the governing equations for nonlinear systems could be found in Felippa [1977], in which two extra terms are added into the equations: nonlinear damping operators $\mathbf{C}(\mathbf{u}, \mathbf{\dot{u}})$ and nonlinear stiffness operators $\mathbf{S}(\mathbf{u})$. These two terms could generate state-dependent corrective force vectors. For the structural analysis in civil engineering, we could also consider the stiffness matrix $\mathbf{K}$ and damping matrix $\mathbf{C}$ in Equation 2.1 are changing over time to include the physical nonlinearity of the system.

2.3.1 The Newmark Method

The Newmark integration schemes are the most commonly used time integration schemes in structural mechanics. The Newmark integration scheme could be implicit or explicit according the choice of parameters, and choosing proper parameters could yield to different well known integrators.

The basic assumptions of Newmark scheme is given as following (Newmark [1959]):

$$^{t+\Delta t}\dot{\mathbf{U}} = {}^t\dot{\mathbf{U}} + [(1 - \gamma)^t\ddot{\mathbf{U}} + \gamma^{t+\Delta t}\ddot{\mathbf{U}}]\Delta t \tag{2.2}$$

$$^{t+\Delta t}\mathbf{U} = {}^t\mathbf{U} + {}^t\dot{\mathbf{U}}\Delta t + [(\frac{1}{2} - \beta)^t\ddot{\mathbf{U}} + \beta^{t+\Delta t}\ddot{\mathbf{U}}]\Delta t^2 \tag{2.3}$$

where the $^{t+\Delta t}\dot{\mathbf{U}}$ represents unknown the velocity at time $t + \Delta t$, similar for the unknown displacement and acceleration. All the terms of quantities at time t are known. The parameters γ and β are to be chosen to determine the properties of the algorithm.

When $2\beta \geq \gamma \geq 1/2$, the Newmark method is an implicit method and it is unconditionally stable. Specially, when the $\beta = 1/4$ and $\gamma = 1/2$, the method is called constant-average-acceleration method (also called trapezoidal rule). This method is unconditionally stable and has accuracy of $O(\Delta t^2)$. Under this condition, no numerical damping is introduced to the analysis. To using this method, the EOMs in Equation 2.1 need to be considered at time $t + \Delta t$. The detailed algorithm using implicit Newmark method is given in Chapter 3, or one can refer to the book written by Bathe [1982].

2.3.2 The Wilson θ Method

Compared to the Newmark constant-average-acceleration method, the Wilson θ method is an extension of linear acceleration method. It assumes a linear variation of acceleration from t to $t + \theta\Delta t$, where $\theta \geq 1$ (Wilson et al. [1973]). The assumption of Wilson θ method for the acceleration is:

$$^{t+\tau}\ddot{\mathbf{U}} = {}^t\ddot{\mathbf{U}} + \frac{\tau}{\theta\Delta t}({}^{t+\theta\Delta t}\ddot{\mathbf{U}} - {}^t\ddot{\mathbf{U}}) \tag{2.4}$$

where the τ denotes the increase in time and $0 \leq \tau \leq \theta\Delta t$. When the $\theta = 1$, the methods is linear acceleration scheme. However, it is known that for only when $\tau \geq 1.37$, the method is unconditionally stable, and it is usually employed as $\theta = 1.4$. For a more clear view, the assumption of Wilson θ method and Newmark constant-average-acceleration is shown in Figure 2.1.
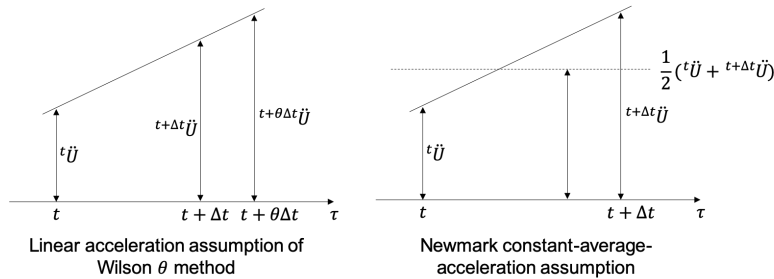
Figure 2.1: Assumption of Wilson θ method and Newmark method (Bathe [1982])

Wilson θ method is also an implicit integration method. Since the linear acceleration variation is assumed, the EOM is considered at time $t + \theta\Delta t$ instead of at time $t + \Delta t$. It is also worthy to note that using Newmark parameters $\gamma = 1/2$ and $\beta = 1/6$ corresponds to the Wilson θ method with $\theta = 1$, which are both linear

acceleration method (Bathe [1982]). This close relationship between these two methods makes it possible to implement both methods in one single computer program (Bathe [1978]).

2.3.3 The Houbolt Method

The Houbolt integration method employs two backward-difference formulas (Houbolt [1950]):

$$^{t+\Delta t}\ddot{\mathbf{U}} = \frac{1}{\Delta t^2}(2^{t+\Delta t}\mathbf{U} - 5^t\mathbf{U} + 4^{t-\Delta t}\mathbf{U} - {}^{t-2\Delta t}\mathbf{U}) \tag{2.5}$$

$$^{t+\Delta t}\dot{\mathbf{U}} = \frac{1}{6\Delta t^2}(11^{t+\Delta t}\mathbf{U} - 18^t\mathbf{U} + 9^{t-\Delta t}\mathbf{U} - 2^{t-2\Delta t}\mathbf{U}) \tag{2.6}$$

The Houbolt integration method has errors of order (Δt^2). It is also an implicit algorithm and the EOMs in Equation 2.1 are considered at time $t + \Delta t$. The time step has no restriction because it is unconditionally stable.

2.3.4 The Central Difference Method

The central difference method is somewhat related to the Houbolt method, and it uses standard finite difference expressions to approximate the acceleration and velocity in terms of displacement (Collatz [1966]). It is assumed that:

$$^t\ddot{\mathbf{U}} = \frac{1}{\Delta t^2}(^{t-\Delta t}\mathbf{U} - 2^t\mathbf{U} + {}^{t+\Delta t}\mathbf{U}) \tag{2.7}$$

$$^t\dot{\mathbf{U}} = \frac{1}{2\Delta t}(-^{t-\Delta t}\mathbf{U} + {}^{t+\Delta t}\mathbf{U}) \tag{2.8}$$

The central difference method is an explicit method since the solution of displacement $^{t+\Delta t}\mathbf{U}$ is calculated based on the EOMs at time t. In another words, it is possible to express the $^{t+\Delta t}\mathbf{U}$ in terms of quantities at time t and earlier time, which are known. The error of the central difference method is of order $(\Delta t)^2$. The central difference method has an advantage that the solution can essentially be carried out on the element level, because there is no stiffness and mass matrices of complete element assemblage need to be calculated if the mass matrix is diagonal, and the stiffness matrix is not required to inverse for each step (Bathe [1982]). However, the disadvantage is that the central difference method requires the time step smaller than a critical value to remain stable. This condition is called Courant, Friedrichs and Lewy (CFL) stability condition (Courant et al. [1928]). More attention will be payed to this method in Chapter 3.

2.4 REVIEW OF COMPARISONS MADE BETWEEN IMPLICIT AND EXPLICIT FINITE ELEMENT METHODS

As mentioned above, the direct time integration methods in finite element analysis could be generally classed as either implicit or explicit. In the implicit method, there is no restriction for adopted time step, however for each time increment, the solution procedure involves the factorization of stiffness matrix and iteration process until the solution satisfies the convergence norms. In the explicit method, the equations are reformulated and can be solved directly at the end of the time increment, without iteration, while a time step smaller than a critical value is needed for explicit method, and in some cases, this critical value may be very small and too many steps need to be taken over the analysis process.

To assess the performance and make the optimal choice for certain type of problem, many studies have been made comparing and discussing the pros and cons of these two methods.

2.4.1 Stability and Accuracy of direct integration methods

To compare these integration schemes, two fundamental concepts are considered: stability and accuracy. The stability means that the initial conditions for the equations with large value $\Delta t/T$ (ratio between time step size and natural period of the system) must not be amplified artificially and thus make the integration of the lower modes worthless, also, any errors in the resulting quantities due to the round-off in the computer do not grow in the integration (Bathe [1982]).

Nickel [1971] investigate the stability of the Newmark method and Wilson averaging method, and they are found to be unconditionally stable for all values of time step size. Specially, the Newmark constant-average-acceleration method was found contains no artificial attenuation, though some vibration period error occurs in the solution. Lax and Richtmyer [1956] examined the stability properties of central difference method and Johnson [1966] proved the stability of Houbolt method. It is found that Houbolt method is also an unconditionally stable method, however it contains both artificial attenuation and period error which are functions of the time step size and natural frequencies of the system.

Similarly, many stability studies based on invoking one of the established theorems are published and many comparison were given by studying the single degree-of-freedom system. However, in dynamic analysis for complex structures, the participation of all modes in the solution is not desirable in most cases, therefore the accuracy is not required for all modes of the complex structure, and the comparison based on the single degree-of-freedom my be not a proper basis for the comparison (Bathe and Wilson [1972]). For this reason, a systematic and fundamental procedure was proposed by Bathe and Wilson [1972] for the stability and accuracy analysis of the direct time integration methods in structural dynamics. They derived an approximation operator $\mathbf{A}$ and a load operator $\mathbf{L}$ which are related explicitly the unknown required variables at time $t + \Delta t$ to previous calculated quantities. For the stability criterion, the spectral decomposition of A is investigated, and the spectral radii of A is defined as $\rho(\mathbf{A}) = max|\lambda_i|$, where λ_i is the eigenvalues of the $\mathbf{A}$. The stability criterion is that $\rho(\mathbf{A}) \leq 1$. According to this, many well-known methods are investigated, the results are shown in Figure 2.2. Similar conclusions can be drawn compared to the studies mentioned above. Moreover the spectral radii of approximation operator of central difference method is also shown in this figure, and to satisfy the condition $\rho(\mathbf{A}) \leq 1$, it is required that $\Delta t/T \leq 1/\pi$.
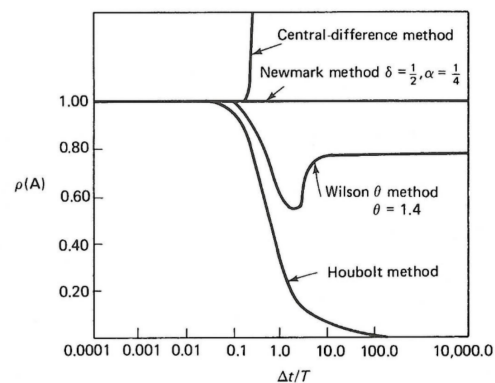
Figure 2.2: Spectral radii of approximation operators, $\xi = 0.0$ (Bathe [1982])

Also the accuracy analysis was reported in the paper of Bathe and Wilson [1972]. the period elongation and amplitude decay caused by the numerical integration method effect are given in Figure 2.3. The curves show that, in genera, the numerical integration using any of the methods are accurate when $\Delta t/T$ is smaller than about 0.01, while when this ratio is large, various characteristics are shown in different integration methods.
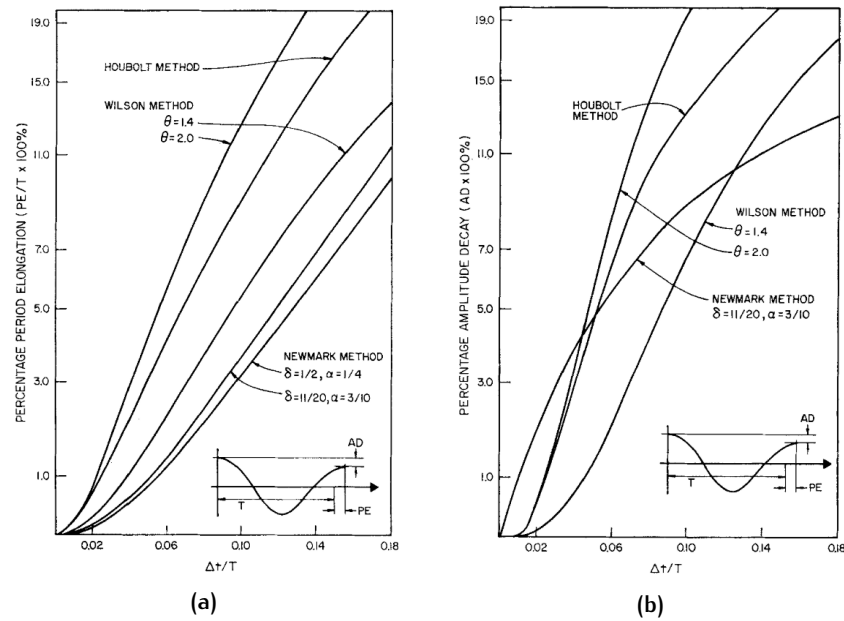
Figure 2.3: (a) Percentage period elongations; (b) Amplitude decays (Bathe and Wilson [1972])

2.4.2 Comparisons in several practical problems

There are several studies have been published comparing two methods in practical problems by using finite element method.

Many of these studies focus on the quasi-static process (e.g. metal forming, thin-wall structure buckling) (Soltani et al. [1994], Choi et al. [2002], Rebelo and Nagtegaal [1992], Kugener [1995], Kugener [1995], Rust and Schweizerhof [2003]).

Soltani et al. [1994] studied the blade forging problem by using implicit elastic-plastic FE code NIKE2D and explicit dynamic FE code DYNA2D. The comparison shows that the effective plastic strain results of two methods have good agreement with each other. While, explicit method is less expensive compared to the implicit method, because the implicit method involves lots of matrices factorization in the iterations, whereas the equations in explicit method are independent.

Choi et al. [2002] made the comparisons of two methods for the hydroforming process. In this study, the influence of mass scaling, which is commonly used in order to save computational time of explicit method is investigated.

Rebelo and Nagtegaal [1992] found that the implicit method is preferable im smaller 2D problems and explicit method has advantages in the contact problems. The reason has been investigated in many studies (Choi et al. [2002], Rebelo and Nagtegaal [1992], and Sun et al. [2000] etc.), and it turns out that the implicit method has severe converging problem when the model involves large deformation or surfaces contact. This superiority was illustrated by Kugener [1995] in his study about metal crimping simulation using implicit FE code ANSYS and explicit FE code OPTRIS. He also pointed out the importance of choosing a improper simulation method can lead to undesirable, lengthy calculation procedure (Kugener [1995]).

In solid mechanics, comparisons were made between implicit and explicit method using crystal plasticity under various 2D and 3D loading conditions by Harewood and McHugh [2007]. It concludes that for directly applied deformation load, the implicit method solves more quickly, this leading is approximately doubled in 3D than 2D problem. Again, the priority of explicit method in contact and element large deformation conditions is mentioned. One interesting found in this paper is when a rate-independent material is used in 2D tension analysis, the small time

step in explicit method could ensure the high nonlinear material behavior is dealt with (Harewood and McHugh [2007]).

Few studies about comparisons in dynamic problems has been found, one of them is given by Sun et al. [2000]. They perform the analysis for the dynamic impact problems of an elastic bar and a cylindrical disk on a rigid wall. The materials adopted in this paper are all linear elastic. The conclusions were drawn that for fast linear impact problems, the cost of explicit method is much less than implicit method. For slow impact case, due to the stability condition, the explicit method needs much smaller time step. If the whole procedure is very long, it will take lots of time increments to finish the analysis. Therefore, the implicit method has advantage for this situation, moreover, implicit method can provide numerical damping to remove the noise and keep results more accurate.

2.5 RECENT DEVELOPMENT OF THE DIRECT TIME INTE-GRATION

The difficulty in making the choice of the time integration methods lies in combining efficiency, accuracy and stability of the algorithm. Implicit methods require iterations but unconditionally stable, On the contrary, explicit methods avoid iterations and convergence problems, but require small time step to remain stable. Therefore, development has been made to take advantage from both families of integration methods.

One way to make the development is to shift from a family to another during the analysis. This could starting with implicit methods in some time intervals which involve only slow dynamic problems with fewer nonlinearities, and when the convergence problem appears, it will shift to an explicit method (Jung and Yang [1998]), in which the time of transition is fixed by user. The automatic shifting criteria is also developed by Noels et al. [2004] for impact problem. Initial conditions, when shifting from explicit to implicit, are also defined to avoid loss of stability and convergence.

Besides, some studies proposed modified explicit or implicit or combined methods to improve the efficiency and ensure the accuracy and stability [Rostami et al. [2012], Shojaee et al. [2015], Albostan et al. [2017]]. The basic idea behind these methods can still be classified as implicit or explicit algorithms. The improvements made by now is still restricted in a certain type of dynamic problems or quasi-static problems, and some improved methods have requirement of programming and computer knowledge to users. Therefore, the knowledge about implicit and explicit methods, as well as their advantages and disadvantages, is still fundamental to the future development of direct time integration.

3 | METHODS AND TOOLS

3.1 OVERVIEW

This chapter elaborates the adopted methods and FE tool in this thesis. First, detailed mathematical expressions for implicit and explicit algorithms are presented. Next, the step-by-step solution procedures for applying the algorithms to linear EOMs are given. Then, some important properties and principles to apply the methods in nonlinear problems are mentioned. Finally, a brief overview of important features of two methods in adopted FE software DIANA FEA 10.3 are given.

3.2 IMPLICIT NEWMARK METHOD

The basic assumptions of Implicit Newmark scheme is, as mentioned above (Newmark [1959]):

$$^{t+\Delta t}\dot{\mathbf{U}} = {}^{t}\dot{\mathbf{U}} + \left[(1-\gamma)\,{}^{t}\ddot{\mathbf{U}} + \gamma\,{}^{t+\Delta t}\ddot{\mathbf{U}}\right]\Delta t \tag{3.1}$$

$$^{t+\Delta t}\mathbf{U} = {}^{t}\mathbf{U} + {}^{t}\dot{\mathbf{U}}\Delta t + \left[(\frac{1}{2}-\beta)\,{}^{t}\ddot{\mathbf{U}} + \beta\,{}^{t+\Delta t}\ddot{\mathbf{U}}\right]\Delta t^2 \tag{3.2}$$

where the $^{t+\Delta t}\dot{\mathbf{U}}$ represents unknown the velocity at time $t + \Delta t$, similar for the unknown displacement and acceleration. Rearranging the above equation to express the acceleration and the velocity at time $t + \Delta t$ as:

$$^{t+\Delta t}\ddot{\mathbf{U}} = \frac{1}{\beta\Delta t^2}(^{t+\Delta t}\mathbf{U} - {}^{t}\mathbf{U}) - \frac{{}^{t}\dot{\mathbf{U}}}{\beta\Delta t} - \frac{{}^{t}\ddot{\mathbf{U}}}{2\beta} + {}^{t}\ddot{\mathbf{U}} \tag{3.3}$$

$$^{t+\Delta t}\dot{\mathbf{U}} = {}^{t}\dot{\mathbf{U}} + \Delta t\left((1-\gamma)\,{}^{t}\ddot{\mathbf{U}} + \gamma\left(\frac{1}{\beta\Delta t^2}\left(^{t+\Delta t}\mathbf{U} - {}^{t}\mathbf{U}\right) - \frac{{}^{t}\dot{\mathbf{U}}}{\beta\Delta t} - \frac{{}^{t}\ddot{\mathbf{U}}}{2\beta} + {}^{t}\ddot{\mathbf{U}}\right)\right) \tag{3.4}$$

The above equations are substituted into the EOMs at time $t + \Delta t$:

$$\mathbf{M}^{t+\Delta t}\ddot{\mathbf{U}} + \mathbf{C}^{t+\Delta t}\dot{\mathbf{U}} + \mathbf{K}^{t+\Delta t}\mathbf{U} = {}^{t+\Delta t}\mathbf{R} \tag{3.5}$$

in which $^{t+\Delta t}\mathbf{R}$ represents the external load vector at time $t + \Delta t$. Rearranging the resulted equation in such a way that the unknown displacement $^{t+\Delta t}\mathbf{U}$ only shows on the left-hand side, and all known quantities show on the right-hand side. It finally yields:

$$\left(\mathbf{M}\frac{1}{\beta\Delta t^2} + \mathbf{C}\frac{\gamma}{\beta\Delta t} + \mathbf{K}\right)^{t+\Delta t}\mathbf{U} = {}^{t+\Delta t}\mathbf{R} + \mathbf{M}\left(\frac{{}^{t}\mathbf{U}}{\beta\Delta t^2} + \frac{{}^{t}\dot{\mathbf{U}}}{\beta\Delta t} + \frac{{}^{t}\ddot{\mathbf{U}}}{2\beta} - {}^{t}\ddot{\mathbf{U}}\right)$$
$$+ \mathbf{C}\left(\left(\frac{\gamma}{\beta\Delta t} - 1\right){}^{t}\dot{\mathbf{U}} + \left(\frac{\gamma}{2\beta} - \gamma - \Delta t + \Delta t\gamma\right){}^{t}\ddot{\mathbf{U}} + \frac{\gamma}{\beta\Delta t^2}{}^{t}\mathbf{U}\right) \tag{3.6}$$

For convenience, Equation 3.6 could be written in short notation as:

$$\hat{\mathbf{K}}^{t+\Delta t}\mathbf{U} = {}^{t+\Delta t}\hat{\mathbf{R}} \tag{3.7}$$

where the $\hat{\mathbf{K}}$ and $^{t+\Delta t}\hat{\mathbf{R}}$ are called effective stiffness matrix and effective loads matrix at time $t + \Delta t$, respectively. In most cases, since the stiffness matrix $\mathbf{K}$ is not diagonal,

the effective stiffness matrix $\hat{\mathbf{K}}$ is not diagonal either. Therefore, the solution of the Equation 3.7 requires solving a system of equations, in matrix calculation, the inverse of effective stiffness matrix $\hat{\mathbf{K}}$ or other factorization of it is needed.

The choices of parameters β and γ have been mentioned in Section 2.3.1. Additionally, numerical damping could be introduced by using $\gamma > 1/2$, to eliminate the undesirable spurious high frequency noise in the solution. However, under this condition the accuracy of the method is reduced to first order $O(\Delta t)$.

3.2.1 Step-by-step solution procedure

A generalized implementation for step-by-step procedure of the implicit Newmark method is given in Algorithm 3.1.

Algorithm 3.1: Step-by-step implicit Newmark method solution procedure

---

1   *Initial calculation*
    input : $\mathbf{K}$, $\mathbf{M}$, $\mathbf{C}$, $^0\mathbf{U}$, $^0\dot{\mathbf{U}}$, $^0\ddot{\mathbf{U}}$, Δt, β and γ ($\gamma \geq 0.5$, $\beta \geq 0.25(0.5 + \gamma)$)
    output: $\hat{\mathbf{K}} = \mathbf{LDL}^T$
2   **begin**
3   Form effective stiffness matrix: $\hat{\mathbf{K}} = \left(\mathbf{M}\dfrac{1}{\beta\Delta t^2} + \mathbf{C}\dfrac{\gamma}{\beta\Delta t} + \mathbf{K} \right)$;
4   Triangularize $\hat{\mathbf{K}}$: $\hat{\mathbf{K}} = \mathbf{LDL}^T$;
5   **end**
6   *Calculation in each time step*
    input : $^t\mathbf{U}$, $^t\dot{\mathbf{U}}$, $^t\ddot{\mathbf{U}}$, $^{t+\Delta t}\mathbf{R}$
    output: $^{t+\Delta t}\mathbf{U}$, $^{t+\Delta t}\dot{\mathbf{U}}$, $^{t+\Delta t}\ddot{\mathbf{U}}$
7   **begin**
8   Calculate the effective loads matrix:

$$^{t+\Delta t}\hat{\mathbf{R}} = {}^{t+\Delta t}\mathbf{R} + \mathbf{M}\left(\frac{^t\mathbf{U}}{\beta\Delta t^2} + \frac{^t\dot{\mathbf{U}}}{\beta\Delta t} + \frac{^t\ddot{\mathbf{U}}}{2\beta} - {}^t\ddot{\mathbf{U}} \right) +$$

$$\mathbf{C}\left(\left(\frac{\gamma}{\beta\Delta t} - 1 \right) {}^t\dot{\mathbf{U}} + \left(\frac{\gamma}{2\beta} - \gamma - \Delta t + \Delta t\gamma \right) {}^t\ddot{\mathbf{U}} + \frac{\gamma}{\beta\Delta t^2}{}^t\mathbf{U} \right);$$

9   Solve for $^{t+\Delta t}\mathbf{U}$: $\mathbf{LDL}^T {}^{t+\Delta t}\mathbf{U} = {}^{t+\Delta t}\hat{\mathbf{R}}$;
10   Calculate $^{t+\Delta t}\ddot{\mathbf{U}}$ and $^{t+\Delta t}\dot{\mathbf{U}}$ according to Equation 3.3 and Equation 3.4;
11   **end**

3.2.2 The implicit integration of nonlinear equations in dynamic analysis

The Algorithm 3.1 shows the solution procedure using implicit Newmark method for linear EOMs. For nonlinear dynamic analysis, this integration scheme can also be employed, however, with iterations to be performed. The obtained results, i.e., displacement, velocity or acceleration, at time $t + \Delta t$ must be checked if they can satisfy the equilibrium equations. If equilibrium equations are satisfied, the analysis will move to next time increment, otherwise, iteration of current time step must continue.

Typical equilibrium equations, ignoring the damping effect, of implicit dynamic analysis at time $t + \Delta t$ could be written as:

$$\mathbf{M}^{t+\Delta t}\ddot{\mathbf{U}}^{(i)} + \mathbf{K}_{NL}\Delta\mathbf{U}^{(i)} + {}^{t+\Delta t}\mathbf{F}^{(i-1)} = {}^{t+\Delta t}\mathbf{R} \tag{3.8}$$

where, $\mathbf{M}$ is the time-independent mass matrix; $^{t+\Delta t}\ddot{\mathbf{U}}^{(i)}$ represents the solution of acceleration at time $t + \Delta t$ after i^{th} iteration; $^{t+\Delta t}\mathbf{F}^{(i-1)}$ represents the nodal point forces at time $t + \Delta t$ after $(i-1)^{th}$ iteration. $\Delta\mathbf{U}^{(i)}$ is the increments in the nodal

point displacements in i^{th} iteration. The relation of displacement solution between each iteration can be expressed as:

$$^{t+\Delta t}\mathbf{U}^{(i)} = {}^{t+\Delta t}\mathbf{U}^{(i-1)} + \Delta\mathbf{U}^{(i)} \qquad (3.9)$$

The nonlinearity of the dynamic system is shown in $\mathbf{K_{NL}}$, which is chosen based on the iteration method. The commonly used iteration methods include Regular Newton-Raphson method and Modified Newton-Raphson method, as shown in Figure 3.1. In the former one, $\mathbf{K_{NL}}$ is evaluated for every iteration step, so it can be written as $\mathbf{K_{NL}} = {}^{t+\Delta t}\mathbf{K_{NL}}^{(i-1)}$ in Equation 3.8. In the latter one, $\mathbf{K_{NL}}$ is evaluated only at the start of every time increment, in another words, $\mathbf{K_{NL}} = {}^{t}\mathbf{K_{NL}}$ in Equation 3.8 for every iteration within time increment $t + \Delta t$.
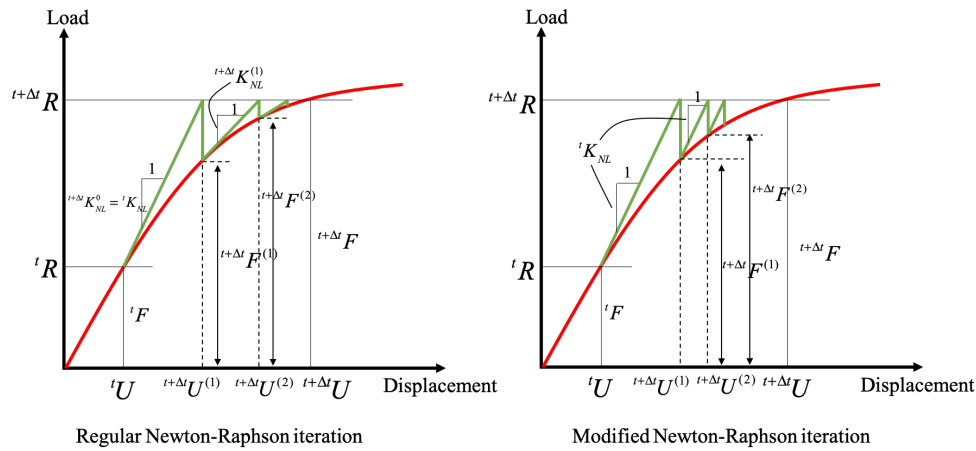
Figure 3.1: Regular and Modified Newton-Raphson iteration methods

To get an insight view of the iteration procedure, one can using Equation 3.9, Equation 3.3 and Equation 3.4 to express the acceleration solution for each iteration step at time $t + \Delta t$, and then substitute it into Equation 3.8 to obtain the $\Delta\mathbf{U}^{(i)}$ for each iteration step. Specially, for the first increment $\Delta\mathbf{U}^{(1)}$ in current time increment $t + \Delta t$, the calculation involves index $i - 1 = 0$, the quantities with this index equal the respective quantities from the solution of previous time increment, which have the index of t.

Combined with Algorithm 3.1, the solution procedure, including the iteration process, for nonlinear dynamic analysis could be summarized as Algorithm 3.2.

An important note is that in the iteration step $i = 1$ for time step $t + \Delta t$, $\Delta\mathbf{U}^{(1)}$ was simply calculated as stated above and accepted as an accurate approximation to the actual displacement increment from time t to time $t + \Delta t$ (HAISLER et al. [1971]). However, it was shown later that this may have a significant influence on the solution for nonlinear dynamic analysis, as it is highly path-dependent. This is because *any error admitted in the incremental solution at a particular time directly affects in a path-dependent manner the solution at any subsequent time* (Bathe and Wilson [1974]). Therefore, the nonlinear dynamic analysis requires more stringently convergence tolerance in the iteration (Bathe [1982]). An illustration example of a simple pendulum is also given by him, it concludes that if the convergence tolerance is not tight enough, the energy of the system will be lost, by the way, if the iteration is not adopted, the predicted response may blow up.

Algorithm 3.2: Implicit Newmark method iteration procedure for nonlinear dynamic analysis

---

1 *Initial calculation* (see Algorithm 3.1)
2 *Calculation in each time step including iteration process*
   input : ${}^{t}\mathbf{U}$, ${}^{t}\dot{\mathbf{U}}$, ${}^{t}\ddot{\mathbf{U}}$, ${}^{t+\Delta t}\mathbf{R}$, ${}^{t}\mathbf{F}$, $\mathbf{K}_{NL}$
   output: ${}^{t+\Delta t}\mathbf{U}$, ${}^{t+\Delta t}\dot{\mathbf{U}}$, ${}^{t+\Delta t}\ddot{\mathbf{U}}$
3 **begin**
4 | ${}^{t+\Delta t}\mathbf{F}^{(0)} = {}^{t}\mathbf{F}$;
5 | ${}^{t+\Delta t}\ddot{\mathbf{U}}^{(0)} = {}^{t}\ddot{\mathbf{U}}$;
6 | ${}^{t+\Delta t}\dot{\mathbf{U}}^{(0)} = {}^{t}\dot{\mathbf{U}}$;
7 | ${}^{t+\Delta t}\mathbf{U}^{(0)} = {}^{t}\mathbf{U}$;
8 | Start from $i = 0$;
9 | **for** $i \leq$ *maximum iteration number (predefined)* **do**
10 | | **if** $\mathbf{M}^{t+\Delta t}\ddot{\mathbf{U}}^{(i)} + \mathbf{K}_{NL}\Delta\mathbf{U}^{(i)} + {}^{t+\Delta t}\mathbf{F}^{(i-1)} = {}^{t+\Delta t}\mathbf{R}$ **then**
11 | | | ${}^{t+\Delta t}\mathbf{U} = {}^{t+\Delta t}\mathbf{U}^{(i)}$;
12 | | | End the loop and return ${}^{t+\Delta t}\mathbf{U}$;
13 | | **else**
14 | | | $i \leftarrow i + 1$;
15 | | | Update $\mathbf{K}_{NL}$ according to the adopted iteration method;
16 | | | Calculate $\Delta\mathbf{U}^{(i)}$ using updated stiffness matrix $\mathbf{K}_{NL}$;
17 | | | ${}^{t+\Delta t}\mathbf{U}^{(i)} = {}^{t+\Delta t}\mathbf{U}^{(i-1)} + \Delta\mathbf{U}^{(i)}$;
18 | | | Calculate ${}^{t+\Delta t}\ddot{\mathbf{U}}^{(i)}$ and ${}^{t+\Delta t}\dot{\mathbf{U}}^{(i)}$ according Equation 3.3 and Equation 3.4;
19 | | **end**
20 | **end**
21 | Calculate ${}^{t+\Delta t}\ddot{\mathbf{U}}$ and ${}^{t+\Delta t}\dot{\mathbf{U}}$ according to Equation 3.3 and Equation 3.4;
22 **end**

3.3 EXPLICIT CENTRAL DIFFERENCE METHOD

As mentioned in Section 2.3.4, the explicit central difference method is using standard finite difference expression to approximate the acceleration and velocity in terms of displacement (Collatz [1966]):

$${}^{t}\ddot{\mathbf{U}} = \frac{1}{\Delta t^2}({}^{t-\Delta t}\mathbf{U} - 2{}^{t}\mathbf{U} + {}^{t+\Delta t}\mathbf{U}) \tag{3.10}$$

$${}^{t}\dot{\mathbf{U}} = \frac{1}{2\Delta t}(-{}^{t-\Delta t}\mathbf{U} + {}^{t+\Delta t}\mathbf{U}) \tag{3.11}$$

The error in above expansion is of order $(\Delta t)^2$. The solution for time $t + \Delta t$ is obtained by considering the EOMs at time t:

$$\mathbf{M}{}^{t}\ddot{\mathbf{U}} + \mathbf{C}{}^{t}\dot{\mathbf{U}} + \mathbf{K}{}^{t}\mathbf{U} = {}^{t}\mathbf{R} \tag{3.12}$$

By substituting Equation 3.10 and Equation 3.11 intoEquation 3.12 and rearranging in such a way that the unknown displacement ${}^{t+\Delta t}\mathbf{U}$ only shows on the left-hand side and all known quantities show on the right-hand side, the result reads:

$$\left(\frac{1}{\Delta t^2}\mathbf{M} + \frac{1}{2\Delta t}\mathbf{C}\right){}^{t+\Delta t}\mathbf{U} = {}^{t}\mathbf{R} - \left(\mathbf{K} - \frac{2}{\Delta t^2}\mathbf{M}\right){}^{t}\mathbf{U} - \left(\frac{1}{\Delta t^2}\mathbf{M} - \frac{1}{2\Delta t}\mathbf{C}\right){}^{t-\Delta t}\mathbf{U}$$
$$\tag{3.13}$$

It can be seen that the calculation of ${}^{t+\Delta t}\mathbf{U}$ is only based on known previous displacements ${}^{t}\mathbf{U}$ and ${}^{t-\Delta t}\mathbf{U}$. Also, there is no requirement for factorization or cal-

culation of inverse of the stiffness matrix, which is usually not a diagonal matrix. Equation 3.13, therefore, can be written in a short format:

$$\mathbf{\hat{M}}^{t+\Delta t}\mathbf{U} = {}^{t}\mathbf{\hat{R}} \tag{3.14}$$

where $\mathbf{\hat{M}}$ is called effective mass matrix, which represents the coefficients of unknown displacement $^{t+\Delta t}\mathbf{U}$ on the left-hand side, and $^{t}\mathbf{\hat{R}}$ is called effective loads at time t, which represents the right-hand side of Equation 3.14.

Another observation is that to calculate $^{t+\Delta t}\mathbf{U}$, the displacement $^{t-\Delta t}\mathbf{U}$ is required. This will require a special starting procedure to start algorithm from $t = 0s$. It can be done by using initial conditions at $t = 0s$ of the system and combined with Equation 3.12, Equation 3.10 and Equation 3.11. Then $^{-\Delta t}\mathbf{U}$ can be calculated and used to start the explicit time integration:

$$^{-\Delta t}\mathbf{U} = {}^{0}\mathbf{U} - \Delta t \, {}^{0}\mathbf{\dot{U}} + \frac{\Delta t^2}{2}\, {}^{0}\mathbf{\ddot{U}} \tag{3.15}$$

It is also worth to mention that if the mass matrix and damping matrix are both diagonal, there is no matrix factorization is involved to solve the Equation 3.13, only matrix multiplications are required to get right-hand side $^{t}\mathbf{\hat{R}}$. In another words, it is not necessary to assemble either stiffness matrix, mass matrix or damping matrix. The required calculation for effective load vector $^{t}\mathbf{\hat{R}}$ can be carried on element level by summing the contributions from each element. Then the whole algorithm procedure could be carried out on the element level, in short notations:

$$^{t+\Delta t}U_i = {}^{t}\hat{R}_i \frac{1}{\hat{m}_{ii}} \tag{3.16}$$

However, this advantage of effectiveness of central difference method only shows up when diagonal mass and diagonal damping matrix are adopted. In practice, this really depends on the problems to be solved.

The most important consideration in using the central difference method is that adopted time step should be smaller than a critical time step. This condition is called Courant, Friedrichs and Lewy(CFL) stability condition, which will be introduced in Section 3.3.2.

3.3.1 Step–by–step solution procedure

The step-by-step solution procedure of central difference method is given Algorithm 3.3, with general mass and damping matrices (i.e. no requirement for diagonal property). If the the mass and damping matrices are both diagonal, triangularize of the effective mass matrix $\mathbf{\hat{M}}$ is not needed, and element level calculation can be carried out according the Equation 3.16.

Compared to the implicit Newmark method solution procedure in Algorithm 3.1, besides the different input parameters, a special start procedure is added in the initial calculation for the central difference method. Moreover, the adopted time step Δt must be smaller than the critical time step Δt_{crit} according to the CFL stability condition.

3.3.2 The critical time step and CFL stability condition

The critical time step and CFL stability condition are utmost important considerations in using of explicit central difference method. It is required that adopted time step Δt must be smaller than a critical value Δt_{crit} to obtain the stability of the algorithm. For each single element, this stability condition, called Courant, Friedrichs and Lewy(CFL) stability condition (Courant et al. [1928]), can be written as:

$$\Delta t \leq \Delta t_{crit} = \frac{2}{\omega_e^h} \tag{3.17}$$

Algorithm 3.3: Step-by-step central difference method solution procedure

1   *Initial calculation*
    input : $\mathbf{K}$, $\mathbf{M}$, $\mathbf{C}$, $^0\mathbf{U}$, $^0\dot{\mathbf{U}}$, $^0\ddot{\mathbf{U}}$, Δt, $\Delta t \leq \Delta t_{crit}$
    output: $\hat{\mathbf{M}} = \mathbf{LDL}^T$

2 **begin**

3   Perform start procedure: $^{-\Delta t}\mathbf{U} = {}^0\mathbf{U} - \Delta t^0\dot{\mathbf{U}} + \dfrac{\Delta t^2}{2}{}^0\ddot{\mathbf{U}}$;

4   Form effective mass matrix: $\hat{\mathbf{M}} = \left(\dfrac{1}{\Delta t^2}\mathbf{M} + \dfrac{1}{2\Delta t}\mathbf{C} \right)$;

5   Triangularize $\hat{\mathbf{M}}$: $\hat{\mathbf{M}} = \mathbf{LDL}^T$

6 **end**

7 *Calculation in each time step*
    input : $^t\mathbf{U}$, $^{t-\Delta t}\mathbf{U}$, $^t\mathbf{R}$
    output: $^{t+\Delta t}\mathbf{U}$ (if needed $^t\dot{\mathbf{U}}$, $^t\ddot{\mathbf{U}}$)

8 **begin**

9   Calculate the effective loads matrix:
    $^t\hat{\mathbf{R}} = {}^t\mathbf{R} - \left(\mathbf{K} - \dfrac{2}{\Delta t^2}\mathbf{M} \right) {}^t\mathbf{U} - \left(\dfrac{1}{\Delta t^2}\mathbf{M} - \dfrac{1}{2\Delta t}\mathbf{C} \right) {}^{t-\Delta t}\mathbf{U}$;

10   Solve for $^{t+\Delta t}\mathbf{U}$: $\mathbf{LDL}^{T\,t+\Delta t}\mathbf{U} = {}^t\hat{\mathbf{R}}$;

11   If needed, calculate $^t\ddot{\mathbf{U}}$ and $^t\dot{\mathbf{U}}$ according to Equation 3.10 and
    Equation 3.11;

12 **end**

---

where the ω_e^h is the highest natural frequency of element e (i.e. the smallest natural period T_e). In another words, the critical time step Δt_{crit} for a single element is calculated based on the highest natural frequency of it. For the whole finite element assemblage, Δt should be smaller than the minimum critical time step $min\{\Delta t_{crit}\}$ of all elements.

The basic idea behind this condition is that if a wave a is moving cross discrete spatial grid, to calculate its amplitude at discrete time step of equal duration, then this duration must be less than the time for the wave to travel to adjacent grid points. Therefore, if the spatial coordinate of the grid is discrete and placed at regular distance, called interval length, and the time is also discrete and divided into equal duration, called time step, then the CFL condition defines the length of the time step as a function of the interval lengths of each spatial coordinate and of the maximum speed that information can travel through the grid space (Courant et al. [1928]). As an example, for linear element, Δt_{crit} could be calculated according to the dilatational wave speed, c, and the length of the element, L:

$$\Delta t \leq \Delta t_{crit} = \frac{2}{\omega_e^h} = \frac{2}{2c/L} = \frac{L}{c} = \frac{L}{\sqrt{E/\rho}} \tag{3.18}$$

In finite element analysis, this critical value Δt_{crit} can be calculated from the mass and stiffness properties of the element. Specifically, the highest natural frequency of each element ω_e^h could be calculated from characteristic equation of each single element: $det\left(\mathbf{K} - \omega^2\mathbf{M}\right)$.

However, one can foresee the disadvantage caused by CFL stability condition, that is in some analysis the critical time step Δt_{crit} may be unduly small calculated from the Equation 3.17. Especially for system with large degrees of freedom, the Δt_{crit} would be very sensitive to the element properties. For example, in a large finite element model, if the mass of the element that has the smallest value of Δt_{crit}, which usually is the element with smallest size, has been further reduced to close to zero, in another words, the mesh size changes even smaller, the value of Δt_{crit} calculated according to the characteristic equation of this element will approach to zero. This means unduly smaller time step is required according to CFL stability

condition. However, since the system has large degrees of freedom and this element size is very small, the influence on the dynamic response of the whole system would be hardly observed. Therefore, even one element mass reduction of the system may heavily reduce the viable time step to be used for the analysis, and similar situation happens when stiffness changes (Bathe [1982]).

3.3.3 The explicit integration of nonlinear equations in dynamic analysis

In nonlinear dynamic analysis, the equilibrium for the finite element system is considered, similar to the linear analysis, at time t to calculate the displacement at time $t + \Delta t$. For illustration purpose, the damping effect is ignored again. In each time step, the equilibrium reads:

$$\mathbf{M}{}^{t}\ddot{\mathbf{U}} + {}^{t}\mathbf{F} = {}^{t}\mathbf{R} \tag{3.19}$$

where the ${}^{t}\mathbf{F}$ is the nodal force at time t. The displacement solution ${}^{t+\Delta t}\mathbf{U}$ is obtained by substitute Equation 3.10 into Equation 3.19.

The advantage of the central difference method compared to the implicit Newmark method in nonlinear dynamic analysis is no iteration process involved, also, as mentioned above, once the mass matrix (and damping matrix, if consider the damping effect) is diagonal, no triangular factorization of the coefficient matrix is needed.

The problem lies in the CFL stability condition. For linear elastic material, the stiffness properties of the element remain the same during the whole analysis, while for nonlinear material, they are changing during the analysis process. It means the actual critical time step for each element is changing as well, however, the adopted constant time step is calculated based on the initial condition of the system, which assumes material is linear elastic. Therefore, in some nonlinear force-displacement relationships (i.e. a stiffening curve), the time step may not satisfy the CFL stability condition during the analysis.

However, though the time step is slightly larger than the critical value and the algorithm is no longer stable, the error accumulation is quite different from what is observed in linear analysis. In linear cases, once the time step is larger than the critical time step, the error will accumulate rapidly and the results will blow up quickly. In nonlinear cases, the error accumulated without an obvious instability in the solution and the response is grossly in error but doesn't blow up. This may lead to severe problems when the high frequency modes of system are oscillated and dominant, since the significant error will accumulated but can hardly be observed (Bathe [1982]).

3.4 IMPORTANT FEATURES OF DIRECT TIME INTEGRA-TION METHODS IN DIANA FEA 10.3

The adopted FE tools in this thesis is the FE software DIANA FEA 10.3, in which both implicit Newmark method and explicit central difference method are implemented. In DIANA FEA 10.3, the dynamic analysis is conducted by including the transient effects of the load on the system. This section will introduce some worthmentioned properties of the adopted direct time integration methods in transient analysis of DIANA FEA 10.3.

3.4.1 Numerical damping in Newmark method

In the implicit Newmark method, Newmark parameter pair β and γ could be defined separately, the basic rule for selection of Newmark parameters has been dis-

cussed in Section 3.2. Also by choosing Newmark parameter pair, numerical damping could be introduced into the system in order to damp out the noise, for example, a commonly used pair is $\beta = 0.3025$ and $\gamma = 0.6$.

3.4.2 Iteration method and convergence criteria

There are several iteration methods available in DIANA FEA 10.3, the one adopted in this thesis is the Regular Newton-Raphson method, as shown in Figure 3.1. Also, some special techniques could be applied for the iteration process, i.e. continuation method and line search algorithm, one can refer to the DIANA FEA documentation (DIANA FEA BV [2019]) to have detailed information about them.

Convergence criteria are crucial to control the iteration process. According to the iteration process introduced in Section 3.2.2, when the results obtained from the iteration process have satisfied the equilibrium conditions, so-called convergence, the iteration process must be stopped. To detect this convergence, several norms are provided including displacement norm, force norm and energy norm. The convergence could be detected when either multiple norms are satisfied at the same time or one of them is satisfied. The choice of the proper norm, as well as the value of the convergence criterion are important to an analysis.

Generally, the displacement norm should not be used when prescribed displacement is applied. Similarly, the force norm is less useful when the structure is very flexible so that the inertial force is hard to generate. The value of the convergence criterion should be chosen according to the accuracy requirement of the analysis. Moreover, In some cases when accuracy is highly required, very strict convergence criteria or multiple convergence norms should be adopted at the same time.

Besides, there is another way to stop the iteration procedure, which is a predefined maximum iteration number. It is used to prevent infinite iterations when the analysis is too hard to converge due to some unexpected reasons. However, when the iteration stopped due to reaching a large maximum number, the problem probably occurs in the finite element model aspect rather than the iteration method.

3.4.3 Mass and damping matrices

For finite element assemblage, the mass matrix and damping matrix could be either consistent or lumped. In practice, lumped or diagonal mass matrix is often used, because they are economic in computation, however, lumped mass may results in inaccurate results due to coarse meshes or irregular element shapes. For implicit Newmark method, both consistent and lumped mass matrix could be used, however, for explicit central difference method, only lumped mass matrix is available in DIANA FEA 10.3.

As for damping matrix, the viscous damping, specifically the Rayleigh damping, is used in this thesis for both methods. The damping matrix $\mathbf{C}$ can be given in form:

$$\mathbf{C} = a\mathbf{M} + b\mathbf{K} \qquad (3.20)$$

where the coefficients a and b are determined by given damping ratios. Similarly to the lumped mass matrix, only lumped damping matrix could be used in central difference method. Moreover, the Rayleigh damping coefficient for stiffness matrix, which is b in Equation 3.20, must be zero, and only damping on mass could be applied.

3.4.4 Start procedure of explicit method and time step definition

As mentioned in Section 3.3, a special start procedure is needed for explicit method. In DIANA FEA 10.3, this start procedure is perform using implicit integration.

In the implicit Newmark method, the time step size is used to define the time increment for the algorithm to proceed, as well as to define the time points for which output could be generated.

For the explicit central difference method in DIANA FEA 10.3, there are different parameters to define either explicit time increment for algorithm or output time points. Their functions and symbols which will be used in this thesis are given in Table 3.1.

Parameters	Function	Example value
Δt_O	The output time interval	e.g. $0.01s$
"dtlim" (Δt_{lim})	The smallest time increment allowed for explicit algorithm	$10^{-15}s$
"dtred" (Δt_{red})	The reduction factor to be multiplied with critical time step in order to define the actual used time increment	0.95
"dtubs" (Δt_{ubs})	The largest time increment allowed for explicit algorithm	$10^{-3}s$

Table 3.1: Central difference method parameters

In DIANA FEA 10.3, the critical time step Δt_{crit} of each element is calculated according to the Equation 3.17 at the start of the analysis. Then, $min\{\Delta t_{crit}\}$ is multiplied with a reduction factor Δt_{red} in order to determine the actual time increment used in the analysis, written as Δt_{ex}. After that, Δt_{ex} is compared with lower bound value Δt_{lim} and upper bound value Δt_{ubs}. If $\Delta t_{lim} \leq \Delta t_{ex} \leq \Delta t_{ubs}$, the explicit algorithm will proceed with time increment Δt_{ex}. However, if Δt_{ex} exceeds the Δt_{lim} or Δt_{ubs}, the analysis will proceed with the upper bound value or lower bound value, depending on which one is exceeded. Finally, the output will generated in a time interval of Δt_O. Moreover, Δt_O will define the number of explicit sub-cycles N_{sub} by simply divided by Δt_{ex}.

3.4.5 Limitation of element order and mass scaling in explicit method

In most cases, the smallest critical time step $min\{\Delta t_{crit}\}$ for the central difference method in a finite element model is usually quite small, therefore hundreds even thousands of explicit sub-cycles may need to be performed for one Δt_O. To fully exploit the efficiency of the explicit method, the internal nodal forces ${}^t\mathbf{F}$ in Equation 3.19 should be calculated very fast. Therefore, only linear interpolated elements should be used in the central difference method.

An important technique used in the explicit time integration for finite element analysis is the mass scaling. The mass scaling technique is activated when Δt_{ex} is smaller than the predefined lower bound value Δt_{lim}, as described in Section 3.4.4. In this situation, the explicit algorithm will adopt the Δt_{lim} as the actual time incremental to proceed the analysis. However, it means the critical time steps of some elements Δt_{crit} are smaller than Δt_{lim}, in another words, the explicit algorithm is no longer stable. To achieve the stability condition, artificial mass is added to these elements which have $\Delta t_{crit} < \Delta t_{lim}$ in order to increase the smallest natural period of the element to at least equal to Δt_{lim}.

Though, the mass scaling is an effective way to avoid unduly small required time step for the explicit algorithm to reduce the computational cost, it only works when the number of problematic elements is low and the mesh sizes and locations of them have almost neglectable influence to the overall dynamic property of the system. However, this may not be the common case. In some complex finite element, especially the model including irregular geometry or many connection parts, the

problematic element may occur in very critical location where added mass will significantly influence the dynamic properties and responses. In this situation, if the element size is small and unimportant to the desired solution, one can directly remove this element.

Moreover, the added artificial mass should not be large compared to the total mass of the model. In practice, the ratio between added artificial mass and total mass, represented as

$$r_M = \frac{M_{added}}{M_{total}} \tag{3.21}$$

should not larger than 10%.

3.4.6 Stability control in explicit method: energy balance

The stability of the explicit method in every time increment is controlled and checked via energy balance. The variation of the total energy of the system in every time increment is calculated and measured with respect to a reference energy value, written in mathematical expressions:

$$W_{total} = |W_{kinetic} + W_{damping} + W_{internal} - W_{external}|$$
$$|\delta W_{total}| < p \cdot W_{ref} \tag{3.22}$$

where the lower index indicate the which type of energy is included in total energy. The reference energy value W_{ref} is calculated according the kinetic energy of the system due to the gravity acceleration, i.e. $W_{ref} = \frac{1}{2}M_{total}(g \cdot \Delta t_{ex})^2$, and p is an abort tolerance parameter.

4 | CASES STUDIES: FINITE ELEMENT MODEL AND ANALYSES SCHEMES

4.1 OVERVIEW

In this chapter, the numerical models of 5 different cases are built up in the DIANA FEA 10.3. The transient analyses using implicit and explicit direct integration methods, as described in previous chapters, are performed. The details of each model, the input signals and all analyses schemes are given for each case.

Three cases with linear elastic material are presented in Section 4.2 to Section 4.4. In Section 4.5, the FE model of a masonry wall are built up. Two sub-cases are considered for this case. The first one is the quasi-static cyclic in-plane shear-compression test, which is performed in the laboratory in Italy by Graziotti et al. [2016]. It is used to verify the material model and parameters. The second sub-case is the in-plane seismic analysis, in which the transient analysis is performed. Section 4.6 is the masonry house model which is also tested by Graziotti et al. [2016] in a shaking table test. The FE model is built up and corresponding seismic signal is applied. However, due to the limitations of hardware and software, unexpected long time is needed to finish the whole analysis. Therefore, simplifications and modifications are applied to the original structure, and only a short duration load is considered. The main purpose of the last case is to illustrate the theoretical viability to perform both implicit and explicit methods in practical real structure seismic analysis.

4.2 CASE 1: A SIMPLY–SUPPORTED BEAM SUBJECTED TO A HARMONIC POINT LOAD

4.2.1 Case description

In this case, a simply-support beam is subjected to a point, sinusoidal in time load. The beam has linear elastic material property. The geometry of the beam is shown in Figure 4.2, as well the FE model.

The harmonic force is applied at a point on the beam, its amplitude is given in expression: $f = Psin(\Omega t)$, with $P = 1N$ and $\Omega = 30rad/s$. The load duration is $1s$, and the load scheme is shown in Figure 4.1. The analytical steady-state response of the beam could be calculated as the reference solution to be compared with the solutions obtained from implicit and explicit time integration methods. However, since the finite element analysis of the beam will include the transient effect, Rayleigh damping is applied to the beam model to damp out the free vibration modes and make it comparable to the analytical steady-state response.

4.2.2 Finite element model

The FE model of this case is quite straightforward, as shown in Figure 4.2. The geometry information is summarized in Table 4.1.
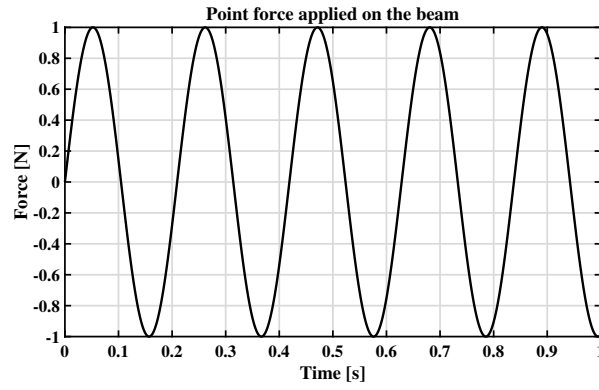
Figure 4.1: The harmonic load scheme of the simply-supported beam
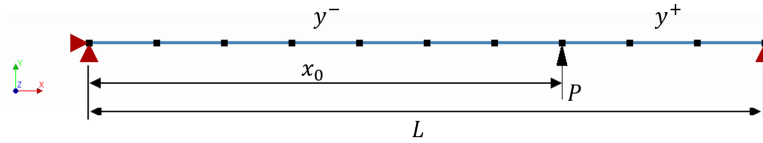
Figure 4.2: Finite element model of the simply-supported beam

Geometry	Length L [m]	Point load location x_0 [m]	Cross-section area A [m^2]	Moment of inertia I [m^4]
Case 1	1	0.7	0.02	4.55×10^{-7}

Table 4.1: Geometry of the simply supported beam

The element type adopted for the beam is L6BEN in DIANA FEA, which is 2-node linear interpolated 2D straight Class-I beam element based on classical Euler-Bernoulli beam theory, as shown in Figure 4.3. Since the polynomial of deflection in y direction u_y is cubic, the integration scheme is chosen as 2 points Gauss integration to get exact polynomials. The material and mesh properties, together with other model information, are given in Table 4.2.

$$u_y(\xi) = b_0 + b_1\xi + b_2\xi^2 + b_3\xi^3$$
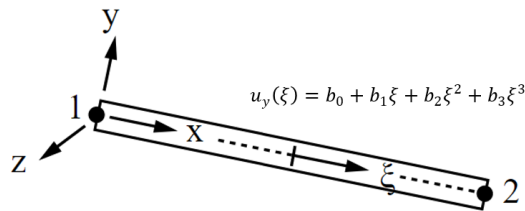
Figure 4.3: 2D Class-I beam element: L6BEN and its polynomial of deflection in y direction

4.2.3 Analyses schemes

Transient analyses with implicit Newmark method and explicit central difference method were performed based on the FE model of the beam. An eigenvalue analysis was performed before the transient analyses, it turns out the first natural frequency of the beam is $49.69 Hz$. According to the experience, the time interval to generate the outputs for both methods are set to be $0.01s$, which is $1/10$ of the first natural period, to ensure the first vibration mode of the system could be generated accurately.

Property	Parameter	Unit	Value
Elastic Material	Young's modulus E	N/m^2	2.2×10^6
	Mass density ρ	kg/m^3	500
Load	$f = Psin(\Omega t)$, with $P = 1N$ and $\Omega = 30rad/s$		
Boundary conditions	Simply supported		
Rayleigh damping	mass coefficient a	$1/s$	30
	stiffness coefficient b	s	0
Element type	2D Class-I straight line (L6BEN)		
Integration scheme	2-point Gauss integration		
Mesh size	Δx	m	0.1
Number of nodes	11		
Number of elements	10		

Table 4.2: Summary of the information of simply-supported beam FE model

Implicit Newmark method scheme

Since the Rayleigh damping is applied to the model, no numerical damping from implicit algorithm is considered. Therefore, the Newmark parameters are chosen as $\beta = 0.25$ and $\gamma = 0.5$. The iteration method is chosen as Regular Newton-Raphson method, and the convergence norm is displacement or force, with tolerance of 0.01. The time step for implicit method, written as Δt_{Im}, is $0.001s$ for a $1s$ duration harmonic load. The transient analysis scheme for implicit method is summarized in Table 4.3.

Direct time integration method	Implicit Newmark method
Newmark parameter	$\beta = 0.25$, $\gamma = 0.5$
Time step Δt_{Im}	$0.001s$
Total steps N_{Im}	1000
Iteration method	Regular Newton-Raphson method
Convergence norm	Displacement or force
Convergence tolerance	0.01
Maximum iteration number	10
Line search	Yes

Table 4.3: Transient analysis scheme for implicit Newmark method

Explicit central difference method scheme

A pretest of the explicit central difference method was made before the complete transient analysis. The aim is to identify $min\{\Delta t_{crit}\}$, which is the smallest critical time step of all the elements, and the result is $min\{\Delta t_{crit}\} = 1.50756 \times 10^{-5}s$. Therefore, to have a preliminary understanding of how the explicit method is controlled by the input settings, two sub-cases are performed. The transient analyses schemes of these two cases are given in Table 4.4. The Sub-case 1 takes $\Delta t_{ex,1} = min\{\Delta t_{crit}\} \times \Delta t_{red}$ as the actual time increment for the explicit algorithm, because the value condition is $\Delta t_{lim} \leq (min\{\Delta t_{crit}\} \times \Delta t_{red}) \leq \Delta t_{ubs,1}$. However, in Sub-case 2, since $(min\{\Delta t_{crit}\} \times \Delta t_{red}) > \Delta t_{ubs,2}$, as a result, the actual time incre-

ment $\Delta t_{ex,2} = \Delta t_{ubs,2}$, which is a time increment further smaller than the critical time step.

Sub-cases	Sub-case 1	Sub-case 2
$\min\{\Delta t_{crit}\}$	1.50756×10^{-5}	
Δt_O	0.001	
Δt_{lim}	$10^{-15}s$	
Δt_{red}	0.95	
$\Delta t_{ubs,i}$	$10^{-3}s$	$10^{-5}s$
$\Delta t_{ex,i}$	$1.43218 \times 10^{-5}s$	$10^{-5}s$
$N_{sub,i}$	70	100

Table 4.4: Transient analyses schemes for explicit method

4.3 CASE 2: A DOUBLE CANTILEVER BEAM SUBJECTED TO A TRANSIENT POINT LOAD

4.3.1 Case description

In case 2, a benchmark analysis from ABAQUS was performed with both implicit and explicit method, and the solution obtained from ABAQUS was selected as reference solution. It concerns the response of an elastic beam, built-in at both ends, subject to a suddenly applied load at its mid-span. The geometry of the beam is similar to the Case 1 except a transient load is applied at the mid-span, and it is shown together with the FE model in Figure 4.5.

The reference solution was obtained from ABAQUS implicit inegration operator: Hilbert-Hughes, with slightly numerical damping, and with three different time steps: $25\mu s$, $50\mu s$ and $100\mu s$. Therefore, to make better comparisons, the similar schemes are also adopted in this thesis with two time integration methods.

The magnitude of the transient load is $2846.7N$ and is applied at the beginning of the analysis. To simulate this transient load, the load scheme in Figure 4.4 but with a duration of $5 \times 10^{-3}s$ is considered in this case.
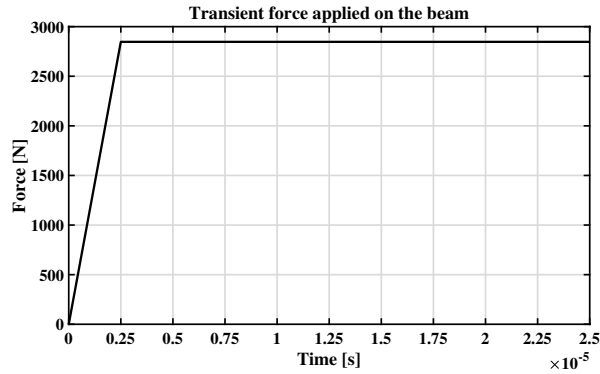
Figure 4.4: The transient load applied on the double cantilever beam

4.3.2 Finite element model

Figure 4.5 gives the finite element model of the beam, the double cantilever boundary conditions are modeled by double fixed boundary conditions. The geometry of the model is included in Table 4.5.
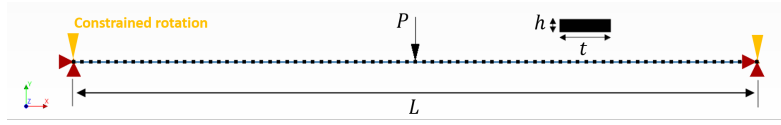
Figure 4.5: The finite element model of the double cantilever beam

Geometry	Length L [mm]	Point load location	Cross-section thickness t [mm]	Cross-section height h [mm]
Case 2	508	Mid-span	25.4	3.2

Table 4.5: Geometry of the double cantilever beam

The element type is using the same one as Case 1, which is 2D Class-I straight line beam element (L6BEN). Considering that slightly numerical damping is included in the reference case, however, the explicit integration method can not include numerical damping, to make a fair comparison, neither numerical damping nor Rayleigh damping is included in implicit and explicit methods. Therefore, the results obtained in this thesis may slightly differ from the reference solution, even though, they are still comparable. The material and mesh properties are presented in Table 4.6.

Property	Parameter	Unit	Value
Elastic Material	Young's modulus E	GPa	206.8
	Mass density ρ	kg/m^3	2710.42
Load	Transient load (Figure 4.4), with duration of $5 \times 10^{-3}s$		
Boundary conditions	Double fixed		
Damping	Not included		
Element type	2D Class-I straight line (L6BEN)		
Integration scheme	2-point Gauss integration		
Mesh size	Δx	mm	6.35
Number of nodes	81		
Number of elements	80		

Table 4.6: Summary of the information of simply-supported beam FE model

4.3.3 Analyses schemes

In the reference case, three different time steps are used to performed analysis with implicit method. Hence, in this section, there are 3 sub-cases for both implicit analysis scheme and explicit analysis scheme.

Implicit Newmark method scheme

For implicit Newmark method, three sub-cases are using the same time steps as the reference case, which are $25\mu s$, $50\mu s$ and $100\mu s$. Neither numerical damping nor material damping is included in all sub-cases. The transient schemes for implicit method are shown in Table 4.7. The lower index of the symbol $[Im, i]$ indicates that it is of the implicit Sub-case i, similar symbol used in the rest of the thesis.

Sub-cases	Sub-case 1	Sub-case 2	Sub-case 3
Time step $\Delta t_{Im,i}$	$25\mu s$	$50\mu s$	$100\mu s$
Total steps $N_{Im,i}$	200	100	50
Newmark parameter	$\beta = 0.25$, $\gamma = 0.5$		
Iteration method	Regular Newton-Raphson method		
Convergence norm	Both displacement and force		
Convergence tolerance	0.01		
Maximum iteration number	50		
Line search	Yes		

Table 4.7: Transient analyses schemes for implicit Newmark method

Explicit central difference method scheme

To identify the minimum critical time step of all elements, a pretest was made before the full analysis. The result shows that $min\{\Delta t_{crit}\} = 7.21291 \times 10^{-7}s$. It is already smaller than any of the time steps in the reference case, therefore, the explicit settings are remain default except using three different output time intervals. The analyses schemes are shown in Table 4.8, note that no damping is considered here either.

Sub-cases	Sub-case 1	Sub-case 2	Sub-case 3
$min\{\Delta t_{crit}\}$	$7.21291 \times 10^{-7}s$		
Δt_{lim}	$10^{-15}s$		
Δt_{red}	0.95		
Δt_{ubs}	$10^{-3}s$		
Δt_{ex}	$6.85226 \times 10^{-7}s$		
$\Delta t_{O,i}$	$25\mu s$	$50\mu s$	$100\mu s$
$N_{sub,i}$	37	73	146

Table 4.8: Transient analyses schemes for explicit method

4.4 CASE 3: A SIMPLY–SUPPORTED THIN PLATE UNDER OUT–OF–PLANE TRANSIENT DISTRIBUTED LOAD

4.4.1 Case description

In case 3, a benchmark from the publication of *NAFEMS Selected Benchmarks for Forced Vibration* (Maguire et al. [1993]) was selected. The benchmark describes a simply supported square plate subjected to various load conditions, one of them is out-of-plane transient uniform distributed load over whole plate with a magnitude $F_0 = 100N/m^2$. This load condition will be performed in this case. The geometry of the plate is $10m \times 10m$ with thickness $t = 0.05m$. The plate is simply supported on the edges and free to deform in out-of-plane direction. The material of the plate is linear elastic with Young's modulus $E = 200 \times 10^9 N/m^2$, Poisson's ratio $\nu = 0.3$ and density $\rho = 8000kg/m^3$.

In the report of Maguire et al. [1993], several reference solutions are provided for this benchmark, including analytical peak displacement, solution from modal analysis using FE code ANSYS and ASAS, and solution from direct time integration method using aforementioned two codes. However, only values of peak displacement, peak stress and static displacement are provided in the report, and the solution obtained from the FE codes are the average value of two codes. One can refer to the report of Maguire et al. [1993] to see more detailed information, but the focus of this case in this thesis is to investigate the performances of the different direct time integration methods.

4.4.2 Finite element model

The finite element model of the plate are shown in Figure 4.6. Since only out-of-plane behavior is interested for this case, all nodes are constrained in x and y directions.

All nodes are constrained in *x* and *y* directions
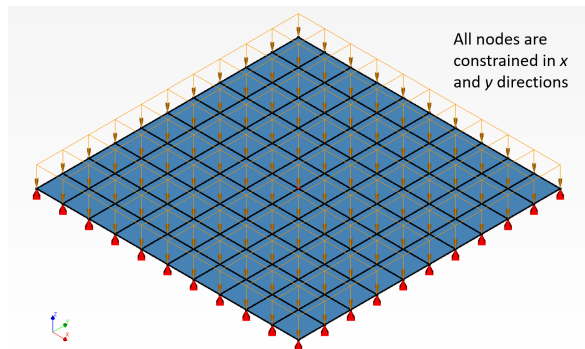
Figure 4.6: The finite element model of the thin plate

The element type adopted for this model is the four-node quadrilateral isoparametric curved shell element Q20SH, as shown in Figure 4.7 together with the polynomials of the linear interpolation. The transient load as shown in Figure 4.6, is applied over the whole plate. The load-time curve is similar to the Figure 4.4 but with a magnitude of $100N/m^2$. The Rayleigh damping parameters are already given in the benchmark, which are $a = 0.299$ and $b = 1.339 \times 10^{-3}$. However, due to the limitation of the explicit method, as introduced in Section 3.4, the parameter b must be set to be zero. The information of the finite element model of the plate is summarized in Table 4.9.

$$u_i(\xi, \eta) = a_0 + a_1\xi + a_2\eta + a_3\xi\eta$$
$$\phi_i(\xi, \eta) = b_0 + b_1\xi + b_2\eta + b_3\xi\eta$$
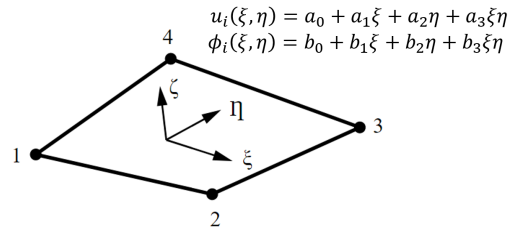
Figure 4.7: The four-node quadrilateral isoparametric curved shell element Q20SH

Property	Parameter	Unit	Value
	Young's modulus E	GPa	200
Elastic Material	Poisson's ratio ν		0.3
	Mass density ρ	kg/m^3	8000
Load	Transient distributed force, with $F_0 = 100N/m^2$		
Boundary conditions	Simply supported		
Rayleigh damping	mass coefficient a	$1/s$	0.299
	stiffness coefficient b	s	0
Element type	Four-node regular curved shell element (Q20SH)		
Integration schemes	Over element area	2×2 Gauss integration	
	Over thickness	3-point Simpson integration	
Mesh size	Δx	m	1
Number of nodes	121		
Number of elements	100		

Table 4.9: Summary of the information of simply-supported plate FE model

4.4.3 Analysis schemes

Since the benchmark report provides few natural frequencies and mode shapes of the thin plate, to verify the dynamic properties of the FE model, the eigenfrequency analysis should be performed first. Then according the first natural period of the system, which is about $0.4s$, the output time step of the direct time integration methods is chosen as $0.01s$, which is smaller than $1/20$ of the first natural period. Moreover, the reference solution of the direct time integration method in the report is obtained using a time step of $0.002s$, to make a better comparison, this time step is also used for the analysis but with a shorter load duration of $2s$.

Implicit Newmark method scheme

Due to Rayleigh damping is already included in the FE model of the plate, no numerical damping is introduced in implicit method. The transient schemes for implicit method are shown in Table 4.10.

Explicit central difference method

The pretest using explicit method shows that $min\{\Delta t_{crit}\} = 1.4597 \times 10^{-4}s$, and the actual adopted time increment for explicit algorithm is $\Delta t_{ex} = \Delta t_{red} \times min\{\Delta t_{crit}\} = 1.38672 \times 10^{-4}s$. The transient analyses schemes for central difference method are presented in Table 4.11.

Sub-cases	Sub-case 1	Sub-case 2
Time step $\Delta t_{Im,i}$	$0.01s$	$0.002s$
Total steps $N_{Im,i}$	500	1000
Newmark parameter	$\beta = 0.25$, $\gamma = 0.5$	
Iteration method	Regular Newton-Raphson method	
Convergence norm	Both displacement and force	
Convergence tolerance	0.01	
Maximum iteration number	50	
Line search	Yes	
Mass Matrix and damping matrix	Lumped	

Table 4.10: Transient analyses schemes for implicit Newmark method

Sub-cases	Sub-case 1	Sub-case 2
$\min\{\Delta t_{crit}\}$	$1.4597 \times 10^{-4}s$	
Δt_{lim}	$10^{-15}s$	
Δt_{red}	0.95	
Δt_{ubs}	$10^{-3}s$	
Δt_{ex}	$1.38672 \times 10^{-4}s$	
$\Delta t_{O,i}$	$0.01s$	$0.002s$
$N_{sub,i}$	73	15

Table 4.11: Transient analyses schemes for explicit method

4.5 CASE 4: THE IN-PLANE LOADING TESTS OF MASONRY WALL EC-COMP2-3

4.5.1 Case description

Case 4 is a masonry specimen from the laboratory test program of *Experimental campaign on a clay URM full-scale specimen representative of the Groningen building stock* performed by EUCENTRE (Graziotti et al. [2016]). In this test program, several full-scale unreinforced clay masonry wall were tested under in-plane cyclic shear-compression load. This in-plane component test is fundamental in calibrating reliable numerical models for the masonry wall, as well as the full-scale URM house model in shaking table tests.

In this report, one of the specimens EC-COMP2-3 was selected and will be used for further seismic analysis to investigate the performance of direct time integration method for quasi-brittle material. For this purpose, the in-plane cyclic shear-compression test will be performed in FEA first. The result of it will be compared with that from experimental test to validate the finite element model of the specimen EC-COMP2-3. Then a seismic signal, which is used in the later shaking table test from the same test program (Graziotti et al. [2016]), will be applied to this model as base excitation. The seismic analysis will be performed using implicit and explicit methods and the results will be compared to evaluate the performance of both methods in seismic analysis for masonry material.

Therefore, this section is divided into two parts. The first part introduce the in-plane cyclic shear-compression test. The second part will describe the seismic analysis of the specimen.

4.5.2 In-plane shear–compression test

The specimen EC-COMP2-3 is a full-scaled clay masonry wall, the dimension of the specimen is given in Table 4.12. The wall was made of clay bricks with unit size $208 \times 100 \times 50mm$ and mortar joints. In the in-plane shear-compression test, the wall was subjected to a vertical compression stress of $\sigma_v = 0.86MPa$. The boundary condition of the specimen is double fixed, the bottom edge of the wall is rigid connected to a Reinforced-Concrete (R.C.) footing, the top edge of the wall is fixed to composite steel/R.C. beam, which is connected to two vertical actuators. Two vertical actuators can apply simultaneously a force equal to the required vertical load and a moment corresponding to the maximum resisting moment at the top section. The horizontal load is applied by a horizontal actuator connected to the top composite steel/R.C beam. More detailed description could be found in the report of Graziotti et al. [2016]. The geometry of the specimen and test set-up for this specimen are shown in Figure 4.8.

Specimen	l $[m]$	t $[m]$	h $[m]$	σ_v $[MPa]$	Boundary condition
EC-COMP2-3	1.2	0.208	2.71	0.86	Double-fixed

Table 4.12: The masonry wall specimen for cyclic in-plane shear-compression test

(a) Geometry of the specimen
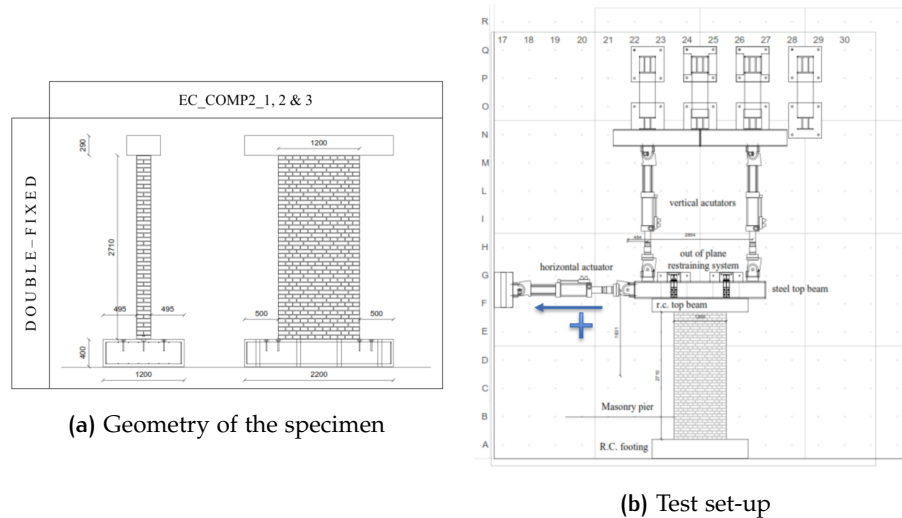
(b) Test set-up

Figure 4.8: Finite element analysis results of simply-supported thin plate

Finite element model

The finite element model according to the geometry and test set-up was built up, as shown in Figure 4.9. The element type is using 8-node quadrilateral isoparametric plane stress (CQ16M), because the out-of-plane stress is zero ($\sigma_{zz} = 0$) in this in-plane test. It is based on quadratic interpolation and Gauss integration, the typical displacement polynomial is presented in Figure 4.10. The element and mesh used in this model is summarized in Table 4.13. The nodes on the bottom edge of the model is fixed in x and y direction, note the nodes of CQ16M has no rotation
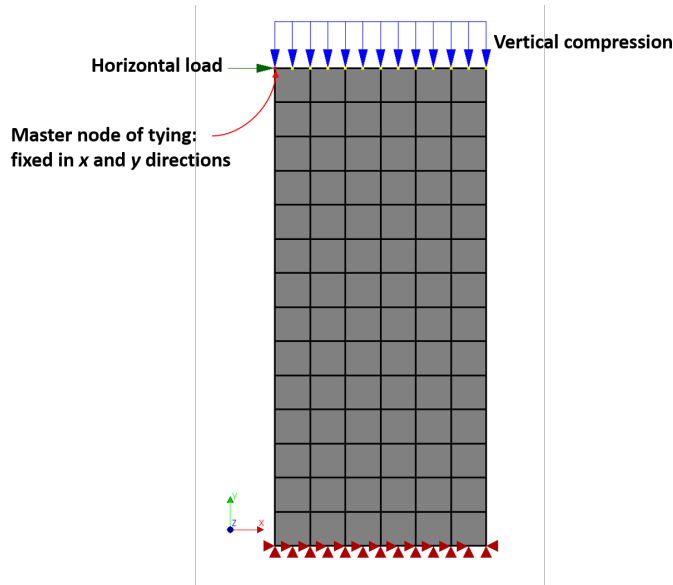
Figure 4.9: FE model of the specimen EC-COMP2-3

$$u_i(\xi, \eta) = a_0 + a_1\xi + a_2\eta + a_3\xi\eta$$
$$+ a_4\xi^2 + a_5\eta^2 + a_6\xi^2\eta + a_7\xi\eta^2$$
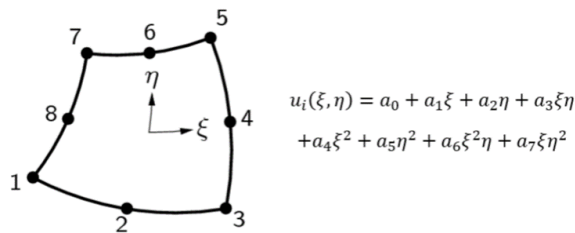
Figure 4.10: 8-node quadrilateral isoparametric plane stress (CQ16M)

Element type	8-node quadrilateral isoparametric plane stress element (CQ16M)
Integration scheme	2×2 Gauss integration
Mesh size	$0.2m$
Element thickness	$0.208m$
Number of nodes	293
Number of elements	84

Table 4.13: The finite element used in the FE model for the masonry wall

degree of freedom. To simulate the top edge of the specimen, which is constrained in rotation but can still move in horizontal and vertical direction, a tying is used in the model. The master nodes of tying is located at the top left corner and fixed in x and y direction and the rest nodes on the top edge are tied to this nodes, which means they have exactly the same displacement during the analysis, in this way, rotation of the top edge is prevented, but horizontal and vertical motions are allowed.

The self-weight of the structure is considered in this model. The vertical compression load is applied through equally distributed force in 2-dimension, which is $q = 178880N/m$. To apply the horizontal prescribed displacement on the top edge, a virtual horizontal support is added to the master node, in this way, applying the prescribed displacement on the master node is equal to apply it on the top edge.

Engineering Masonry material model (DIANA FEA BV [2019])

The Orthotropic material model Engineering Masonry model in DIANA FEA 10.3 is selected to simulate the quasi-brittle behavior of the masonry. This section will briefly introduce the constitutive laws of Engineering Masonry material model, one can also refer to the DIANA FEA 10.3 Documentation (DIANA FEA BV [2019]) to learn more detailed information about it.

The Engineering masonry model is based on the smear cracking concept. It considers the anisotropy of the masonry resulting from different stiffness in directions of the bed joints and head joints. There are four predefined cracks in the plane of the element, which are in the direction of bed joint, in the direction of head joint and in two diagonal directions.

The tensile crack is assessed in the direction either normal to the bed joint or to the head joint, and secant nonlinear unloading and reloading behavior is assumed. The crushing is also assessed in the direction normal to the bed joint or to the head joint, and the unloading and reloading behavior is considered to be non-secant, in order to simulate highly nonlinear behavior of the masonry. The shear failure mechanism is based on the standard Coulomb friction failure criterion.

The constitutive laws for Engineering Masonry model in tensile cracking, compressive crushing and shear behavior are presented as shown in Figure 4.11. It describes the unloading behavior more realistically by strong stress decay with the original linear stiffness. Therefore it is recommended for static nonlinear cyclic or transient dynamic nonlinear analyses of components and full structure (DIANA FEA BV [2019]).
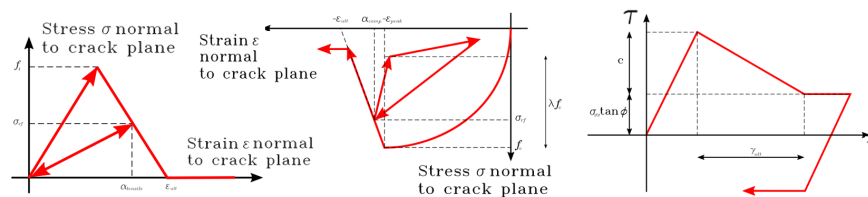
Figure 4.11: The constitutive laws for Engineering Masonry model in tensile cracking, compressive crushing and shearing (DIANA FEA BV [2019])

According to the laboratory tests and experience, the following (Table 4.14) material parameters are used in the FE model.

Cyclic loading scheme

The cyclic load is introduced through the horizontal actuator by imposing the prescribed displacements to the top edge of the masonry wall. In the FE model, the cyclic prescribed displacement is applied on the master node of tying on the top edge of the model using displacement control.

Property	Parameter		Unit	Value
Elasticity	Young's modulus	Perpendicular to head joints E_x	Mpa	4916.5
		Perpendicular to bed joints E_y	MPa	9833
	Shear modulus G_{xy}		MPa	3933.2
	Mass density ρ		kg/m^3	1979
Cracking	Head joint failure type	Tensile strength head joint defined by friction		
	Tensile strength	Bed-joint strength f_{ty}	MPa	0.23
		Minimum head-joint strength f_{tx}	MPa	0.69
	Fracture energy in tension G_{ft}		N/m	15
	Stepped diagonal crack angle α		Degree	45
Crushing	Compressive strength f_c		MPa	6
	Fracture energy in compression G_{fc}		N/m	40000
	Factor to strain at compressive strength n			4
	Unloading factor λ			0.4
Shear	Friction angle Φ		Degree	26
	Cohesion f_{v0}		MPa	0.18

Table 4.14: Material properties for Engineering masonry model

In the laboratory tests, the cyclic load protocol includes 16 cycles in total and each cycle has three identical runs. Since the test was conducted in quasi-static condition, no transient effect was included in the FE analysis, and the number of identical runs for each cycle was reduced to two, in order to save computational time. The target amplitude of displacement for each cycle in test protocol and applied prescribed displacement for each cycle in FE model are given in Table 4.15, and the cyclic scheme with a time dependent factor is shown in Figure 4.12.

Cycle	Target loading amplitude [mm]	FE analysis loading amplitude [mm]
1_1	0.41	0.4
1_3	0.85	0.8
1_4	0.99	1
1_D	1.32	1.2
2_D	2.10	2
3_D	2.68	2.6
4_D	4.10	4
5_D	5.44	5
6_D	6.82	6.5
7_D	8.20	8
8_D	10.89	10.5
9_D	13.59	13.5
10_D	16.35	16.2
12_D	21.89	21.6
13_D	27.40	27
14_D	34.28	34.2

Table 4.15: Cyclic loading protocol in laboratory test and FE analysis
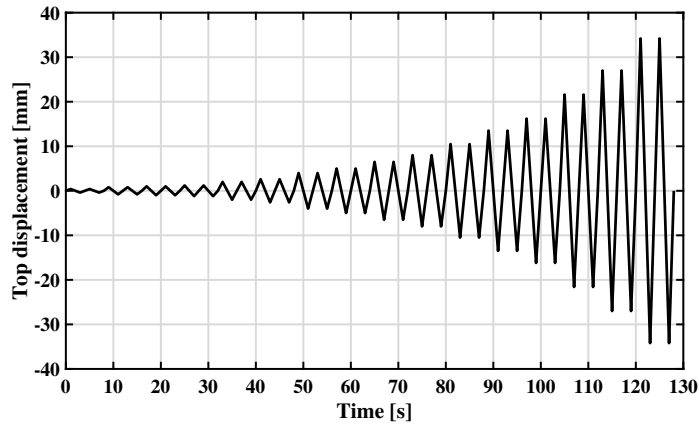
Figure 4.12: Time history of the cyclic loading in FE analysis

Quasi-static analysis scheme

The purposes of performing quasi-static analysis are to validate the material parameters in the FE model and also identify the the nonlinear behavior of the masonry wall.

Therefore, a monotonic pushover loading with maximum magnitude of prescribed displacement of 34.2mm was first applied on model in order to investigate the load bearing capacity softening behavior of the masonry material. Moreover, few eigenfrequency analyses are performed during the monotonic pushover procedure, these analyses will provide valuable information about how the material nonlinearity influences the natural frequency of the structure, which is important to determine the critical time step in explicit method. The monotonic pushover analysis scheme and the corresponding eigenfrequency analyses are given in Table 4.16. Note both physically and geometrically nonlinear effects are considered.

Load steps	Self-weight	1
	Vertical compression	1
	Monotonic pushover	100
Iteration method	Regular Newton-Raphson	
Maximum iteration number	50	
Line search	Yes	
Convergence norm	Both displacement and force	
Convergence tolerance	0.01	
Eigenfrequency check	Every 10 pushover load steps	

Table 4.16: Monotonic pushover analysis scheme and corresponding eigenfrequency analyses schemes

Then the cyclic loading scheme presented in Table 4.15 is applied and results will be compared with the experimental results. The analysis scheme for cyclic loading test is shown in Table 4.17. The transient effect is ignored in FEA, and the cyclic load is applied using displacement control via several load steps.

4.5.3 In-plane seismic analysis

The in-plane seismic analysis is based on the previous quasi-static analysis of the masonry wall specimen, but taking into account the transient effect of the seismic loading and using direct time integration method to obtain the dynamic response of the structure.

	Self-weight	1
Load steps	Vertical compression	1
	Cyclic pushover	1866
Iteration method	Regular Newton-Raphson	
Maximum iteration number	50	
Line search	Yes	
Convergence norm	Both displacement and force	
Convergence tolerance	0.01	

Table 4.17: Cyclic pushover analysis scheme

The material parameters of the Engineering masonry is using the validated ones through quasi-static analyses, given in Table 4.14. However, since the masonry wall is quite stiff for in-plane base acceleration load, some modifications are applied to the model to increase the inertial effect generated by the base acceleration on the wall.

Modified finite element model

First, the real masonry wall is usually simultaneously carrying the dead weights and inertia forces of the upper structures, such like floor and roof, in the seismic events. To simulate this loading condition, a large density ($\rho = 160000 kg/m^3$) linear elastic beam is added on the top of the masonry wall to provided extra vertical loading and increase the inertia force. The length of the beam is the same as the width of the masonry wall, which is 1.2m. The cross-section of the beam has thickness of 0.208m and height of 0.2m. Above all, the total mass of beam is 7.9872t.

Second, considering the element limitation for the explicit method, which is only linear interpolated element is available, to ensure the accuracy of the results, the mesh size is reduced to half of the value in Table 4.13, and linear plane stress element type Q8MEM is adopted. The new element properties are given in Table 4.18.

	Masonry wall	**Beam**
Element type	4-node quadrilateral isoparametric plane stress element (Q8MEM)	2D Class-I straight line beam element (L6BEN)
Displacement polynomial	$u_i(\xi, \eta) = a_0 + a_1\xi + a_2\eta + a_3\xi\eta$	$u_y(\xi) = b_0 + b_1\xi + b_2\xi^2 + b_3\xi^3$
Integration scheme	2×2 Gauss integration	2-point Gauss integration
Mesh size	0.1m	0.1m
Element thickness	0.208m	0.208m
Total number of nodes	364	
Total number of elements	336	

Table 4.18: The finite element used in the FE model for the masonry wall

Third, the tying at the top of the model is removed because the load is no longer applying on the top edge. Also, the virtual support at the top left node of the model is removed, because external load is not prescribed displacement. Instead, a seismic acceleration load is applied at the base of the wall.

Last, the Rayleigh damping with damping ratio of 5% is added to the model to eliminate the undesired high frequency noise. The Rayleigh parameters are calculated from two selected frequencies. The first frequency is the first non-zero natural frequency, and the second one is the highest frequency that has the cumulative effective mass percentage larger than 90% in the seismic load direction. Through these two parameters, a low level of damping would be introduced for the zone between the selected two frequencies. The resulting Rayleigh damping parameters are $a = 5.5$ and $b = 2.5 \times 10^{-4}$. Again, since lumped mass is adopted for direct time integration, b is set to be zero.

The modified FE model of the masonry wall is presented in Figure 4.13.
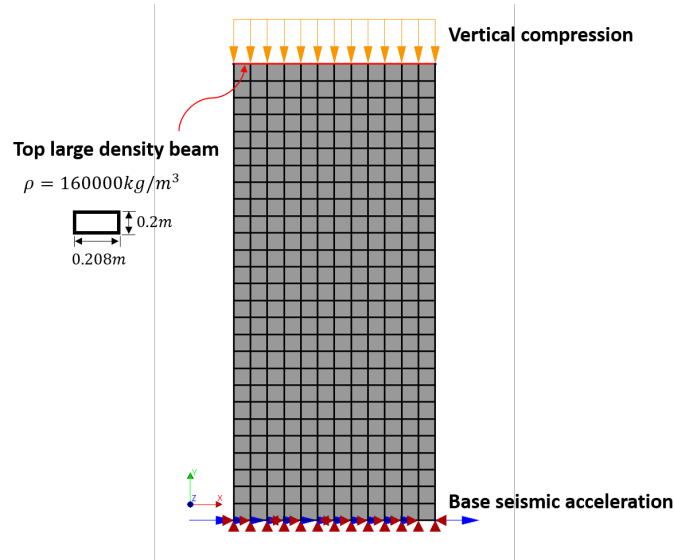
Figure 4.13: FE model of the specimen EC-COMP2-3 for seismic analysis

Input seismic signal

The input signal was given in the Graziotti et al. [2016], the one adopted for this model is the signal $SC2\_400\%$, which is scaled from the original signal $SC2$ to 400%.

The signal $SC2$ is obtained from the experiment data of base acceleration history. It has a peak ground acceleration (PGA) of $0.140335g$. Correspondingly, the $SC2\_400\%$ has PGA value of $0.56134g$. The acceleration time history of $SC2\_400\%$ is given in Figure 4.14a. Since the accelerations after $10s$ are relatively small and have minor influence on the overall nonlinear behavior of structure, to save the computational time, the interval between $1s - 10s$ was adopted as actual input, as shown in Figure 4.14b. Moreover, normalized Fourier spectrum of the signal $SC2\_400\%$ is calculated and presented in Figure 4.15.

(a) Acceleration time history of $SC2\_400\%$

(b) Input acceleration time history
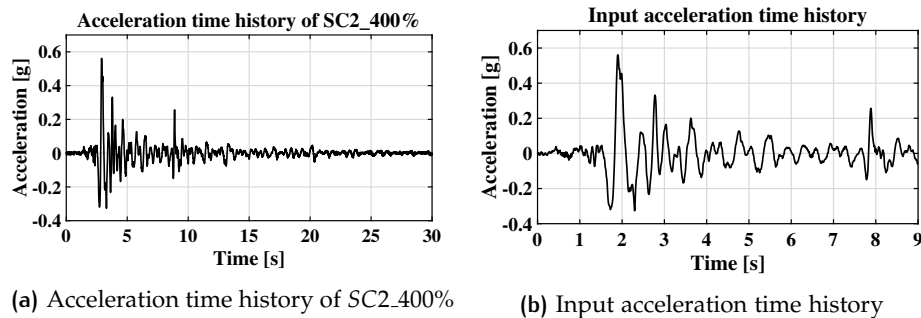
Figure 4.14: Input signal for seismic analysis
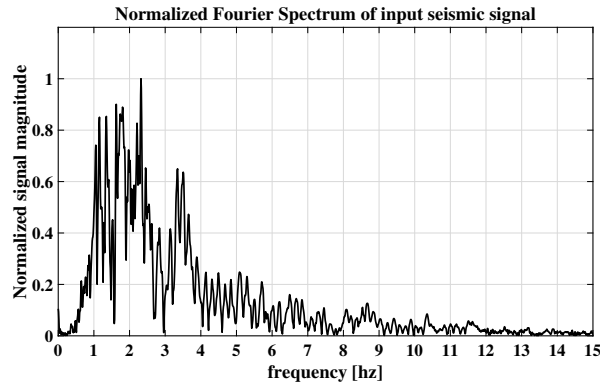
Figure 4.15: Normalized Fourier spectrum of seismic signal $SC2\_400\%$

Analysis schemes

First an eigenfrequency analysis was made to identify the dynamic property of the structure. It turns out the first eigen frequency of the structure is $10.71Hz$, therefore, to ensure the first eigen mode could be generate accurately, the output time interval of the results are chosen as $0.005s$, which is about $1/20$ of the first natural period.

Both physical nonlinearity and geometry nonlinearity are included in the transient analysis. Since the Rayleigh damping is already included in the structure, no extra numerical damping is introduced. In both implicit method and explicit method, the self-weight is first applied on the structure through one load step, and then vertical compression is applied, finally the seismic base acceleration with a duration of $9s$.

The transient analysis scheme using implicit Newmark method is presented in Table 4.19.

Implicit method	Newmark method
Time step Δt_{Im}	$0.005s$
Total steps N_{Im}	1800
Newmark parameter	$\beta = 0.25$, $\gamma = 0.5$
Iteration method	Regular Newton-Raphson method
Convergence norm	Energy
Convergence tolerance	0.0001
Maximum iteration number	200
Line search	Yes
Mass Matrix and damping matrix	Lumped

Table 4.19: Transient analyses schemes for implicit Newmark method

Moreover, since the eigenfrequency of the structure may change when the nonlinear behavior is activated, therefore, eigenfrequency analyses were performed every $0.5s$ during the implicit method procedure.

For explicit method, the $min\{\Delta t_{crit}\}$ is first identified as $min\{\Delta t_{crit}\} = 4.50268 \times 10^{-5}s$. Then two sub-cases are performed with the first sub-case using $min\{\Delta t_{crit}\} = 4.50268 \times 10^{-5}s$ and the second one using $\Delta t_{ex} = 5 \times 10^{-6}s$. The transient analysis using explicit central difference method is given in Table 4.20

Sub-cases	Sub-case 1	Sub-case 2
$\min\{\Delta t_{crit}\}$	$4.50268 \times 10^{-5}s$	
Δt_{lim}	$10^{-15}s$	
Δt_{red}	0.95	
$\Delta t_{ubs,i}$	$10^{-3}s$	$5 \times 10^{-6}s$
$\Delta t_{ex,i}$	$4.27754 \times 10^{-5}s$	$5 \times 10^{-6}s$
Δt_O	0.005	
N_{sub}	1800	

Table 4.20: Transient analyses schemes for explicit method

4.6 CASE 5: THE URM FULL–SCALE BUILDING TESTS

4.6.1 Case description

Case 5 is the full-scale building on the shaking table test conducted by Graziotti et al. [2016] in laboratory test program of *Experimental campaign on a clay URM full-scale specimen representative of the Groningen building stock.* The test performed a shaking table test on a single-story full-scale clay Unreinforced Masonry (URM) building at the EUCENTRE laboratory in Pavia (Italy), in order to investigate the seismic behavior of typical pre-1940 URM Dutch residential building.

In this section, the geometry of the full-scale house will be introduced first, then the finite element model was built up and the weakest seismic signal was applied on the model. Few preliminary analyses were performed using the linear elastic material property. However, due to the limitations of the hardware and software, extremely long computational time is required for the explicit method. So, some simplifications and modifications are applied to the model, as well as a short duration of seismic load is adopted. The nonlinear material properties and strong seismic signal are considered then in the analysis of of Simplified model. These simplifications may lead to the results of the finite element analyses not quite comparable to the experiment results, but the the comparison between results from implicit and explicit methods can still provide valuable information about differences between these two methods.

Therefore, the main purpose of this case is to illustrate the theoretical viability and also provide some insight views of differences in the results of both method for real structure seismic analysis. Moreover, this case also gives important information about the mass scaling technique in the complex structure seismic analyses.

4.6.2 Geometry and general characteristics of the house

The house is a single-story full-scale structure built up with clay-brick masonry bricks and a timber floor and roof structure. The house has plan dimensions of $5.33m \times 5.77m$, and the height of $6.23m$. The house plan is not symmetric, because a re-entrant corner exists in one of the longitudinal masonry walls (west side wall). The irregular plan with re-entrant may magnify the torsional effects when uniaxial seismic excitation is applied at the base.

A plane view of the house at the ground floor level is given in Figure 4.16. Figure 4.17 shows the elevation views from four lateral sides of the house. The overall view of the house at the end of the construction works is given in Figure 4.18.

The timber floor and roof structure are shown in Figure 4.19. The connections between floor beams to the east and west wall are using steel anchors which are embedded in the masonry wall, and the ends timber floor beam are also partially embedded in the masonry wall. The floor-wall connections basically prevent both relative displacement and rotation of the floor beam, therefore it could be modeled as rigid connections, i.e. shared nodes, in the FE model. Some pictures of the connections are shown in Figure 4.20. The connections between roof structure and the longitudinal walls are shown in Figure 4.21. These connections of the wall plate embedded in mortar are modeled by share nodes with masonry wall in the FE model. The connections between orthogonal roof beams, which are nailed together, could be modeled as short stiff elastic beam.
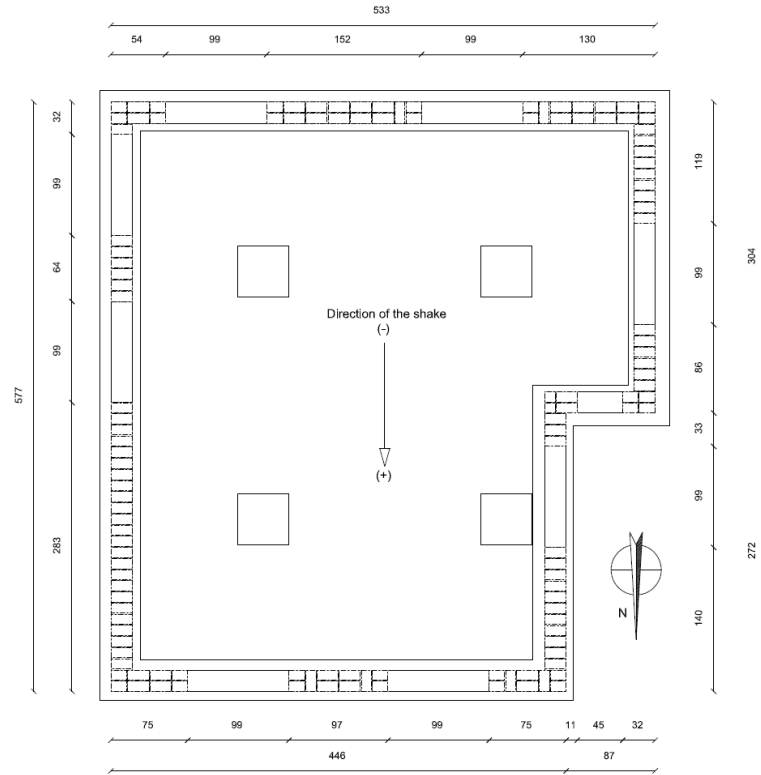
Figure 4.16: Plan view of the house at ground floor level (in *cm*) (Graziotti et al. [2016])

Figure 4.17: Elevation views of the house from four lateral sides (in *cm*) (Graziotti et al. [2016])

Figure 4.18: The test house at the end of the construction works (Graziotti et al. [2016])
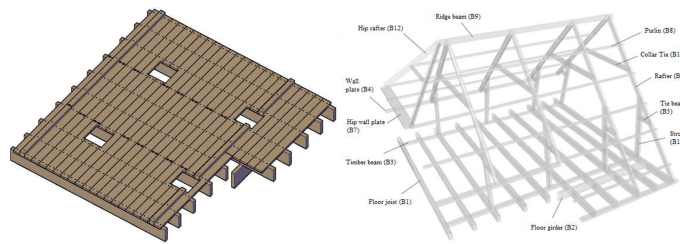
Figure 4.19: The timber floor and roof structure (Graziotti et al. [2016])
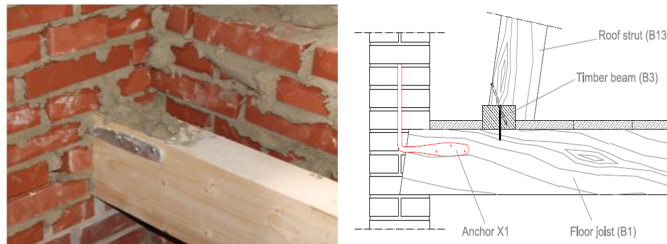
Figure 4.20: Connections between floor beams and masonry walls (Graziotti et al. [2016])
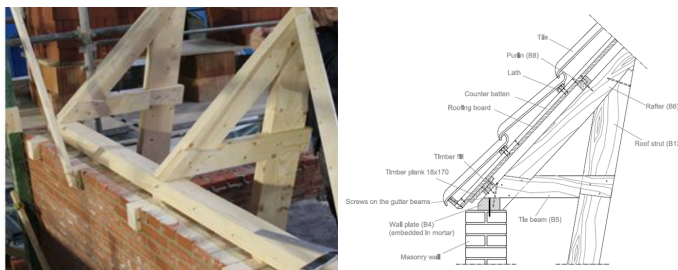
Figure 4.21: Connections between Roof beams and longitudinal walls (Graziotti et al. [2016])

Above the roof timber beam structure, $18mm \times 200mm$ timber roofing boards are placed. However, these boards are light in weight and have almost no contribution to the loading capacity of the house, therefore, they are not included in the FE model.

Moreover, there are 8 laminated rubber blocks are placed on the first floor to provide extra load. The total mass of the blocks are $1.31t$, including six $600mm \times 700mm$ blocks with $200kg$, and two $350mm \times 400mm$ blocks with $55kg$. The list of masses contributing to the total mass of the specimen are given in Table 4.21.

Mass of masonry	28.96
Total mass of the roof	1.87
Total mass of the floor	1.78
Total mass of the house	32.61

Table 4.21: List of masses contributing to the total mass of the house (unit:[t])

Additionally, a rigid steel frame has been built and fixed on the shaking table. The steel frame is firmly bolted to the surface of the shaking table. The columns of the steel frame pass through the first floor of the house without any connection or contact between them. The main purpose of this steel frame is to establish the reference points and place instruments for measurement. Therefore, it will not included in the FE model either.

4.6.3 Finite element model

The full FE model of the test-house was built up in DIANA FEA 10.3, as shown in Figure 4.22. The full FE model is consisted by masonry wall structure model, first floor structure model and roof structure model. All nodes on the bottom edge of the model are fixed and prescribed uniaxial acceleration in x direction (north-south direction) is applied to all of them.
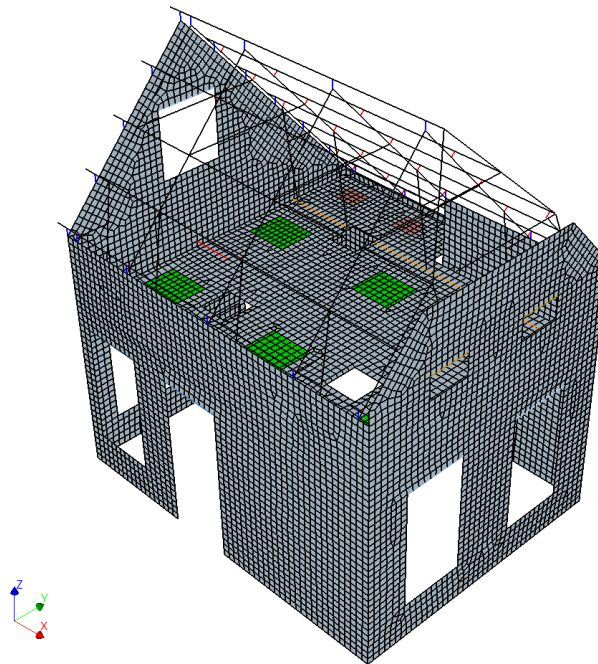
Figure 4.22: Full FE model of the test-house

Limitations for modeling strategy

Before introducing the details of this FE model, it is important to mention some limitations for modeling strategy in DIANA FEA. Due to the fact that the critical time step of explicit method is calculated based on the natural frequency of each element in the model, zero-volume (i.e zero-mass) element types could not be used in the model, otherwise, the critical time step is close to zero and explicit algorithm can't successfully proceed. Besides, the tying can't properly function in explicit algorithm either. Therefore, all the necessary connections are modeled as rigid connections in this model.

Model of masonry wall

The model of the masonry walls is shown in Figure 4.23a. The element type adopted for the masonry wall is the four-node quadrilateral isoparametric curved shell element (Q20SH), because the curved shell element could represent both in-plane and out-of-plane deformations of the wall. Each node of the element has 5 degree of freedoms: three displacements u_x, u_y, u_z and two rotations Φ_x and Φ_y.

Additionally, due to limitation of explicit method, only first order element type is adopted. The four-node quadrilateral curved shell element Q20SH has linear interpolations in both displacement and translations. The element topology and polynomials are shown in Figure 4.23b. The integration over element are is regular 2×2 Gauss integration, and in the direction of thickness the 3-point Simpson is used by default. However, few three-node triangular isoparametric curved shell elements T15SH occur in the FE model, this is because the irregular geometry of the structure. Since not more than 20 of this kind of element included in the model, compared to total number of more than 10000 elements, the influence of them is neglected.

To have better accuracy, the mesh size is set to be $0.1m$ and the thickness of the element is aligned with the length of the brick which is $208mm$. The effect of presence of timber lintel is modeled with liner elastic 3D 2-node first order Class-I beam element L12BE, and the cross-section is assigned with $100mm \times 50mm$.

(a) Geometry of FE model of masonry walls

(b) Element type for masonry walls
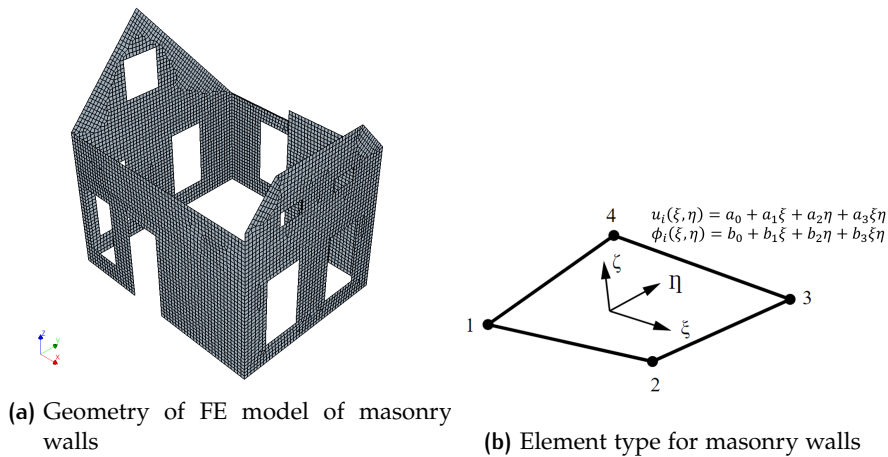
Figure 4.23: FE model for masonry wall structure

Model of first floor structure

The model of the first floor is composed of first floor beams, north-south direction girder, anchors, laminated rubber mass blocks and the timber floor panel. The FE model of entire floor structure and models of components are presented in Figure 4.24. The floor panel and mass blocks are using the same element type as the masonry wall, i.e. Q20SH. The thickness of the first floor panel $24mm$. The four rectangular holes on the floor panel is used for the rigid steel frame to pass through. The mass of each block is corresponding to the experiment report.

The floor beams and anchors are modeled with 3D 2-node first order Class-I beam elements L12BE, based on the classical Euler-Bernoulli beam theory. The girders are using the 3D 2-node Class-III beam element L12BEA, based on Mindlin-Reissner theory, to take into account the shear deformation by assuming the displacements and rotations of the beam axis normals are independent and are respectively interpolated from the nodal displacements and rotations. The cross-section dimensions of these beam elements are aligned with the dimensions in the report of Graziotti et al. [2016]. Both aforementioned 3D beam elements have six degree of freedoms at each node, which are three displacement along three axes and three rotations

around three axes. Since the class-I beam is based on Euler-Bernoulli beam theory, the polynomials for transverse deformation are cubic and 2-point Gauss integration is adopted. The 3D class-III beam element has independent rotation and displacement, therefore the polynomials are both linear and 1-point integration scheme is used.
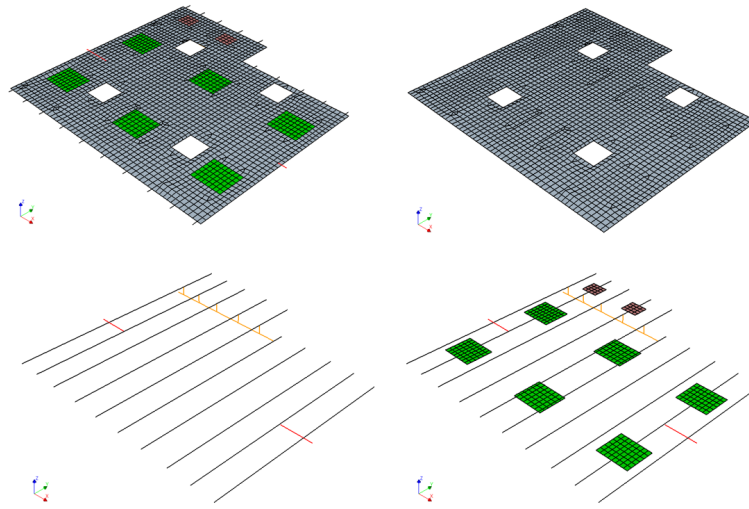
Figure 4.24: FE model of first floor of the house

Model of roof structure

The Figure 4.25 shows FE model of roof structure. The model reproduce the real roof beam structures for the test-house. All the beams are built up in the FE model according to the information provided in the report. The 3D 2-node class-III beam element L12BAE is adopted for all rafters, struts and purlins components, and class-I beam element L12BE is adopted for connection components of the roof structure. According to the experiment report, different cross-section dimension and properties are assigned to different pert of the roof beams, e.g. purlins, rafters and connections. The roof structure is connected to and supported from the masonry walls by timber plate panel embedded in mortar of the longitudinal east and west walls and also by roof struts fixed on the first floor. Both connection types are modeled with rigid connection, i.e, sheared nodes. Besides, the connections between roof rafters and roof purlins, which are nailed together in real structure, are modeled with very short and stiff elastic beam elements.

Overview of element type and properties

An overview of used finite element type and mesh properties are summarized in Table 4.22.

The masonry walls are modeled with Engineering masonry model, with the material properties exactly the same as used in Section 4.5 for the masonry wall, as shown in Table 4.14. The other parts of the model are assumed to be linear elastic. The linear elastic material properties of different components of the model are given in Table 4.23.

4.6.4 Input seismic signal

During the test, the house is subjected to three different typologies of motion: a random white noise ($RNDM$), and two types of earthquake signals ($SC1$ and $SC2$). The purpose of signal $RNDM$ is for table calibration and structural identification,
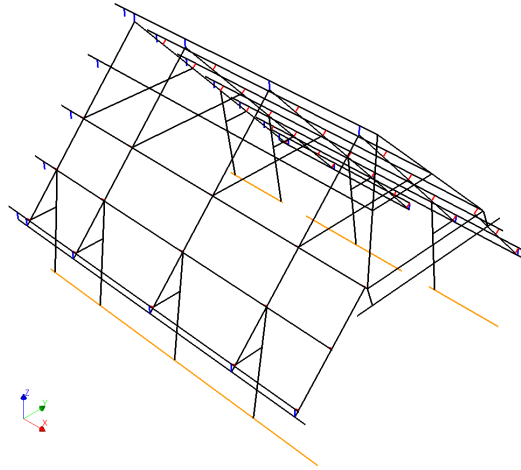
Figure 4.25: FE model of roof structure of the house

Structure components	Masonry wall & floor panel & mass blocks	Roof rafters, struts & floor girders	Other timber beams
Element type	Curved shell element (Q20SH)	Class-III beam element (L12BEA)	Class-I beam element (L12BE)
Integration scheme	$2 \times 2 \times 3$	1-point	2-point
Mesh size		0.1m	
Number of elements	9727	873	666
Total Number of nodes		10631	
Total number of elements		11266	

Table 4.22: List of used element types and mesh properties

Elasticity	Young' modulus $[N/m^2]$	Poisson's ratio	Mass density $[kg/m^3]$
Floor beams	1.1×10^{11}	0.3	450
Floor anchors	2×10^{11}	0.3	7800
Roof beams	1.1×10^{10}	0.3	450
Roof connections	2×10^{10}	0.2	540
First floor	$E_x = 1.1 \times 10^{10}$ $E_y = E_z = 4.5 \times 10^8$ $G_{xy} = 2 \times 10^6$	0.3	540

Table 4.23: List of used linear elastic material properties

so it is not included in the FEA. The characteristics of two earthquake signals are summarized in Table 4.24.

Input	PGA [g]	Waveform name	5 − 75% significant duration [s]
$SC1$	−0.096	00201L	0.39
$SC2$	0.155	01703L	1.73

Table 4.24: Characteristics of selected earthquakes signals

The input earthquake signals for the FE model are obtained from the accelerometers data placed on the shaking table. The accelerations time history of input signals are shown in Figure 4.26. In the later tests, the signals will be scaled to 50%, 150% etc, named as the original signal names plus the scale factor, e.g., $SC2\_400\%$. The acceleration response spectra are provided in the report, as shown in Figure 4.27.

(a) $SC1\_100\%$ (b) $SC2\_100\%$
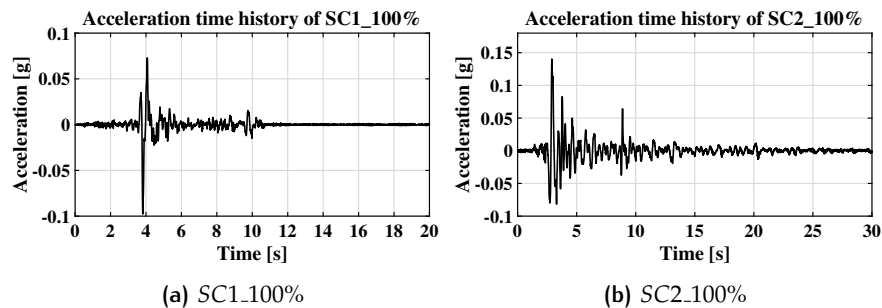
Figure 4.26: Acceleration time history of selected input earthquake signals
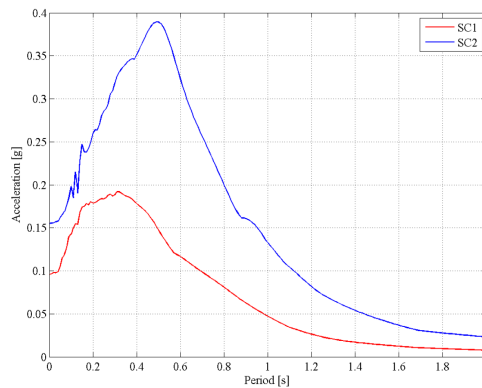
Figure 4.27: Acceleration response spectra comparison (Graziotti et al. [2016])

4.6.5 Preliminary analyses and results

Eigenfrequency analysis

The first preliminary analysis would be the eigenvalue analysis to identify the dynamic characteristics of the structure. The first 5 eigenfrequencies and their corresponding vibration mode shapes are calculated in DIANA FEA 10.3.The results are given in Table 4.25, and the corresponding mode shapes are shown in Figure 4.28.

Mode	Eigenfrequency [Hz]
1	9.5622
2	13.141
3	15.7
4	19.052
5	21.649

Table 4.25: First 5 eigenfrequencies of the model

(a) Mode 1   (b) Mode 2   (c) Mode 3

(d) Mode 4   (e) Mode 5
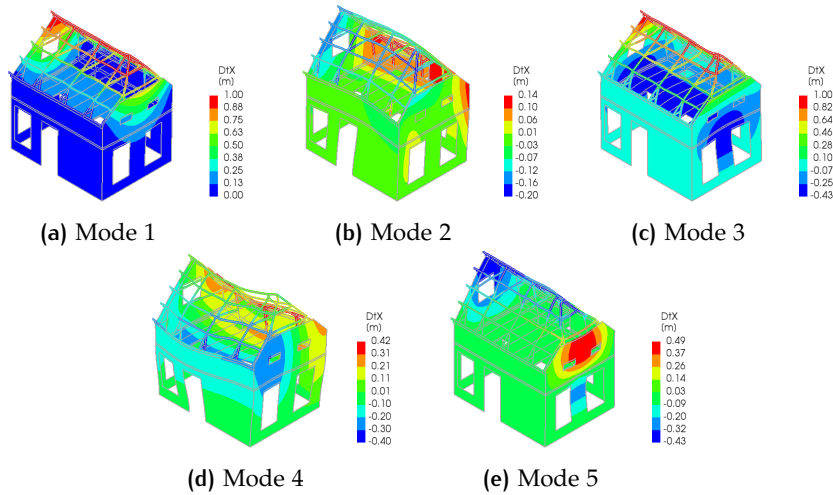
Figure 4.28: Mode shapes of the model

The first egigenfrequency of the undamaged structure is $9.5662Hz$ from numerical analysis, and the experiment report gave the value of $10Hz$. From the mode shape #1, it can be observed that the first mode is governed by the flexible roof structure vibration, and it agrees with the experiment observation, which is shown in Figure 4.29.

(a) First mode shape from numerical result   (b) First mode shape from experiment
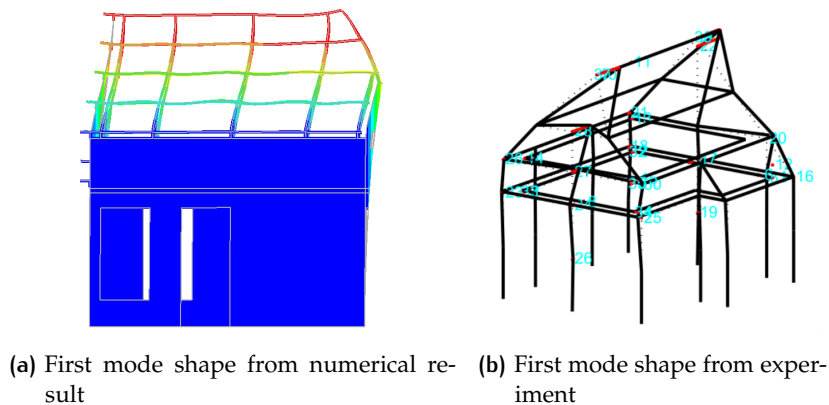
Figure 4.29: Comparison of the first mode shape of the model

The second mode shaped identified from the numerical results is a torsional motion due to irregular plan geometry of the structure. This mode is most likely excited by the seismic input in the east-west direction. Since uniaxial north-south direction seismic signal is the only input signal, this mode is not identified in the experiment.

The third mode of the numerical result was identified during the experiment. In this vibration mode, not only the flexible roof structure, but also the masonry walls, influence the mode shapes. The frequency identified in experiment is $18Hz$ and the numerical result is $15.7Hz$. The difference may come from the fact that the real structure is stiffer than the FE model at the first floor level in the north-south direction due to additional anchors installed on the floor beams. Though, the overall vibration mode, which involves significant deformation of masonry walls of north and south sides, is similar, as shown in Figure 4.30.

(a) Second mode shape from numerical result **(b)** Second mode shape from experiment
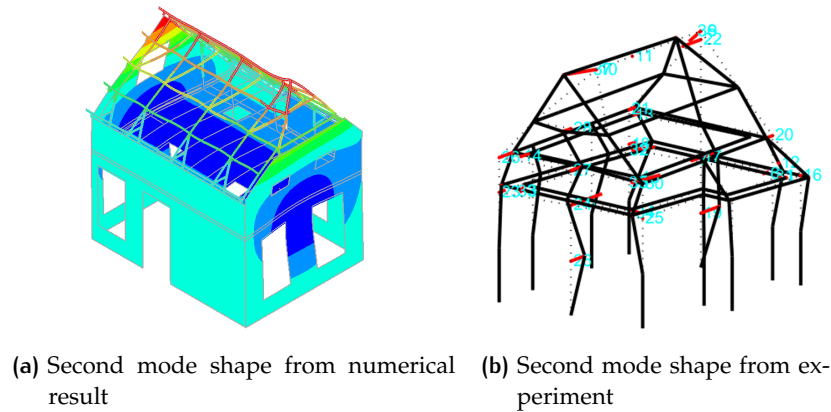
Figure 4.30: Comparison of the second mode shape of the model

Seismic analysis in linear elastic phase

The preliminary seismic analyses using direct time integration methods are performed. The main purposes of these analyses are to have a first sight of the validation of the model as well as the viability of two interested direct time integration methods: implicit Newmark method and explicit central difference method.

For such a complex structure, it is suggested to start with linear elastic material property. According to the experimental results, when the structure subjected to the signal $SC1\_100\%$, no visible crack and obvious nonlinear behavior were observed on the house, hence it can be assume that the house is almost remaining linear elastic. Therefore, all the materials, including masonry, are assumed to be linear elastic, and the signal $SC1\_100\%$ was adopted. The Rayleigh damping was added to the model according to the eigenvalue analysis and the cumulative effective mass method mentioned in Section 4.5.

According to the experimental results, the following results are investigated: the displacement time history of the first floor (East and West sides) and of roof level; the positive and negative displacement envelopes recorded at first floor (East and West sides) and at roof level; the hysteretic response in terms of base shear vs first-floor average displacement. As marked in Figure 4.31, the displacement of East side is obtained by taking average value of nodes #5599 and #5619, and for West side, nodes #7174 and #5678. The roof displacement is obtained from node #10314.

First, the unconditionally stable implicit method is used. Consider the complexity of the structure, the time step is selected to be $0.05s$, and the total analysis time to be $20s$. Slightly numerical damping is included in the Newmark method ($\beta = 0.3025$, $\gamma = 0.6$). The displacement time history of first floor East side is shown in Figure 4.32. The other results of the implicit method are shown in Appendix A.
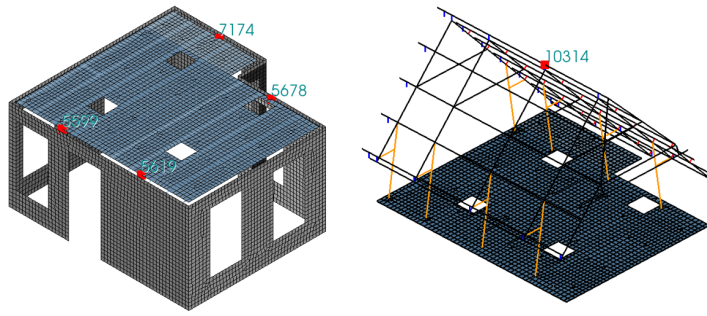
Figure 4.31: Target nodes to obtain interested results
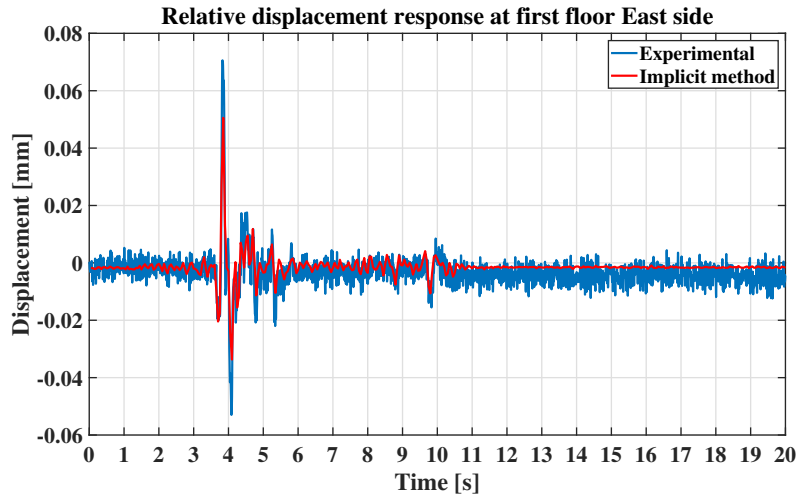
(a) East side

Figure 4.32: Comparisons of displacements time history of the first floor East side

The results comparisons of the preliminary analysis using implicit method show that results from numerical results generally agree with the experimental results. The displacement responses have very similar trends in both results. However, the numerical results have slightly lower peak values for the first floor displacement response on both East and West sides, which can be also observed from the displacement envelope comparison, this is because the linear elastic material properties are assumed for the model while in the experiment nonlinear properties of the material influence the response even without obviously visible crack. This can be proved by the hysteretic curves of base shear versus average first floor displacement results, and it can be observed that much more energy was dissipated due to the nonlinearity in the experimental results than the numerical solution. Therefore, calibrations of the model are still needed, but in general, the comparisons between results from the implicit method solution and the experimental solution verify the validity of the FE model.

Then, the explicit method was adopted for the analysis. However, due to the irregular geometry of the model and also high density meshes, it turns out that $min\{\Delta t_{crit}\}$ is extremely small. Therefore the parameter in the explicit method Δt_{lim} is used to force the time step adopted for the algorithm to become larger. As a result, this will add artificial mass on the model and may change the dynamic property of the model.

Few analyses with different Δt_{ex} were performed. The results of relative displacement response at first floor east side are given in Figure 4.33.
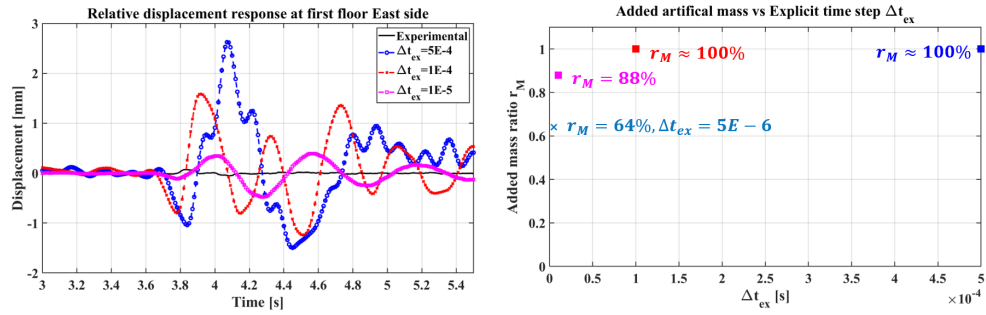
Figure 4.33: Explicit method solution vs Experimental results

It can be observed that the results are unacceptable for explicit method. The displacement is much larger than the experimental results, because the added mass is too large compared to the original model mass. The artificial added mass ratios for different Δt_{ex}, including a extra smaller one 5×10^{-6}, are shown in Figure 4.33. It shows that with decreasing added mass ratio, the solution of explicit method is becoming better and better. However, the smallest explicit time step $\Delta t_{ex} = 5 \times 10^{-6}$ shows that the ratio between artificial mass and total mass of the model is 64%, which is unacceptably large, and the solution of such a time step is either unreasonable. Additionally, to investigate how is the distribution of elements which have added mass with time step $\Delta t_{ex} = 5 \times 10^{-6}$, positions of these elements are checked in FE model, some typical added mass elements are shown in Appendix B.

All of these preliminary analyses results and discussions above turn out the necessity of a simplified model of the house as well as a shorter duration of the load, in order to make explicit method run faster.

4.6.6 Simplified model

The simplifications will change the original properties of the structure. But considering that the implicit method can obtain a reasonable results for the seismic analysis, as well as the main focus of this research is compare the solutions from implicit method and explicit method, the comparisons for the simplified model will be made between the solutions obtained from implicit method and explicit method.

The first simplification is removing the roof structure, because the roof structure provides limited loading capacity to the structure which is subjected to the base acceleration. Also, the roof structure is relatively light-weighted and unimportant to study the nonlinear behavior of the quasi-brittle masonry material.

Then, parts of masonry walls above the first floor level is removed too, because the out-of-plane stiffness of these walls are very low due to the absence of roof structure and the out-of-plane failure of these walls will always occur as one can expect. Moreover, these masonry walls have irregular shapes, removing them is also good for a regular meshing.

Finally, the mesh size is increased to $0.2m$ to speed up the analysis. Particularly, the first floor structure is re-meshed in order to generally increase the mass (in the term of mesh size) of these elements.

The simplified model of the house is shown in Figure 4.34. The other aspects of the model remain unchanged. The nonlinear behavior of the masonry is considered in analyses for the rest of the part of this thesis. A list of element type and number are shown in Table 4.26
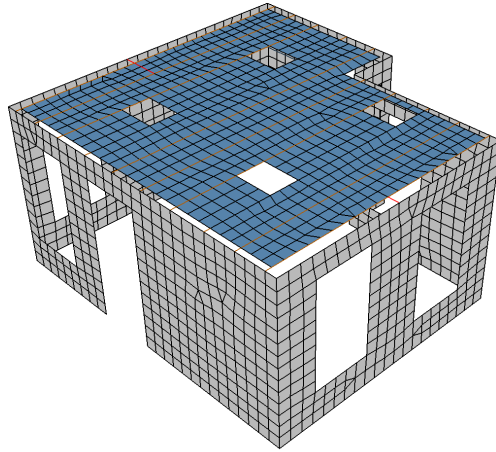
Figure 4.34: Simplified model of the house

Structure components	Masonry wall & floor panel & mass blocks	floor girders	Other timber beams
Element type	Curved shell element (Q20SH)	Class-III beam element (L12BEA)	Class-I beam element (L12BE)
Integration scheme	$2 \times 2 \times 3$	1-point	2-point
Mesh size	0.2m		
Number of elements	2301	379	15
Total Number of nodes	2481		
Total number of elements	2695		

Table 4.26: List of used element types and mesh properties in simplified model

Modified input seismic signal

The input signal is also modified so that the most interested nonlinear behavior of the structure could be activated. According to the report, obvious cracks are observed after the signal $SC2\_400\%$, where the building experienced a substantial level of damage. Hence, the signal $SC2\_400\%$ was adopted in this case. Similar to the Case 4 in Section 4.5, the input acceleration time history was selected to be the interval between $1s - 10s$ of signal $SC2\_400\%$, because the most significant strong acceleration is included in this interval and the rest part of the signal has limited influence on the nonlinear behavior of the structure. Therefore, the input acceleration time history is the same as one in Case 4, as shown in Figure 4.14b.

Analyses schemes

For the simplified model, the eigenfrequency analysis is needed to have a insight view of the dynamic property of the structure. Also, according to the eigefrequency analysis, the Rayleigh damping parameter and the output time interval could be determined. The first natural frequency of the model is 13.4Hz, and the Rayleigh

parameters, according to the cumulative effective mass method, are chosen as $a = 8.1$ and $b = 0$. The output time interval is selected as $0.005s$, which is much smaller than the first natural period of the structure.

Then implicit method with lumped mass and damping matrices and no introduced numerical damping is used to perform the transient analysis with a load duration of $9s$. The analysis scheme using implicit Newmark method is listed in Table 4.27.

Implicit method	Newmark method
Time step Δt_{Im}	$0.005s$
Total steps N_{Im}	1800
Newmark parameter	$\beta = 0.25$, $\gamma = 0.5$
Iteration method	Regular Newton-Raphson method
Convergence norm	Displacement or force
Convergence tolerance	0.01
Maximum iteration number	200
Line search	Yes
Mass Matrix and damping matrix	Lumped

Table 4.27: Transient analyses schemes for implicit Newmark method

The minimum critical time step in the simplified model is $min\{\Delta t_{crit}\} = 1.8485 \times 10^{-6}s$. Since this time step is still pretty small, few analyses with slightly larger explicit time steps Δt_{ex} are performed, and one analysis with this $min\{\Delta t_{crit}\}$ is performed finally. The analyses schemes are given in Table 4.28

Sub-cases	Sub-case 1	Sub-case 2	Sub-case 3	Sub-case 4
$min\{\Delta t_{crit}\}$		$1.8485 \times 10^{-6}s$		
$\Delta t_{lim,i}$	$5 \times 10^{-5}s$	$10^{-5}s$	$5 \times 10^{-6}s$	$10^{-6}s$
Δt_{red}		0.95		
Δt_{ubs}		$10^{-3}s$		
Δt_O		$0.005s$		
$\Delta t_{ex,i}$	$5 \times 10^{-5}s$	$10^{-5}s$	$5 \times 10^{-6}s$	$1.756 \times 10^{-6}s$
$N_{sub,i}$	100	500	1000	2847

Table 4.28: Transient analyses schemes for explicit method

5 | CASES STUDY: RESULTS COMPARISONS AND DISCUSSIONS

5.1 OVERVIEW

In this chapter, the numerical solutions of the transient analyses described in the Chapter 4 for every case are presented. The comparisons between the solution of implicit and explicit method are made. For convenience, a list of the analyses schemes for each case is reviewed again. The comparison for linear cases are mainly in terms of displacement response, and for nonlinear cases additional aspects, such as crack patterns, hysteretic curves, are also considered. Necessary discussions were made to have a better understanding and interpretation of the results. Finally, these results and discussions will form the answers to the research questions proposed at the start of this thesis.

5.2 CASE 1

In Case 1, the mid-span (node #8) deflection of the beam is selected as the interested results, as shown in Figure 5.1. The deflection time history of node #8 will be compared between analytical solution, implicit method solution and explicit solution.
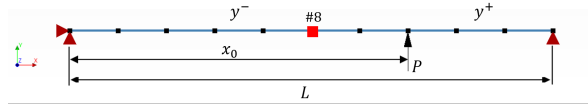
Figure 5.1: The interested point (node #8) on the simply-supported beam

5.2.1 Analytical solution

The reference solution of the steady-state response of the beam is obtained by solving the classical governing equation of the beam.

The equation of the motion of the beam is:

$$\rho A \frac{\partial^2 y}{\partial t^2} + EI \frac{\partial^4 y}{\partial t^4} = 0 \tag{5.1}$$

The boundary conditions are:

$$
\begin{aligned}
x = 0: \quad & y^- = \partial^2 y^- / \partial x^2 = 0 \\
x = L: \quad & y^+ = \partial^2 y^+ / \partial x^2 = 0
\end{aligned} \tag{5.2}
$$

The interface conditions are:

$$
\begin{aligned}
x = x_0: \quad & y^- = y^+ \\
& \partial y^- / \partial x = \partial y^+ / \partial x \\
& \partial^2 y^- / \partial x^2 = \partial^2 y^+ / \partial x^2 \\
& EI(\partial^3 y^+ / \partial x^3 - \partial^3 y^- / \partial x^3) = P sin(\Omega t)
\end{aligned} \tag{5.3}
$$

The steady-state solution is assumed to be:

$$y(x,t) = Y(x)sin(\Omega t) \tag{5.4}$$

By substituting the assumed solution into governing equations, we can get the general solution in the frequency domain as:

$$Y^-(x) = A^- cosh(\beta x) + B^- sinh(\beta x) + C^- cos(\beta x) + D^- sin(\beta x)$$
$$Y^+(x) = A^+ cosh(\beta x) + B^+ sinh(\beta x) + C^+ cos(\beta x) + D^+ sin(\beta x) \tag{5.5}$$

where β is defined as $\beta^4 = \dfrac{\rho A}{EI}\Omega^2$.

Equation 5.5 has 8 unknowns, by substituting these general solution into 4 boundary conditions and 4 interface conditions, they can be solved. Then, according to the equation 5.4, the analytical solution $y(x,t)$ can be obtained for any location on the beam at any time. The Figure 5.2 shows the steady-state response of mid-span of the beam in 1 seconds duration.
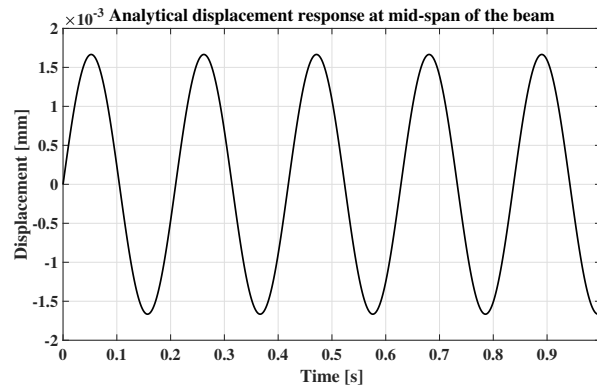
Figure 5.2: The analytical solution for mid-span deflection time history

5.2.2 Numerical solutions

Review of analyses schemes

Analyses	Damping	Δt_O [s]	$min\{\Delta t_{crit}\}$ [s]	Δt_{ex} [s]
Implicit	No	0.001	—	—
Explicit Sub-case 1	No	0.001	1.50756×10^{-5}	1.43218×10^{-5}
Explicit Sub-case 2	No	0.001	1.50756×10^{-5}	10^{-5}

Table 5.1: Review of transient analysis scheme for Case 1

Solutions

First, a simple eigenfrequency analysis was performed to identify the natural frequency of the beam. The result turns out the first natural frequency is $49.69Hz$.

The implicit method solution at mid-span (node #8) according to the analysis scheme in Table 4.3 is plotted in Figure 5.3a. The explicit method solutions according to analysis scheme Table 4.4, which include two sub-cases, are plotted in Figure 5.3b.

(a) The implicit method solution

(b) Two explicit sub-cases' solutions
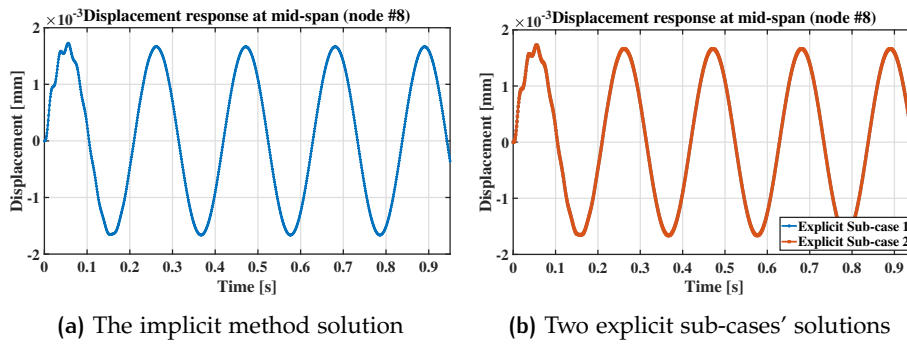
Figure 5.3: Numerical solutions for mid-span deflection time history

5.2.3 Comparison of the solutions

Since it has been observed that the two explicit sub-cases have exactly the same result, the sub-case 1 which uses the minimum critical time step was used for the following comparisons. The three solutions obtained from different methods are compared together with zooming in different time history intervals, as shown in Figure 5.4.

(a) Time interval $0 - 0.2s$

(b) Time interval $0.6 - 0.9s$
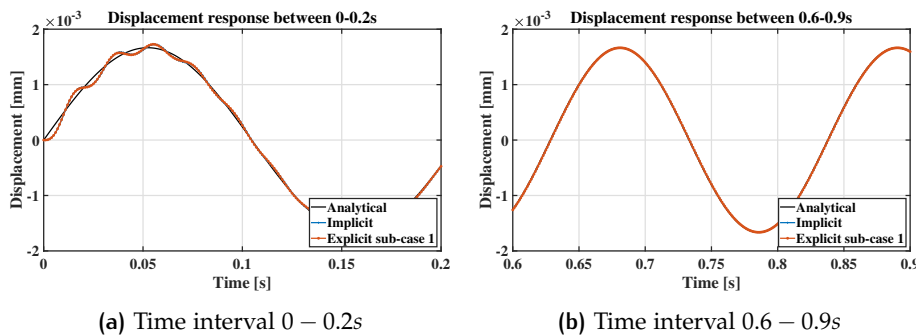
Figure 5.4: Comparison of the solutions in different time intervals

It can be observe that both direct time integration methods accurately reproduce the steady-state displacement response at the mid-span in a short time after the load was applied. In the time interval $0 - 0.2s$ slight differences are observed in numerical solutions. This is the first vibration mode of the beam, corresponding to the first natural frequency $49.96Hz$. Since the steady-state response needs time to reach, the transient effect shows up at the beginning of the analysis. In the time interval $0.6 - 0.9s$, three solutions are fully overlapped due to the damping effect.

Moreover, the same results of two explicit method sub-cases shows that once the stability condition is reached in the linear elastic system, which means the $min\{\Delta t_{crit}\}$ is used for the explicit algorithm, the explicit method could accurately generate the displacement response of the structure, the further decrement for the explicit time step is not necessary.

5.3 CASE 2

In Case 2 (Section 4.3), the mid-span (node #1) is selected for the results comparison. The node #1 is the node on which the transient load was applied, as shown in Figure 5.5. Three different time steps are used to generate the output of the displacement response of the node #1, which are $25\mu s$, $50\mu s$ and $100\mu s$. The analyses schemes are described in Table 4.7 and Table 4.8. The reference solutions are

calculated in ABAQUS using implicit solver with slight numerical damping. The comparison of each case is made in the following section.
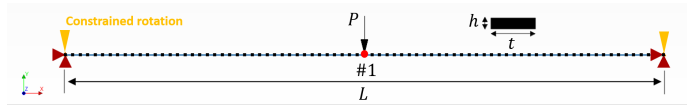
Figure 5.5: The interested point (node #1) in FE model

Review of analyses schemes

Analyses	Damping	Δt_O [μs]	$min\{\Delta t_{crit}\}$ [s]	Δt_{ex} [s]
Implicit Sub-case 1	No	25	—	—
Implicit Sub-case 2	No	50	—	—
Implicit Sub-case 3	No	100	—	—
Explicit Sub-case 1	No	25	7.21291×10^{-7}	6.85226×10^{-7}
Explicit Sub-case 2	No	50	7.21291×10^{-7}	6.85226×10^{-7}
Explicit Sub-case 3	No	100	7.21291×10^{-7}	6.85226×10^{-7}

Table 5.2: Review of transient analysis scheme for Case 2

5.3.1 Sub–case 1: solutions of time step $25\mu s$

The solutions of sub-case 1 from different methods with using output time step of $25\mu s$ are given in Figure 5.6.
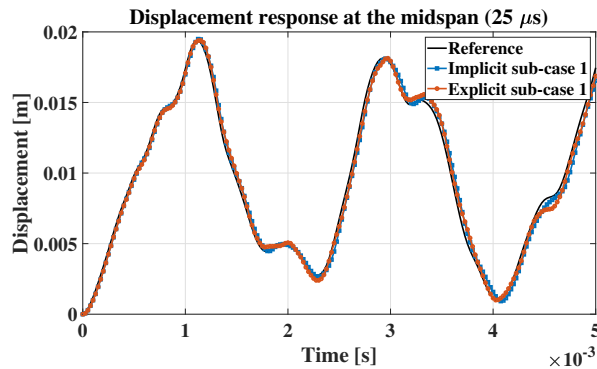
Figure 5.6: The displacement response at node #1 with time step $25\mu s$

With output time step $25\mu s$, the solution are accurately generated in all methods, the results are quite close to each other and no obvious difference is observed.

5.3.2 Sub–case 2: solutions of time step $50\mu s$

A larger output time step is used in sub-case 2, which is $50\mu s$. The comparison of solutions are shown in Figure 5.7 The results are still match each other in general, but
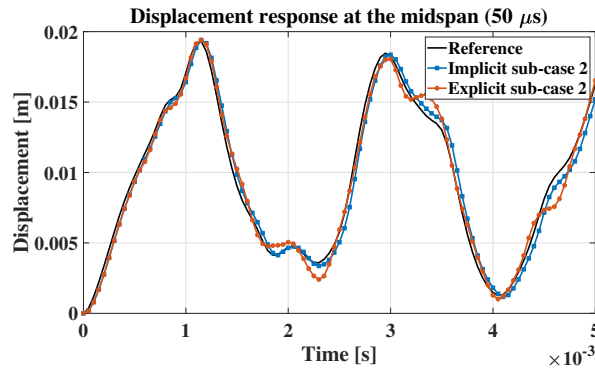
Figure 5.7: The displacement response at node #1 with time step $50\mu s$

slight difference starts to show up in the comparison. A larger amplitude of high frequency component is contained in the explicit solution. The implicit and reference solution are more closer to each other. However, since the reference solution is also calculated by implicit method, this can be expected to happen.

5.3.3 Sub-case 3: solutions of time step $100\mu s$

A much larger time step of $100\mu s$ is used for sub-case 3. The results are shown in Figure 5.8. Even with much coarser resolution of the solution, the explicit solution
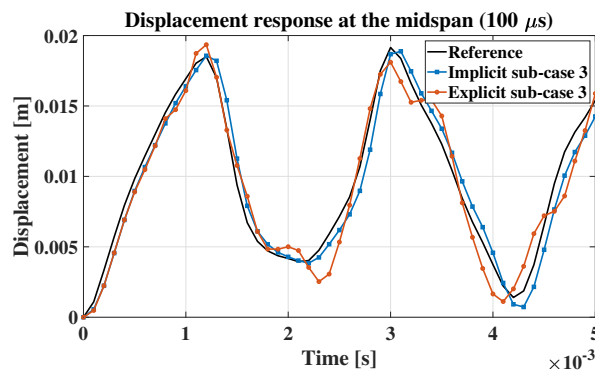
Figure 5.8: The displacement response at node #1 with time step $100\mu s$

still remains the information about high frequency components. However, in the implicit solutions, these information has been mainly lost.

5.3.4 Comparisons of solution from different time steps

The comparison between three implicit sub-cases are given in Figure 5.9a, and similar comparison is made for three explicit sub-cases, shown in Figure 5.9b.
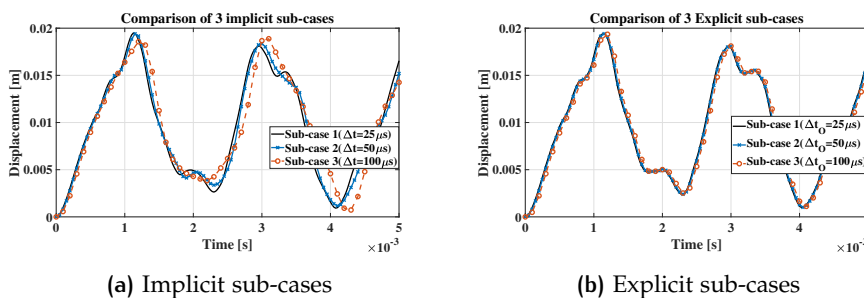
(a) Implicit sub-cases

(b) Explicit sub-cases

Figure 5.9: Comparisons of solutions from different time steps

It can be observed that the time step has very significant influence on the implicit method solutions. The amplitude of the displacement response as well as the high frequency components are changing due to the changes of the time step. The larger time step used, the less of high frequency components are reproduced. This is because the time step for implicit method is too large to capture the high frequency wave traveling through the nodes, so the information is lost. Though, the implicit method is unconditionally stable, the accuracy will be lost due to the large time step.

While in the explicit method solution, almost no difference could be observed in three sub-cases. This is because the explicit algorithm actually calculates the solution at the $min\{\Delta t_{crit}\} = 7.21291 \times 10^{-7}s$, which is determined to be able to represent the highest frequency wave traveling through the element nodes, according to the CFL stability condition. So, even with different output time step Δt_O, the accurate response is always calculated, the only influence of Δt_O is the resolution of the solution. Once the resolution is good enough to show the high frequency vibration modes, the results could be considered to be accurate.

5.4 CASE 3

The Case 3 investigates the response of simply-supported thin plate to out-of-plane transient distributed force, as described in Section 4.4. The reference solution is given at the middle point (node #1) of the plate in Maguire et al. [1993], as shown in Figure 5.10. The numerical solution of peak displacement in out-of-plane direction, peak stress and their corresponding time points will be compared with the reference solution in Maguire et al. [1993]. The analyses schemes are described in Table 4.10 and Table 4.11.
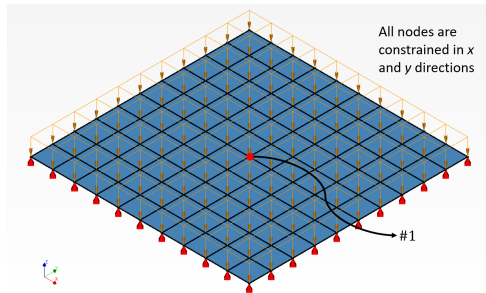
Figure 5.10: The interested point (node #1) in FE model

Review of analyses schemes

Analyses	Damping	Δt_O [s]	$min\{\Delta t_{crit}\}$ [s]	Δt_{ex} [s]
Implicit Sub-case 1	Rayleigh Damping	0.01	—	—
Implicit Sub-case 2	Rayleigh Damping	0.002	—	—
Explicit Sub-case 1	Rayleigh Damping	0.01	1.4597×10^{-4}	1.38672×10^{-4}
Explicit Sub-case 2	Rayleigh Damping	0.002	1.4597×10^{-4}	1.38672×10^{-4}

Table 5.3: Review of transient analysis scheme for Case 3

5.4.1 Eigenfrequencies

The first eight eigenfrequencies and the corresponding mode shapes are identified for the FE model, as shown in Figure 5.11. The comparison of the identified eigenfrequencies and reference values are listed in Table 5.4. The results show good agreement with the reference solution.

(a) Mode 1, 2.4026Hz (b) Mode 2 & 3, 6.1853Hz (c) Mode 4, 9.9345Hz

(d) Mode 5 & 6, 13.160Hz (e) Mode 7 & 8, 16.849Hz
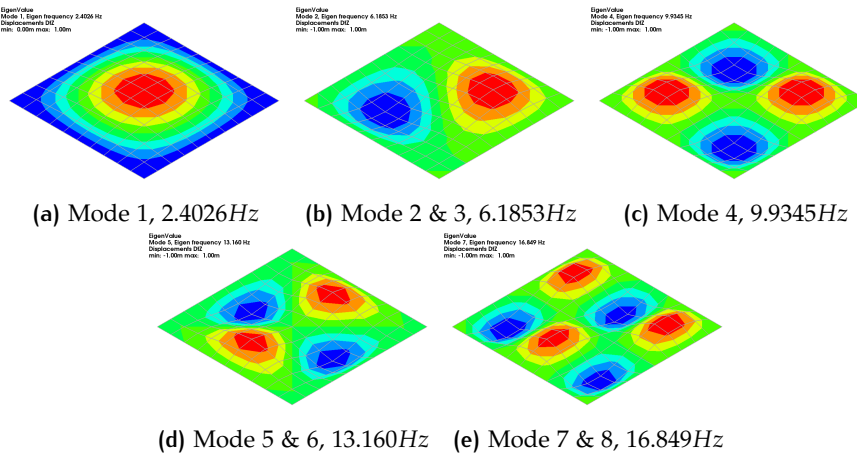
Figure 5.11: First eight eigenfrequencies and the corresponding mode shapes

Eigenfrequencies	Reference [Hz]	Identified [Hz]
f_1	2.398	2.4026
f_2 & f_3	6.1195	6.1853
f_4	9.89	9.9345
f_5 & f_6	12.845	13.160
f_7 & f_8	16.582	16.849

Table 5.4: Identified eigenfrequencies vs reference values

According to the eigenfrequencies of the model, two output time steps which are 0.01s and 0.002s, the first one guarantees the first mode will be generated accurately and the second one provides the possibility for up to eighth mode.

5.4.2 Displacement time history in out–of–plane direction

The solution of displacement time history of node #1 in out-of-plane direction from implicit method is shown in Figure 5.12a and from explicit method is shown in Figure 5.12b. Almost no difference could be observed in implicit sub-cases, neither in explicit sub-cases. The displacement response could be calculated accurately in both methods.

5.4.3 Stress σ_{xx} time history

The solution of displacement time history of node #1 in out-of-plane direction from implicit method is shown in Figure 5.12a and Figure 5.12b show the stress σ_{xx} time history solution at node #1 calculated by implicit and explicit method respectively.

In the stress results, differences are observed between implicit sub-cases, the solution from different time steps show different high frequency contents. This may imply that high vibration mode ares excited even though it doesn't clearly show

(a) Implicit sub-cases

(b) Explicit sub-cases
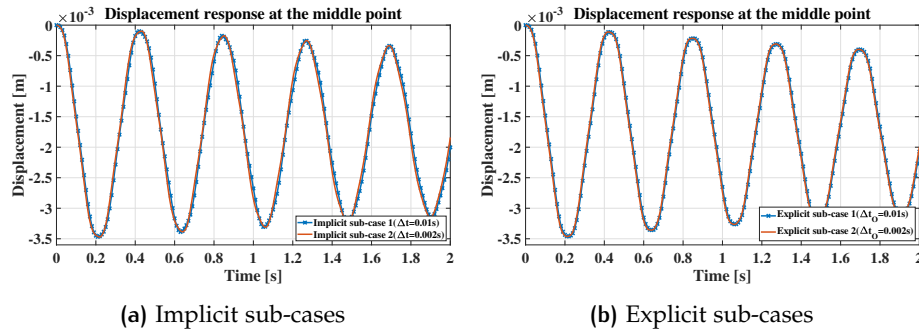
Figure 5.12: Comparisons of displacement time history of node #1 in out-of-plane direction

(a) Implicit sub-cases

(b) Explicit sub-cases
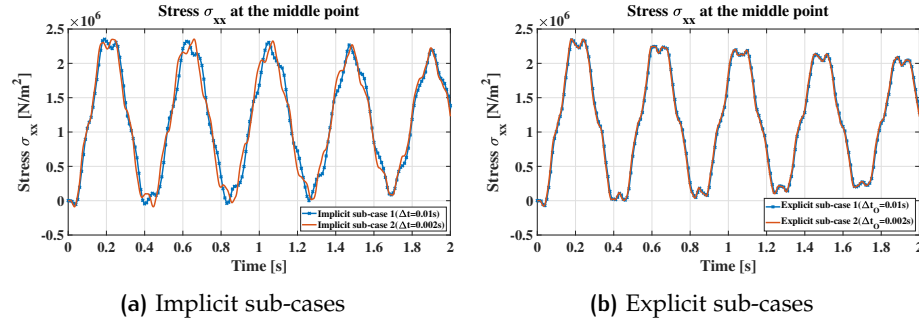
Figure 5.13: Comparisons of stress σ_{xx} time history of node #1

in the displacement response. While, the explicit sub-cases have exactly the same stress time history, but still, higher vibration mode is observed which isn't reproduced in displacement response.

5.4.4 Comparisons and discussions

The peak displacement and peak stress values in implicit and explicit solutions are compared with the reference solution, as well as the corresponding time points. The results are given in Table 5.5.

	Peak displacement		Peak stress
	δ_p (mm)	t_p (s)	σ_{xx} (N/mm^2)
Reference solution	3.507	0.216	2.484
Implicit solution	3.472	0.218	2.353
Explicit solution	3.463	0.210	2.355

Table 5.5: Comparison of peak response

The numerical solutions show good agreement with the reference solution. The difference between the peak displacements is smaller than 1.5%, and the time points for peak values are also very close. The peak stress has about 5% deviation, it may cause from the influence of high frequency vibration mode in the numerical solutions, but they are still very close to each other.

To investigate the difference in the stress σ_{xx} time history, the implicit solutions and explicit solution are plotted together in Figure 5.14. In addition, the Fast Fourier Transform (FFT) of the σ_{xx} time history is calculated and plotted in Figure 5.15.
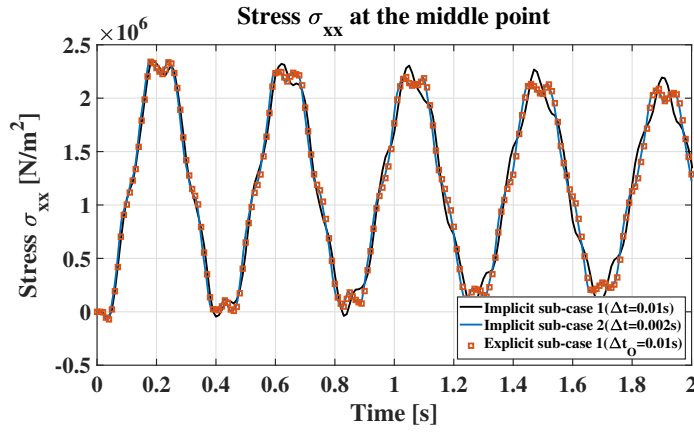
Figure 5.14: Comparison between implicit and explicit solutions of σ_{xx}
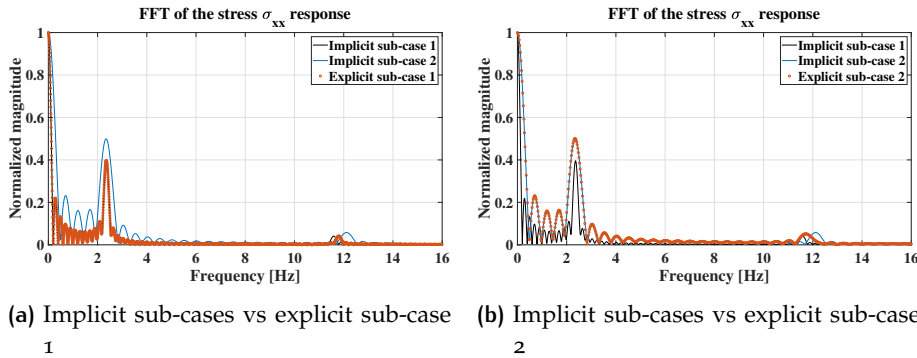
(a) Implicit sub-cases vs explicit sub-case 1

(b) Implicit sub-cases vs explicit sub-case 2

Figure 5.15: Comparisons of FFT of stress σ_{xx} time history

Figure 5.14 shows that the explicit solution has very close results to implicit sub-case 2, which has the smaller time step than implicit sub-case 1. Though, the explicit has a lower resolution of the solution, which is $\Delta t_O = 0.01s$, compared to the implicit sub-case 2 with $\Delta t = 0.002s$, it still contains accurate high frequency information, which is better than the implicit sub-case 1.

The comparisons of FFT show that the dominant frequency component in the stress time history is $2.333Hz$, which is corresponding with the first natural free vibration frequency $2.398Hz$, the difference is come from the Rayleigh damping included in the model. The different amplitudes at this frequency come from the different resolutions of the signals, as a result lower resolution of the signal has more leakage in the Fourier spectrum. It can be proved in Figure 5.15a and Figure 5.15b, the amplitudes of the first peak of explicit solutions are the same with the corresponding resolution of implicit solution, in this case, the output time step.

However, another important peak value occurs at around $11.5Hz$ to $12.5Hz$, which is corresponding to the 5th and 6th vibration modes, again, the value is reduced due to damping. The implicit sub-case 1 has peak value at $11.59Hz$, the implicit sub-case 2 at $12.12Hz$, the explicit cases at $11.71Hz$. This is the reason why different high frequency vibrations occurred in stress response time history. It turns out that with smaller time step, the implicit method could generate high frequency vibration more accurately, while the explicit is not influenced by that. The larger time step in implicit method tends to make this frequency shift towards left, i.e. smaller, which will lead to inaccurate representation of high frequency mode vibration.

The reason why only first and $5th$ (or $6th$) modes are excited is that transient distributed load is applied on the all plate surface, so the symmetric modes are more easily to be activated. However, since the energy contained in the high frequency mode is so low, it is hard to observe it in displacement response.

5.5 CASE 4

The results of the Case 4 (Section 4.5) will be presented in two parts, the first part is the in-plane shear-compression quasi-static analysis results and the second part is the in-plane seismic analysis results. The in-plane quasi-static analysis aims to validate the material parameters in the FE model and study the nonlinear behavior of the masonry wall. The seismic analysis will take into account the transient effect of seismic loading and investigate the performance of implicit and explicit method for nonlinear quasi-brittle material.

5.5.1 In-plane shear–compression test

As described in Section 4.5.2 and Figure 4.9, the wall is subjected to prescribed displacement applied at the top edge. Since the typing is used in the model, the prescribed displacement is directly applied at the master nodes, as a result, the base shear force could be obtained either from reaction forces of nodes at bottom edges or from the virtual support reaction force at the master node.

The in-plane tests include a monotonic pushover analysis with eigenfrequency check and a cyclic pushover analysis. The results of capacity curves and hysteresis curves are generated and compared to the experimental results. Also, the nonlinear behavior of the model and its influence on the eigenfrequency are also discussed.

Monotonic pushover results

As shown in Table 4.16, a prescribed horizontal displacement of 34.2*mm* was applied at the master node on the model. The capacity curve in terms of displacement versus base shear force is plotted in Figure 5.16a, and the first eigenfrequency evolution during the monotonic pushover process is plotted in Figure 5.16b.

(a) Capacity curve   (b) First eigenfrequency evolution
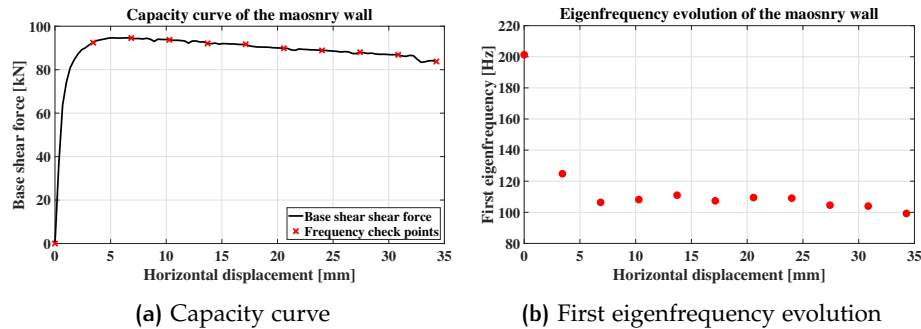
Figure 5.16: Monotonic pushover results

The maximum shear capacity in numerical results is 94.67*kN*, which is quite close to the reference value obtained from cyclic pushover test 92.52*kN* in positive direction and 92.55*kN* in negative direction. Moreover, the softening behavior is also shown in the capacity curve due to the crack in the model. Hence, the stiffness of the material is reduced and the natural frequency of the structure as well as the element is decreased, as proved in the first frequency evolution result. The first natural frequency drops from 201.3*Hz* to around 99.27*Hz* at the end. Few figures of the crack width evolution during the pushover procedure together with the corresponding first natural frequency are shown in Figure 5.17 to illustrate this softening behavior.
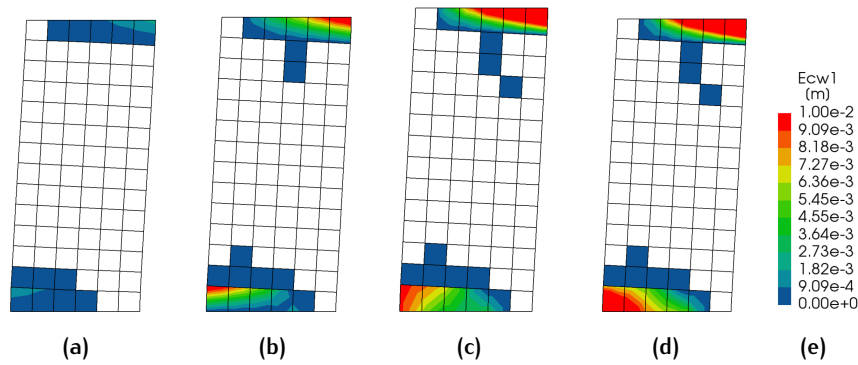
Figure 5.17: Crack evolution with corresponding top displacement Dx and frequency f: (a) $Dx = 3.428mm$, $f = 124.8Hz$; (b) $Dx = 13.712mm$, $f = 111Hz$; (c) $Dx = 27.424mm$, $f = 104.6Hz$; (d) $Dx = 34.28mm$, $f = 99.27Hz$ (e) The legend.

Cyclic pushover results

The cyclic pushover analysis scheme is given in Table 4.17. The hysteresis curve of horizontal displacement versus base shear force are plotted in Figure 5.18 with comparing to the experimental result.
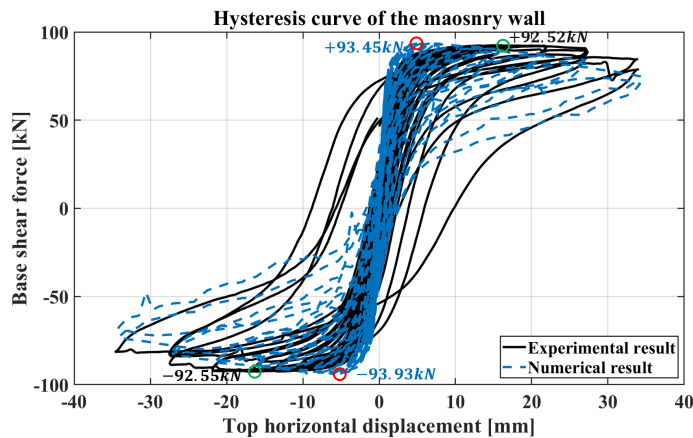
Figure 5.18: The hysteresis curve of masonry wall

The numerical results have a good agreement with the experimental results. The initial stiffness is almost the same. The maximum loading capacity in positive and negative direction of numerical results are $+93.45kN$ and $-93.93kN$, which are slightly higher than experimental results of $+92.52kN$ and $-92.55kN$, the difference is around 1%. The decrease of the capacity with increasing cycles and the unloading-reloading curve of the numerical results match the experimental results very well. However, the stiffness at the end of the loading shows some differences, it might be caused by the fact the wall in the experimental test are exhibits intensive toe crushing at the base in the end of loading cycles, so that the structure is unable to carry load anymore. This failure of the wall can be observed from the curves of last three cycles in the experimental results. Most of the energy is dissipated in these three cycles as well.

The masonry wall model first cracked at the bottom edge and the bricks below the wall-top beam. At this point, the pier has a pure rocking behavior, until the first diagonal cracks appear above the base. Then the specimen exhibits intensive toe crushing mechanism at the base. After that, diagonal crack appears in the top half of the pier, rendering the wall is unable to carry vertical load anymore. The failure mode is a hybrid failure mode, which means the rocking mechanism and

toe crushing first happened and after the maximum flexural capacity of the pier reached, then shear failure occurs. In general, this crack evolution and the failure mode are shared between test results and numerical results. Few illustrations of the crack width evolution are shown in Figure 5.19.

(a) $+1mm$ (b) $-1.44mm$ (c) $+4mm$ (d) $-5mm$

(e) $+6.5mm$ (f) $-8mm$ (g) $+13.5mm$ (h) $-27mm$

(i) $+34.2mm$ (j) $-34.2mm$ (k)

Ecw1
(m)
1.00e-3
9.09e-4
8.18e-4
7.27e-4
6.36e-4
5.45e-4
4.55e-4
3.64e-4
2.73e-4
1.82e-4
9.09e-5
0.00e+0
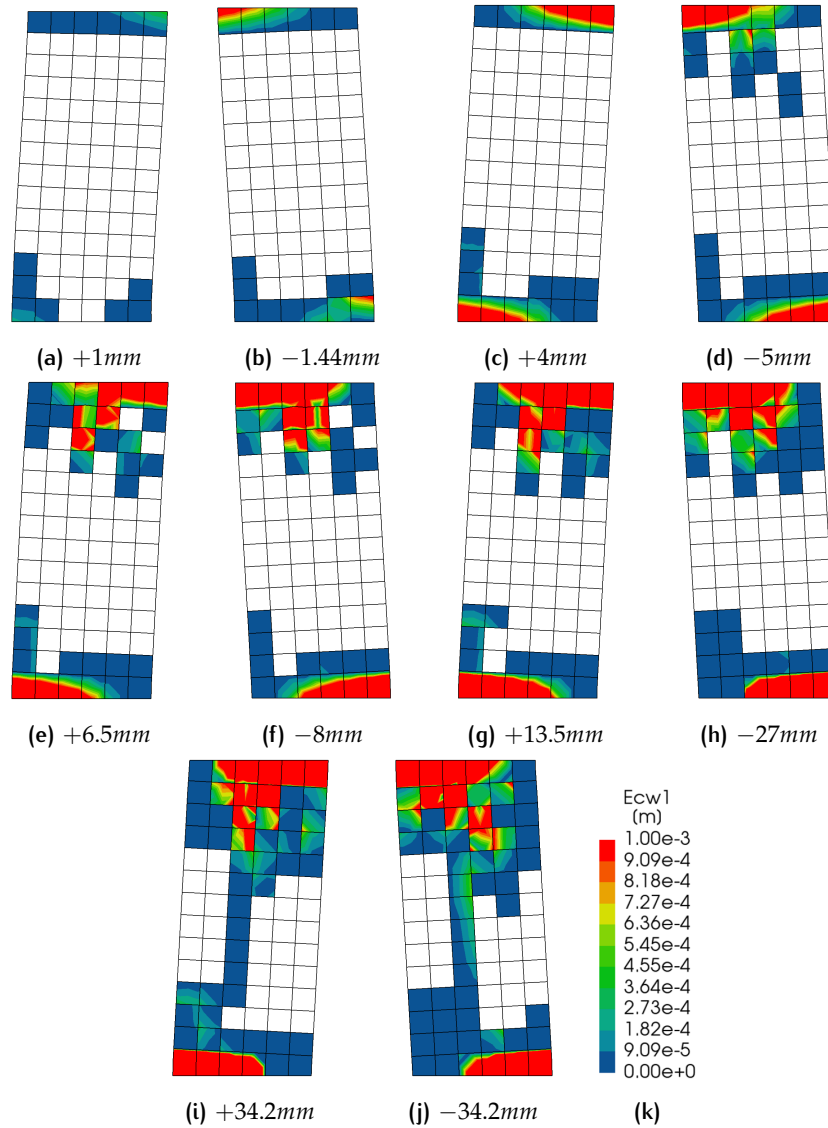
Figure 5.19: Crack width evolution with corresponding top displacement

5.5.2 In-plane seismic analysis

The Section 4.5.3 has given the detailed information about the modified FE model, seismic input signal and the analyses schemes. The node #2 are selected to show the results comparisons for this model, as shown in Figure 5.20.
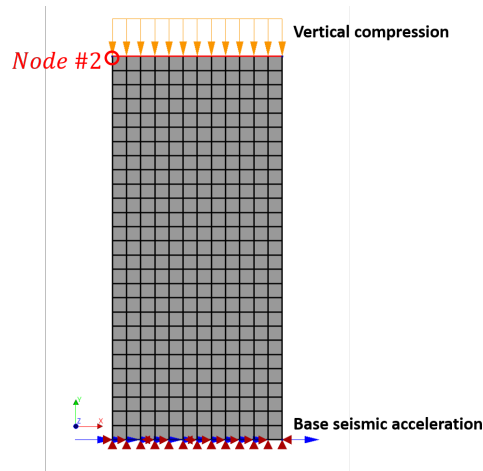
Figure 5.20: The interested node #2 on the modified FE model for seismic analysis

Review of analyses schemes

Analyses	Damping	Δt_O [s]	$min\{\Delta t_{crit}\}$ [s]	Δt_{ex} [s]
Implicit	Rayleigh Damping	0.005	—	—
Explicit Sub-case 1	Rayleigh Damping	0.005	4.50268×10^{-5}	4.27754×10^{-5}
Explicit Sub-case 2	Rayleigh Damping	0.005	4.50268×10^{-5}	5×10^{-6}

Table 5.6: Review of transient analysis scheme for Case 4

Eigenfrequency analysis

The eigenfrequencies and mode shapes are first identified for the mode. Since the double-fixed boundary condition was changed to free at top edge with a high density steel beam, the eigenfrequency was reduced a lot compared to the model in quasi-static analysis. The mode shapes and the corresponding eigenfrequencies related to the vibration in seismic excitation's direction are presented in Figure 5.21.

Compared with the Fourier spectrum of the input seismic signal (Figure 4.15), in which most of the energy was contained by the frequency components below $12Hz$, it can be predicted that the response of the structure to this seismic input will be governed by the first vibration mode.

Displacement responses of node #2

The transient analysis scheme using implicit method was performed according to Table 4.19, and explicit method according to Table 4.20. The relative displacement time history of node #2 with respect to the base is plotted in Figure 5.22a and Figure 5.22b.

(a) $10.707Hz$　　　　　**(b)** $85.240Hz$　　　　　**(c)** $217.050Hz$
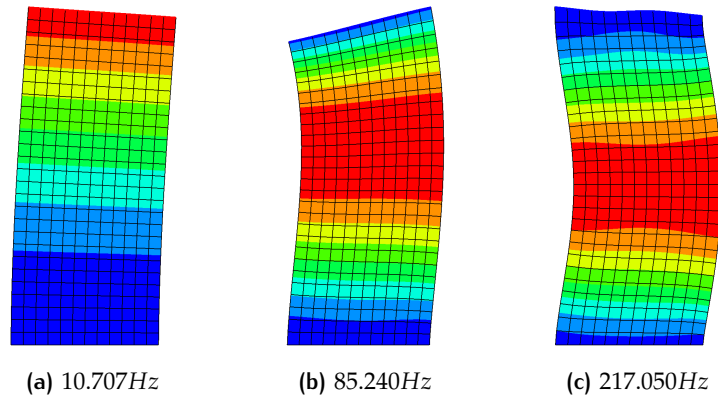
Figure 5.21: Eigenfrequencies and mode shapes

(a) Implicit method solution　　　　　**(b)** Explicit method solutions
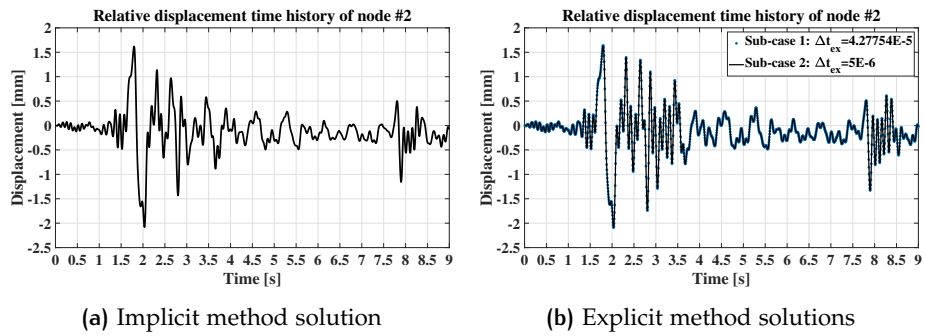
Figure 5.22: Relative displacement time history of node #2 with respect to the base

Both methods produced reasonable displacement response. Two explicit sub-cases with different explicit time step Δt_{ex} provide the same solution again, because they are both equal or smaller than the $min\{\Delta t_{crit}\}$, in another word, satisfy the CFL stability condition. Differences could be observed in the results. The comparison and discussion will be made later with referring to other aspects of the results.

Eigenfrequency evolution in seismic analysis

The first eigenfrequency of the masonry wall was checked every $0.5s$ through the seismic analysis. Evolution of the first eigenfrequency is plotted in Figure 5.23, together with the relative displacement of node #2 at every time point.
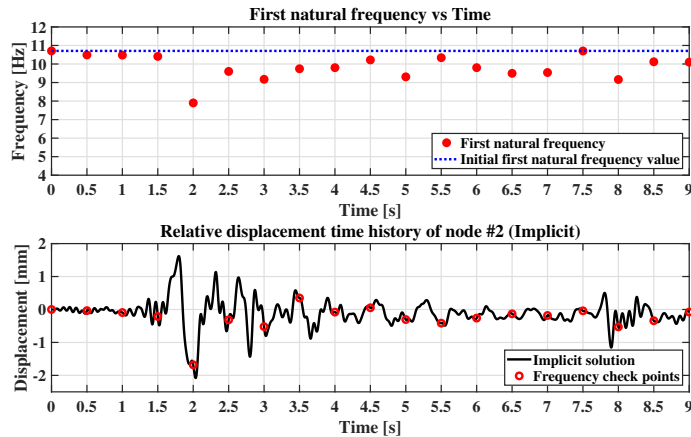
Figure 5.23: Evolution of the first eigenfrequency of the structure and relative displacements of node #2 at corresponding time points

The results show that the first natural frequency didn't surpass the value when structure is in linear elastic phase. The values of the first natural frequencies during the seismic analysis is calculated of the current deformation or crack state of the material, which means at the moment when all cracks are closed, the natural frequency reaches the value of linear elastic phase, and when cracks open again the material has softer stiffness and frequency decreases. Therefore, it can conclude that for material has softening behavior, the critical time step for explicit method determined based on the linear elastic phase is always safe and satisfy the CFL stability conditions.

Hysteresis curve of base shear force versus relative displacement of node #2

The base shear force are calculated by summing up the nodal reaction force at the base edge of the model. The hysteresis curves of base shear force versus relative displacement of node #2 are plotted in Figure 5.24.

(a) Implicit method solution　　　　(b) Explicit method solutions
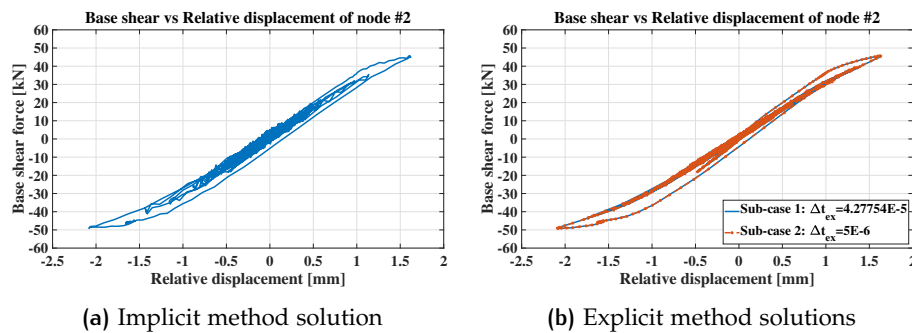
Figure 5.24: Hysteresis curve of base shear force versus relative displacement of node #2

The hysteresis curves from both methods have good agreement with each other on maximum shear force, energy dissipation and reloading-unloading behaviors. The explicit sub-cases show the same results again. However, the explicit solutions show much smoother than the implicit solution, in which slightly chaos values occur after the largest hysteresis loop. This implies that it is hard for implicit method to reach convergence criterion after the strong peak of the seismic signal.

5.5.3　Comparisons and discussions

Since the explicit sub-cases get the same solution, therefore the sub-case 1 is used for the following comparisons.

First, the comparison of displacement obtained from implicit method and explicit method are plotted together inFigure 5.25. Based on comparison, two time intervals are zoomed in to show better views of the differences in response, plotted in Figure 5.26a and Figure 5.26b. Fast Fourier Transform (FFT) is also applied on both solutions, as shown in Figure 5.26c.
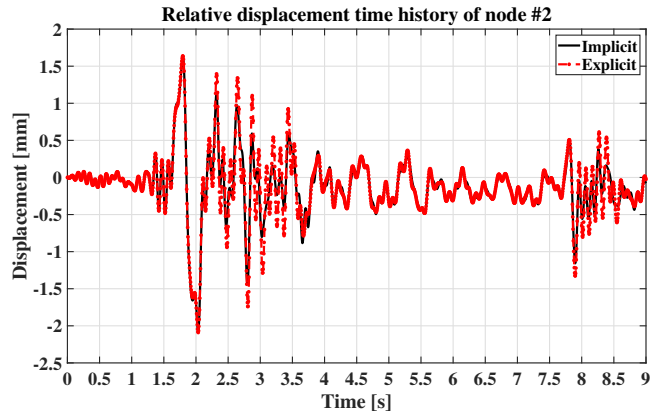
Figure 5.25: Comparisons between implicit and explicit method solutions of relative displacement time history of node #2
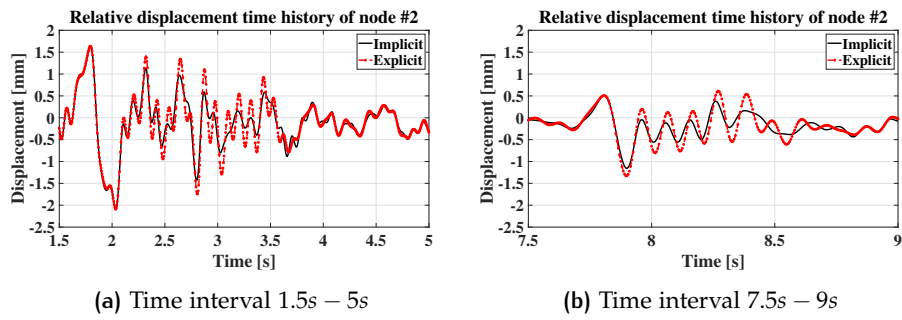
(a) Time interval $1.5s - 5s$

(b) Time interval $7.5s - 9s$
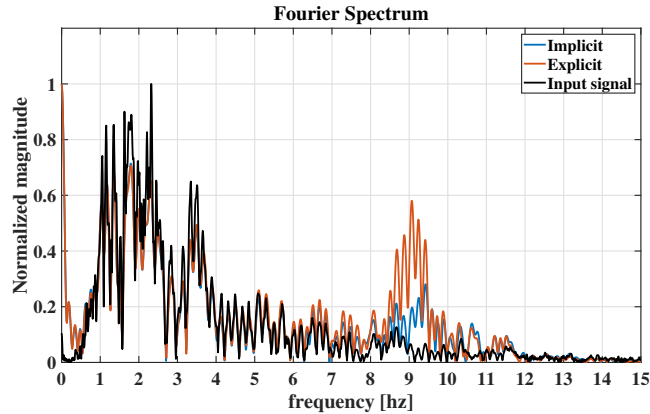
(c) Fourier spectra

Figure 5.26: Differences in displacement responses and Fourier spectra

The differences show after the peak displacement response, the explicit solution shows larger amplitude vibration after the peak response than the implicit solution, this can be observed either in time interval of $1.5s - 5s$ or $7.5s - 9s$. Then, the amplitude difference gradually disappears if no other peak arrives. This implies that more energy was dissipated in implicit method solution for the strong base acceleration than the explicit solution. This can be proved in the Fourier spectra of the response. Compared with the spectra with the input seismic signal, both solutions include the same dominant frequencies contents of the input signal, which is between $1 - 4Hz$. Moreover, the responses also have the first natural frequency content at around $9.5Hz$, the value is slightly smaller because the damping is introduced. That means the first natural mode was activated by the seismic signal, however, the explicit spectrum has mush larger magnitudes around the first natural frequency than implicit spectrum. So, in total, the energy contained in explicit

spectrum is larger, because the implicit dissipated more energy due to the nonlinear behavior of the model.

To have a insight view of the nonlinear behavior in the seismic response, few figures about crack pattern, which is indicated by the state parameter $NCRACK = 1$ (in this case red color), at different time point during the time interval $1.5s - 2.5s$ are presented in Figure 5.27.
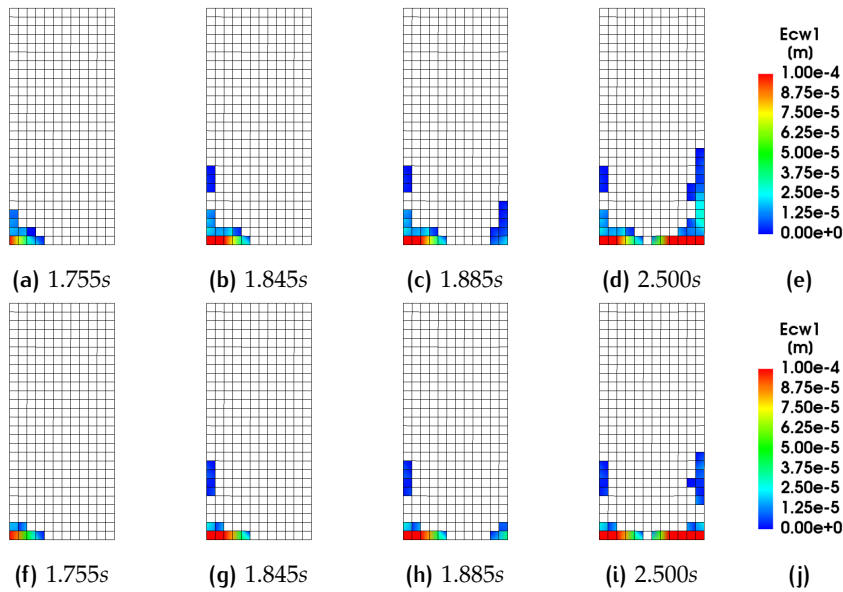
Figure 5.27: Crack patterns development during $1.5s - 2.5s$: (a)-(d) implicit solutions; (e)-(h) explicit solutions

It can be observed that the implicit solution has more cracks occur than explicit solution during the strong peak acceleration of the seismic signal, therefore, more energy is dissipated through these cracks for implicit solution.

The comparison of the hysteresis curves plotted in Figure 5.28 also show this difference in energy dissipation. Though, the difference are not obvious, but still it corresponds to the nonlinear behavior of the model.
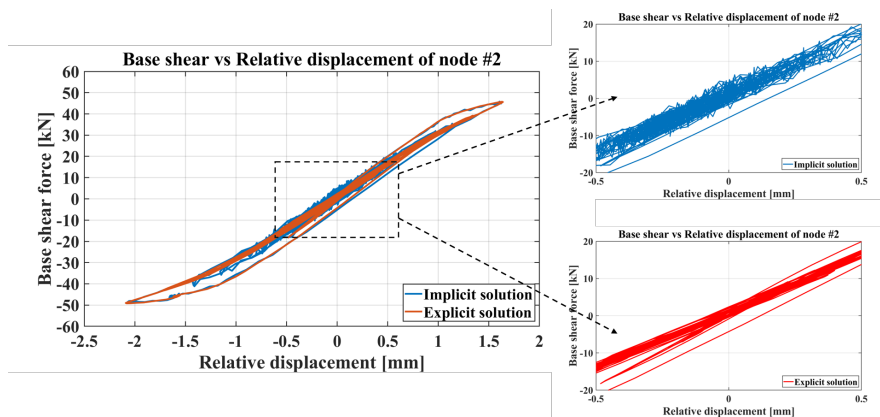
Figure 5.28: Comparisons between implicit and explicit method solutions of hysteresis curves of base shear vs relative displacement

In general, it can be concluded that for this masonry wall model with quasi-brittle material properties, both implicit and explicit methods could generate reasonable nonlinear dynamic response. The peak displacement responses are close to each other for the solutions from both methods. Similar crack patterns were observed during the seismic analysis. The energy dissipated due to the nonlinear behavior can be represented in the hysteresis curves.

However, slightly differences in nonlinear dynamic response under intense base acceleration are observed. The explicit method solution show less cracks and less energy dissipation than the implicit method solution, meanwhile, the displacements responses after the peak displacement are also larger because less material cracked or failed. The difference could be resulted from the fact that implicit method may have problems to reach the convergence criteria when significant nonlinear behavior was activated due to the strong motion of the base. The chaos part in the hysteresis curve of implicit solution provide some clues for this reason. The explicit method has no convergence problem for nonlinear behavior of the material, and its solutions also show very smooth transitions for cracks and energy dissipation process. This illustrates the advantage of the explicit method for the nonlinear dynamic problem. However, the disadvantage is that very small time step is required, in this case, with regular geometry and well-meshed model, the critical time step still reaches $min\{\Delta t_{crit}\} = 4.50268 \times 10^{-5}s$, as a result, it takes longer time to be finished than implicit method.

5.5.4 Additional analysis: using the explicit critical time step in implicit method

According to the comparisons above, the most significant factor for difference existing between implicit and explicit solutions is the convergence problem in the implicit method. The convergence problem will occur when nonlinear behavior happens in a relatively large time step in the implicit method so that the equilibrium of the system is hard to satisfy in a limit number of iterations.

This convergence problem could be eliminated using very small time step in the implicit method. When the time step is extremely small, the stiffness could be seen as linear within each time step, so the iteration will converge very fast.

To compare the all converged solution in implicit method using very small time step with the explicit method solution, which involves no iteration process, one specially analysis using implicit method with time step equaling to explicit critical time step value is performed.

However, in this way, the most important advantage of implicit method, which is unconditional stability with large time step, is abandoned. Using such a small time step will make implicit method run extremely long. One can expect a very good agreement between implicit and explicit solution, since all iterations should converge immediately, but this kind of implicit method strategy is neither economic nor practical. Still, it could provide an insight view of influence of convergence during iteration process. Hence, the detailed analysis scheme and results comparison are presented in Appendix C.

5.6 CASE 5

According to the preliminary analyses described in Section 4.6.5, the simplified model of the masonry house is used for seismic analyses, as shown in Figure 4.34. The transient analyses schemes are listed in Table 4.27 and Table 4.28. The eigenfrequencies of the model will be identified first. Then the displacement time history of the first floor level and the hysteresis curves about base shear versus first floor average displacement will be checked. Also, the deformed shapes and crack patterns will be compared between implicit and explicit method solutions.

Review of analyses schemes

Analyses	Damping	Δt_O [s]	$min\{\Delta t_{crit}\}$ [s]	Δt_{ex} [s]
Implicit	Rayleigh Damping	0.005	−	−
Explicit Sub-case 1	Rayleigh Damping	0.005	1.8485×10^{-6}	5×10^{-5}
Explicit Sub-case 2	Rayleigh Damping	0.005	1.8485×10^{-6}	1×10^{-5}
Explicit Sub-case 3	Rayleigh Damping	0.005	1.8485×10^{-6}	5×10^{-6}
Explicit Sub-case 4	Rayleigh Damping	0.005	1.8485×10^{-6}	1.756×10^{-6}

Table 5.7: Review of transient analysis scheme for Case 5

5.6.1 Eigenfrequency analysis

The eigenfrequency analysis was first performed to identify the dynamic properties of the simplified model. The first four vibration modes in the direction of seismic input were identified and shown in Figure 5.29.

(a) $13.414Hz$ (b) $27.939Hz$ (c) $29.480Hz$ (d) $38.538Hz$
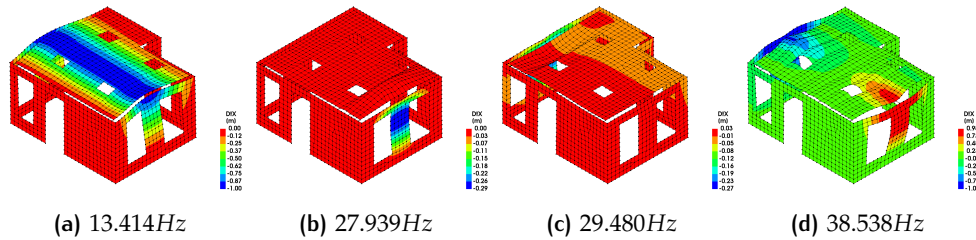
Figure 5.29: Mode shapes of the simplified model

Since the Fourier spectrum of seismic signal shows that most of energy is carried below the $12Hz$, the first vibration of the model will be the utmost important in seismic analysis. Compared to the natural frequencies and mode shapes of full model of the house, which are shown in Figure 4.28 and the similar mode shape in seismic input direction is at frequency $15.7Hz$, the simplified model doesn't significantly change the dominant vibration mode of the structure.

5.6.2 Added mass ratios

To save computational time, first three explicit sub-cases have time steps larger than the critical value according to CFL condition. Therefore, extra artificial mass was

added on the model depending on the actual adopted explicit time step. The results of added mas ratio in each explicit sub-case are given in Table 5.8.

Explicit sub-cases	$\Delta t_{ex,i}$ [s]	Total mass [kg]	Added mass [kg]	Added mass ratio
Sub-case 1	5×10^{-5}	8.47×10^5	8.25×10^5	97%
Sub-case 2	1×10^{-5}	5.23×10^4	2.97×10^4	57%
Sub-case 3	5×10^{-6}	2.76×10^4	4.93×10^3	18%
Sub-case 4	1.756×10^{-6}	2.26×10^4	0	0%

Table 5.8: Added mass ratios in each explicit sub-case

The first sub-cases have more than 50% of added mass, so the overall dynamic properties of the model might be significantly changed, one can predict that huge differences may occur between implicit and explicit method.

The explicit sub-case 3 has relatively small added mass ratio, which is 18%. The positions of these elements with added mass were checked. It turned out that the mainly added mass was concentrated on the first floor level, including some beam elements and curved shell elements. The reason is that first floor structure has the material of timber, which has low density, also the timber floor is quite thin, therefore, the masses of elements of the floor are small. As a result, the natural periods of these elements are small compared to those of masonry wall elements. However, this means the nonlinear behavior of the masonry wall will not be strongly influenced. The results of implicit and explicit method may have differences, but the magnitudes of them won't be very large.

As for the explicit sub-case 4 with zero added mass, the model has completely same properties as the original model, the similar solution should be expected for implicit and explicit methods.

5.6.3 Relative displacement response at first floor

The relative displacement of the first floor level is obtained at the same locations shown in Figure 4.31. The displacement solutions are compared between the implicit method solutions and four explicit sub-cases solutions.

East side

The solutions of relative displacement at the east side of the first floor are plotted in Figure 5.30a to Figure 5.30e, and in these figures, the implicit method solution is selected as the reference.

Since the first three explicit sub-cases have Δt_{ex} larger than the $min\{\Delta t_{crit}\}$, the solutions of them have huge deviations from the implicit solution. However, the explicit solutions are approaching the implicit solution with smaller explicit time steps Δt_{ex}. Finally, with $\Delta_t ex = 0.95 \times min\{\Delta t_{crit}\} = 1.75603 \times 10^{-6}s$ in explicit sub-case 4, the explicit method solution matches the implicit method solution for the relative displacement at first floor east side.

West side

The solutions of relative displacement at the west side of the first floor are plotted in Figure 5.31a to Figure 5.31e, the implicit method solution is selected as the reference again.

The similar approaching process could be observed for west side relative displacement as the east side. The explicit sub-case 4 finally has a very close solution to the implicit method solution. Slight difference could be observed in the peak values of

the response, the explicit sub-case 4 has higher amplitudes for these peaks than the implicit solution. In general, they have a very good agreement.

(a) Implicit method solution

(b) Explicit sub-case 1

(c) Explicit sub-case 2

(d) Explicit sub-case 3

(e) Explicit sub-case 4
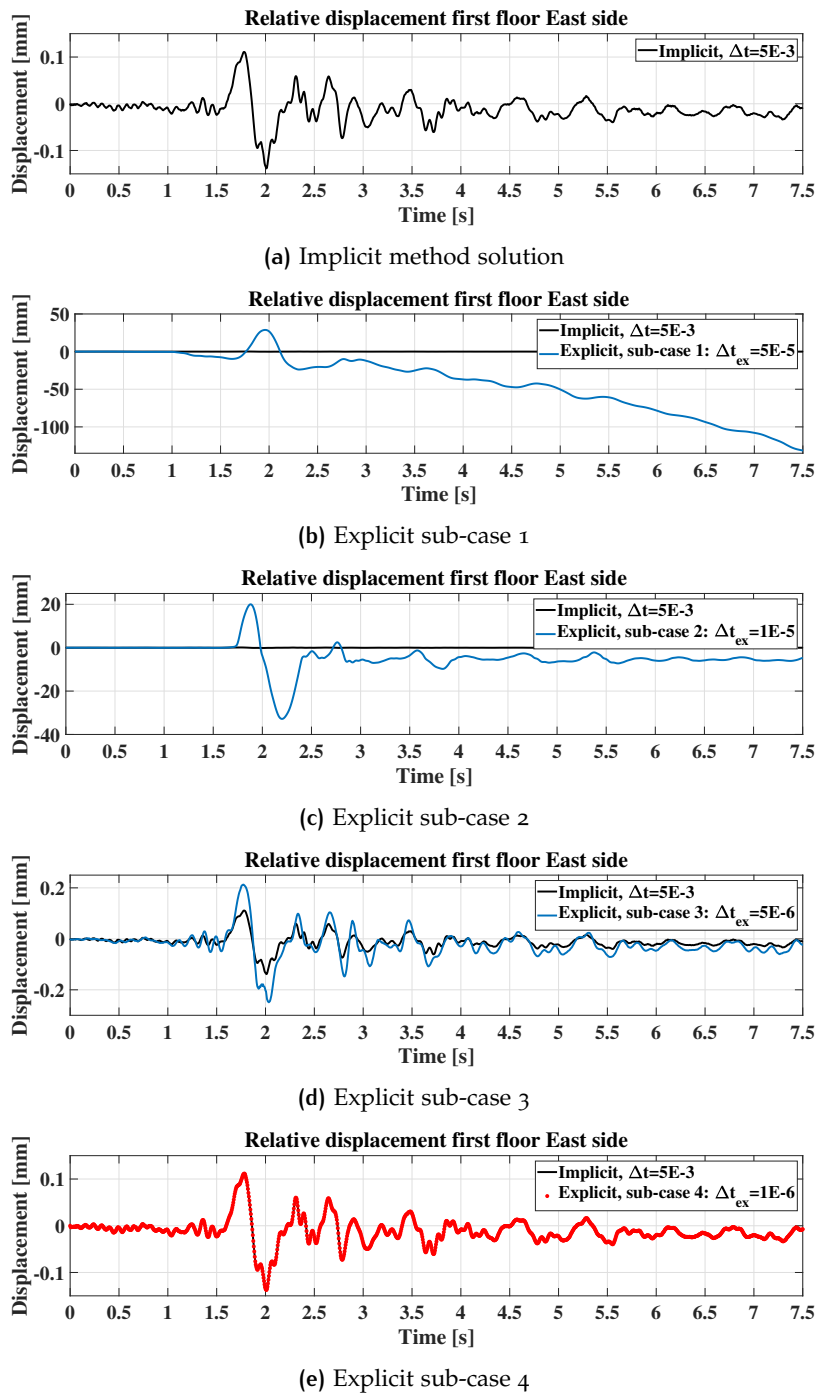
Figure 5.30: Relative displacement response at first floor East side
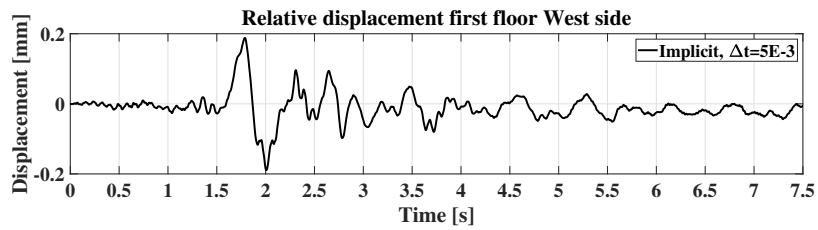
(a) Implicit method solution
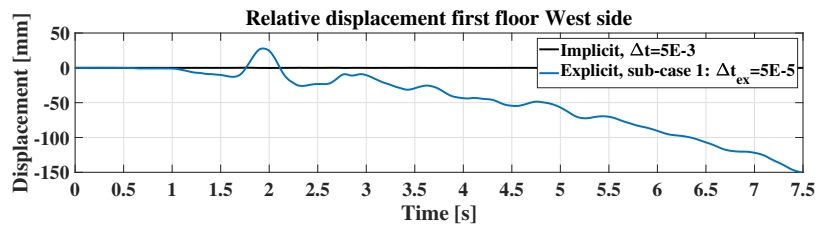
(b) Explicit sub-case 1
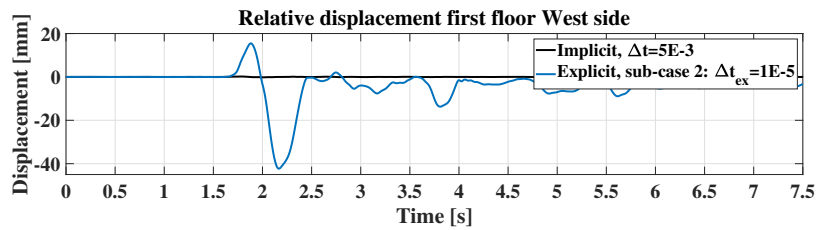
(c) Explicit sub-case 2
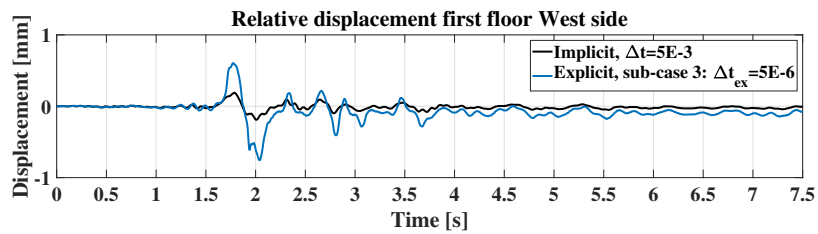
(d) Explicit sub-case 3
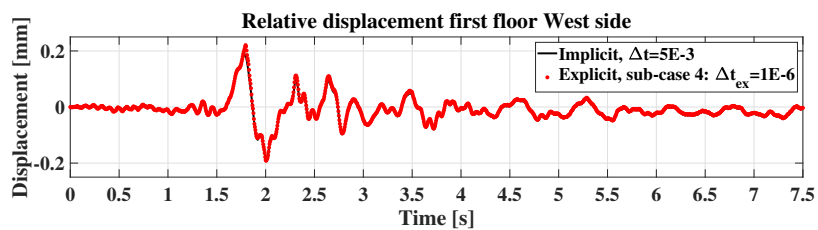
(e) Explicit sub-case 4

Figure 5.31: Relative displacement response at first floor West side

5.6.4 Hysteresis curves of base shear versus first floor average displacement

The first floor average displacement is calculated by taking average of east side and west side displacements. The base shear forces are obtained by summing up reaction forces at all base nodes in seismic input direction. The resulting hysteresis curves of implicit method and explicit method solution are plotted in Figure 5.32, and based on the displacement results, the explicit sub-case 4 is plotted for later comparisons.
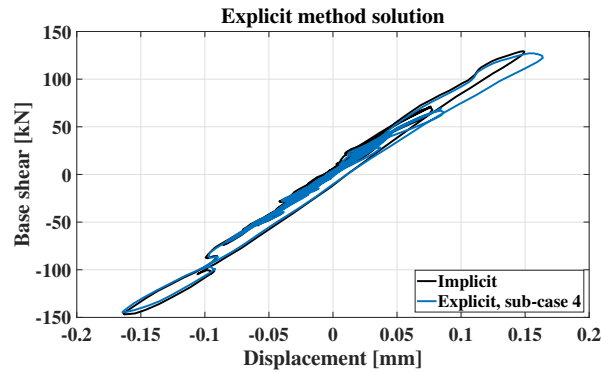
Figure 5.32: Hysteresis curves of base shear versus first floor average displacement

It can be observed that both methods have a good agreement, while the explicit method solution shows lower base shear forces for positive displacement on first floor level and slightly higher energy dissipation than implicit solution.

5.6.5 Deformed shapes and crack patterns

The deformed shapes of the model are almost the same for both methods, the results from explicit sub-case 4 at the maximum positive and maximum negative displacement moments aer shown in Figure 5.33.

(a) 1.795s

(b) 2.005s
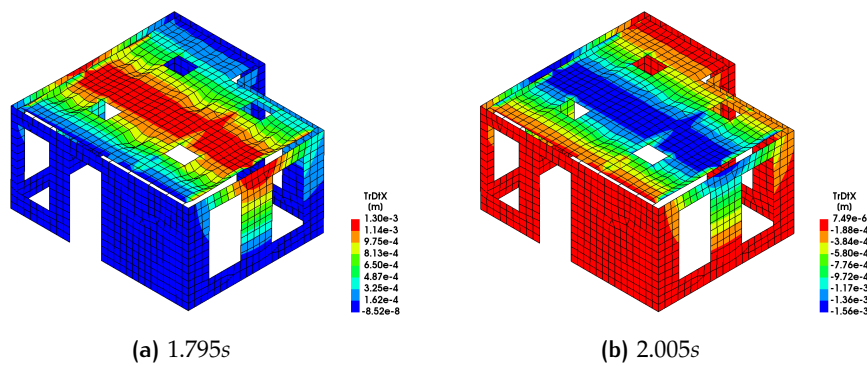
Figure 5.33: Deformed shapes of the model from explicit sub-case 4

The deformed shapes show that the first vibration mode in seismic input direction mainly governs the dynamic response of the model.

The final crack patterns are shown in Figure 5.34a and Figure 5.34b. The similar crack patterns were generated. The dominant cracks were at bottom edges of the north and south wall due to the out-of-plane vibration, and these cracks also developed along the diagonal from bottom edge to the lower corner of the opening on the wall. The cracks occur at the upper boundary of the wall is mainly due to the beam and anchor connections, the self-weight of the floor and extra mass blocks give large additional vertical load to this beam-wall point connections. The main

difference in the crack pattern was at the north lower corner of west side wall, at where the explicit has more cracks and larger crack widths.

(a) Implicit solution   (b) Explicit sub-case 4
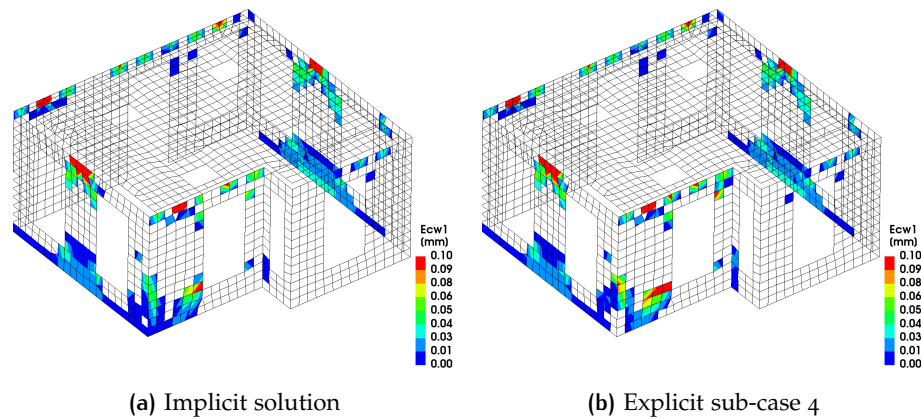
Figure 5.34: Final crack patterns of the model

5.6.6   Comparisons and discussions

The results from implicit method and explicit sub-case 4 generally match each other very well. Minor differences were observed, such as the peak displacement response on west side of first floor level, it also corresponds to the differences in crack pattern and hysteresis curves. The possible reason is still from the different incremental procedures of implicit and explicit methods. The implicit method has the risk of no convergence problems when the nonlinear behavior happened. Especially under strong base acceleration, the implicit might take lots of iterations to reach the convergence.

Thanks to the mass scaling technique, few time steps larger than the critical value could also be used in explicit method to improve the speed the the analysis. However, the influence of the mass scaling, as presented in displacement responses, is significant. The percentage of the added mass ratio need to be controlled under a small value. Otherwise the results cannot represent the real response of the structure. Moreover, once added mass ratio is using in the model, one should also check th positions and properties of these elements which are applied added mass. If the added mass was applied to the elements that has minor influence on the dynamic properties of the structure, the results could be considered acceptable. On the contrary, if these elements are at critical part of the structure or around the interested location, the mass scaling must be used carefully and its effect must be considered in the analysis.

Besides the mass scaling technique, one can also consider directly removing the elements that limit the critical time step for the explicit method. Again, this modification also need to be consider the influence of the removed elements and should used with great care.

Overall, the Case 5 illustrate the theoretical viability of both implicit and explicit method for real structure seismic analysis. For the structure with significant nonlinearity, the explicit method may be more preferable than implicit method due to no iteration involved. To use the explicit method, the model of the structure model may need modifications. With proper modifications and careful control of mass scaling effect, the explicit method could reproduce the real response of the structure very well.

6 | CONCLUSIONS AND RECOMMENDATIONS

6.1 CONCLUSIONS

In this research, the commonly used direct time integration methods in dynamic time-history analysis, i.e., implicit Newmark method and explicit central difference method, are used in five cases studies. The first three cases are using linear elastic materials, and the last two cases with quasi-brittle nonlinear materials are selected from the laboratory tests conducted by Graziotti et al. [2016]. The transient analyses using implicit method and explicit method are all performed in finite element software DIANA FEA 10.3. The results of the two methods are obtained and compared in several aspects to investigate the differences and evaluate the performances of both methods.

To perform the transient analyses, the finite element model of each case was first built up. For the first three cases, the models include a simply-supported elastic beam, a double cantilever elastic beam, and a simply-supported thin plate. Then harmonic point, transient point load, and distributed out-of-plane transient load are applied to the first three models, respectively. For the last two cases with quasi-brittle nonlinear material properties, the finite element model was built up according to the laboratory tests, including a masonry wall and a full-scaled clay URM house. The quasi-static pushover analyses were first performed to validate the finite element model. Then seismic loads were applied, and necessary modifications were made to perform the analyses.

Then a series of analyses were performed in each case in order to investigate the influence of the adopted time step, which is the most important parameter for the direct time integration method.

Finally, comparisons were made between the results obtained from implicit method and explicit method. The comparison was made mainly in displacement responses for the first three cases, and also in crack patterns and capacity curves for the last two cases.

From the analyses and results comparisons, the following conclusions can be drawn to answer the sub-questions and finally reach the answer to the main research questions of this thesis:

For linear elastic material:

- In all three cases, the displacement responses of the linear elastic material could generally be reproduced accurately by using proper time steps in implicit and explicit methods.

- In the explicit method, using the critical time step, determined by CFL stability conditions ($\Delta t_{ex} = min\{\Delta t_{crit}\}$), could generate accurate responses of the system. Further decreasing of the adopted time step, i.e., $\Delta t_{ex} < min\{\Delta t_{crit}\}$, is not necessary to improve the accuracy for explicit method solutions. Instead, decreasing the output time step Δt_O is more likely to improve the resolution of the results, as a result, provide more accurate presentations of high frequency vibration modes.

- The adopted time step (Δt in implicit method and Δt_O in explicit method) has a more significant influence on the solutions from implicit method than

that from explicit method. This can be observed from comparisons in Case 2 and Case 3. The solution of implicit method with small Δt has more accurate displacement responses and more high frequency contents than the solution from large Δt. However, in the explicit method, the solution is the same for different Δt_O. It means the explicit solutions always contain the same displacement response and high frequency contents no matter how long is time interval for output. However, this accuracy will be lost when the time step is not small enough in implicit method. Since the unconditional stability of the implicit method, these lost or changes of the accuracy in solutions are hard to be detected, which could be a problem when high frequency vibrations are important to the analysis.

- The above conclusion is also proved in the Case 3 stress comparisons. It also illustrates that though the displacement responses have no visible difference between implicit and explicit solutions, the stress responses could show different high frequency vibrations as well, and explicit method could maintain the accuracy better than implicit method.

For quasi–brittle material

- In general, both implicit and explicit methods could reproduce the dynamic responses of the structure with quasi-brittle material in terms of displacement response, hysteresis curves, and cracks patterns.

- The results of eigenfrequency evolution analyses show that for quasi-brittle material, which has softening behavior due to the nonlinearity, the critical time step determined by CFL stability condition $\Delta t_{ex} \leq min\{\Delta t_{crit}\}$ based on the initial linear elastic stage will always satisfy the stability condition when the nonlinear behavior is activated.

- Similarly to the conclusion in linear elastic material cases, further decreasing of the adopted time step is not necessary to improve the accuracy for explicit method solutions.

- Slight differences between implicit and explicit methods may exist for the strong nonlinear behavior of the model. The implicit method could have difficulties to reach convergence during the integration, especially when the time step Δt is relatively large. Non-converged iterations or hardly converged iterations could lead to structure cracking earlier or later than the real situation. The explicit method shows its advantage for no iteration involving. The solutions of explicit method have smoother displacement transitions and hysteresis curves. For this reason, the explicit method should be recommended for the analyses with nonlinear material properties. However, the disadvantage is the limitation in critical time step. Both Case 4 and Case 5 require very small time steps to keep explicit algorithm stable. As a result, very long computational time is needed.

- The mass scaling technique could improve the speed of the explicit method by adding artificial mass on specific elements and allowing Δt_{ex} larger than $min\{\Delta t_{crit}\}$ of the original model. In this way, the finite element model is changed. Therefore, one should carefully check the locations of mass-scaled elements and evaluate the reliability of the results of explicit method.

6.2 RECOMMENDATIONS

To have a general conclusion about in which situation either implicit or explicit method should be recommended, more general and realistic cases are still needed

to be studied. Based on the analyses and conclusion presented in this thesis, I would like to give the following recommendations for future research:

- A series of sequenced incremental scaled seismic signals could be considered to be applied to the model, in this way, the analyses could be performed with consideration of accumulated damage of the structure.

- Other types of connections (e.g., structural interface, spring-dash connection), rather than rigid connection, for the models of real structures could be considered in the analyses.

- Different types of nonlinear behaviors could be studied for implicit and explicit methods, such as stiffening or yielding.

- Other popular implicit and explicit time integration methods could also be used for comparisons to show their advantages/disadvantages and give valuable recommendations.

BIBLIOGRAPHY

Utku Albostan, Tunc Bahcecioglu, Yalin Arici, and Ozgur Kurc. Nonlinear seismic dam and foundation analysis using explicit newmark integration method with static condensation. *Procedia Engineering*, 199:316 – 321, 2017. ISSN 1877-7058. doi: https://doi.org/10.1016/j.proeng.2017.09.055. URL http://www.sciencedirect.com/science/article/pii/S1877705817334859. X International Conference on Structural Dynamics, EURODYN 2017.

K. J. Bathe and E. L. Wilson. Stability and accuracy analysis of direct integration methods. *Earthquake Engineering & Structural Dynamics*, 1(3):283–291, 1972. doi: 10.1002/eqe.4290010308. URL https://onlinelibrary.wiley.com/doi/abs/10.1002/eqe.4290010308.

Klaus-Jürgen Bathe. *ADINA-A Finite Element Program for Automatic Dynamic Incremental Nonlinear Analysis*. acoustics and Vibration Laboratory, Department of Mechanical Engineering, Massachusetts Institute of Technology, Cambridge, Mass, 1978.

Klaus-Jürgen Bathe. *Finite Element Procedures in Engineering Analysis*. Englewood Cliffs, New Jersey, 1982.

Klaus Jürgen Bathe and Edward L. Wilson. Nonsap — a nonlinear structural analysis program. *Nuclear Engineering and Design*, 29(2):266 – 293, 1974. ISSN 0029-5493. doi: https://doi.org/10.1016/0029-5493(74)90128-9. URL http://www.sciencedirect.com/science/article/pii/0029549374901289. Special Issue: Papers Presented at the Conference.

Ted Belytschko. A survey of numerical methods and computer programs for dynamic structural analysis. *Nuclear Engineering and Design*, 37(1):23 – 34, 1976. ISSN 0029-5493. doi: https://doi.org/10.1016/0029-5493(76)90050-9. URL http://www.sciencedirect.com/science/article/pii/0029549376900509.

H.-H. Choi, S.-M. Hwang, Y.H. Kang, J. Kim, and B.S. Kang. Comparison of implicit and explicit finite-element methods for the hydroforming process of an automobile lower arm. *The International Journal of Advanced Manufacturing Technology*, 20(6):407–413, Sep 2002. ISSN 1433-3015. doi: 10.1007/s001700200170. URL https://doi.org/10.1007/s001700200170.

Lothar Collatz. *The Numerical Treatment of Differential Equations*. Springer-Verlag, New York, N.Y., 1966.

R. Courant, K. Friedrichs, and H. Lewy. Über die partiellen Differenzengleichungen der mathematischen Physik. *Mathematische Annalen*, 100:32–74, 1928. doi: 10.1007/BF01448839.

DIANA FEA BV. *DIANA 10.3 Documentation release 10.3*. DIANA FEA BV, Delftechpark 19a, 2628 XJ Delft, The Netherlands, 2019. URL https://dianafea.com/manuals/d103/Theory/Theory.html.

C A Felippa and K C Park. Direct time integration methods in nonlinear structural dynamics. 17118:277–313, 1979.

Carlos A. Felippa. Procedures for computer analysis of large nonlinear structural systems. In ALVIN WEXLER, editor, *Large Engineering Systems*, pages 60 – 101. Pergamon, 1977. ISBN 978-0-08-021295-1. doi: https://doi.org/10.1016/B978-0-08-021295-1.50010-9. URL http://www.sciencedirect.com/science/article/pii/B9780080212951500109.

F. Graziotti, U. Tomassetti, A. Rossi, B. Marchesi, S. Kallioras, M Mandirola, A. Fragomeli, E. Mellia, S. Peloso, F. Cuppari, G. Guerrini, A. Penna, and G. Magenes. Shaking table tests on a full-scale clay-brick masonry house representative of the Groningen building stock and related characterization tests. Technical report, 2016.

W. E. HAISLER, J. H. HONG, J. E. MARTINEZ, J. A. STRICKLIN, and J. R. TILLERSON. Nonlinear dynamic analysis of shells of revolution by matrix displacement method. *AIAA Journal*, 9(4):629–636, 1971. doi: 10.2514/3.6240. URL https://doi.org/10.2514/3.6240.

F. J. Harewood and P. E. McHugh. Comparison of the implicit and explicit finite element methods using crystal plasticity. *Computational Materials Science*, 39(2): 481–494, 2007. ISSN 09270256. doi: 10.1016/j.commatsci.2006.08.002.

John C. Houbolt. A recurrence matrix solution for the dynamic response of elastic aircraft. *Journal of the Aeronautical Sciences*, 17(9):540–550, 1950. doi: 10.2514/8. 1722. URL https://doi.org/10.2514/8.1722.

Thomas J. R. Hughes, Karl S. Pister, and Robert L. Taylor. Implicit-explicit finite elements in nonlinear transient analysis. 18:159–182, 1979.

D. E. Johnson. A proof of the stability of the houbolt method. *AIAA Journal*, 4(8): 1450–1451, 1966. doi: 10.2514/3.3702. URL https://doi.org/10.2514/3.3702.

D. Jung and D. Yang. Step-wise combined implicit–explicit 1nite-element simulation of autobody stamping process. *Journal of Materials Processing Technology*, 83:245–260, 1998.

S. Kugener. Simulation of the crimping process by implicit and explicit finite element methods,. *AMP Journal of Technology*, 4:8–15, 1995.

Nikos Lagaros, Chara Mitropoulou, and Papadrakakis Manolis. *Time History Seismic Analysis*, pages 3751–3767. 01 2015. doi: 10.1007/978-3-642-35344-4_134.

P. D. Lax and R. D. Richtmyer. Survey of the stability of linear finite difference equations. *Communications on Pure and Applied Mathematics*, 9(2):267–293, 1956. doi: 10.1002/cpa.3160090206. URL https://onlinelibrary.wiley.com/doi/abs/10.1002/cpa.3160090206.

J. Maguire, D. J. Dawswell, and L. Gould. NAFEMS: Selected Benchmarks for forced vibration. Technical report, 1993.

Belgasmia Mourad and Moussaoui Sabah. Comparison between static nonlinear and time history analysis using flexibility-based model for an existing structure and effect of taking into account soil using domain reduction method for a single media. *KSCE Journal of Civil Engineering*, 19(3):651–663, Mar 2015. ISSN 1976-3808. doi: 10.1007/s12205-015-0351-y. URL https://doi.org/10.1007/s12205-015-0351-y.

N. Newmark, M. A method of computation for structural dynamics. *ASCE J. Eng. Mech. div.*, 85:67–94, 1959. URL http://ci.nii.ac.jp/naid/20000316988/en/.

Robert E. Nickel. On the stability of approximation operators in problems of structural dynamics. *International Journal of Solids and Structures*, 7(3):301 – 319, 1971. ISSN 0020-7683. doi: https://doi.org/10.1016/0020-7683(71)90028-X. URL http://www.sciencedirect.com/science/article/pii/002076837190028X.

L. Noels, L. Stainier, and J.-P. Ponthot. Combined implicit/explicit time-integration algorithms for the numerical simulation of sheet metal forming. *Journal of Computational and Applied Mathematics*, 168(1):331 – 339, 2004. ISSN 0377-0427. doi:

https://doi.org/10.1016/j.cam.2003.12.004. URL http://www.sciencedirect.com/science/article/pii/S0377042703009968. Selected Papers from the Second International Conference on Advanced Computational Methods in Engineering (ACOMEN 2002).

N. Rebelo and J.C. Nagtegaal. *Numerical Methods on Industrial Forming Process*, pages 99–108, 1992.

Sobhan Rostami, Saeed Shojaee, and Ali Moeinadini. A parabolic acceleration time integration method for structural dynamics using quartic B-spline functions. *Applied Mathematical Modelling*, 36(11):5162–5182, 2012. ISSN 0307904X. doi: 10.1016/j.apm.2011.11.047. URL http://dx.doi.org/10.1016/j.apm.2011.11.047.

Wilhelm Rust and Karl Schweizerhof. Finite element limit load analysis of thin-walled structures by ANSYS (implicit), LS-DYNA (explicit) and in combination. *Thin-Walled Structures*, 41(2-3):227–244, 2003. ISSN 02638231. doi: 10.1016/S0263-8231(02)00089-7.

Saeed Shojaee, Sobhan Rostami, and Asghar Abbasi. An unconditionally stable implicit time integration algorithm: Modified quartic B-spline method. *Computers and Structures*, 153:98–111, 2015. ISSN 00457949. doi: 10.1016/j.compstruc.2015.02.030. URL http://dx.doi.org/10.1016/j.compstruc.2015.02.030.

Behzad Soltani, Kjell Mattiasson, and Alf Samuelsson. Implicit and dynamic explicit solutions of blade forging using the finite element method. *Journal of Materials Processing Tech.*, 45(1-4):69–74, 1994. ISSN 09240136. doi: 10.1016/0924-0136(94)90320-4.

J. S. Sun, K. H. Lee, and H. P. Lee. Comparison of implicit and explicit finite element methods for dynamic problems. *Journal of Materials Processing Technology*, 105(1):110–118, 2000. ISSN 09240136. doi: 10.1016/S0924-0136(00)00580-X.

E. J. Wilson, I. Farhoomand, and K. J. Bathe. Nonlinear dynamic analysis of complex structures. *Earthquake Engineering & Structural Dynamics*, 1(3):241–252, 1973. doi: 10.1002/eqe.4290010305. URL https://onlinelibrary.wiley.com/doi/abs/10.1002/eqe.4290010305.

A | APPENDICES

The interested preliminary results in Section 4.6.5 are shown in Figure A.1 to Figure A.4.
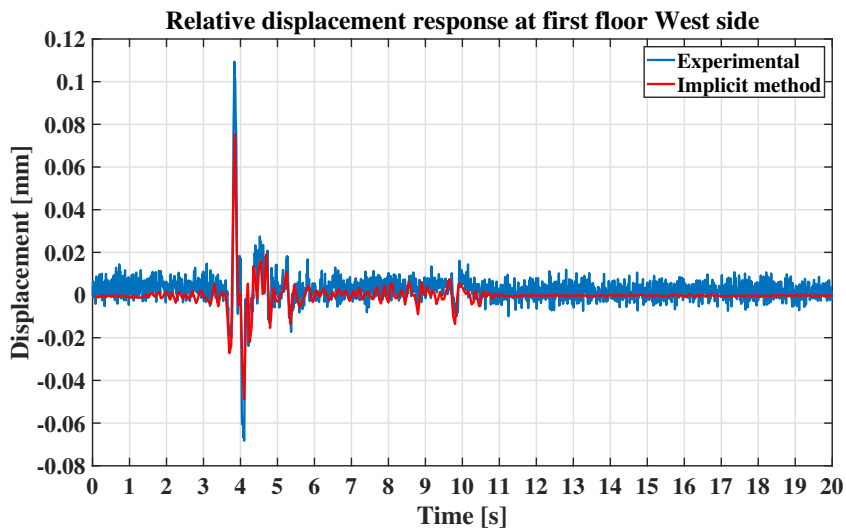
Figure A.1: Comparisons of displacements time history of the first floor West side and roof level
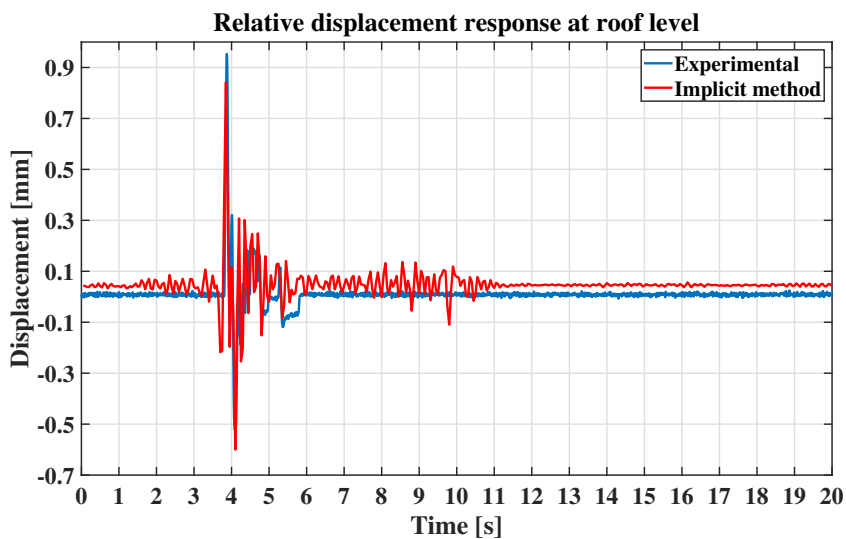
Figure A.2: Comparisons of displacements time history of roof level

87

(a) Displacement envelope for East side   **(b)** Displacement envelope for West side
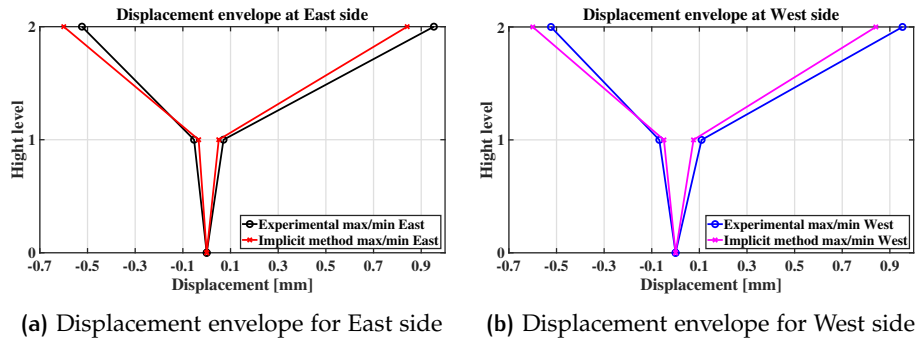
Figure A.3: Comparisons of displacement envelopes (Height level $0, 1, 2$ represent ground, first floor and roof levels respectively)
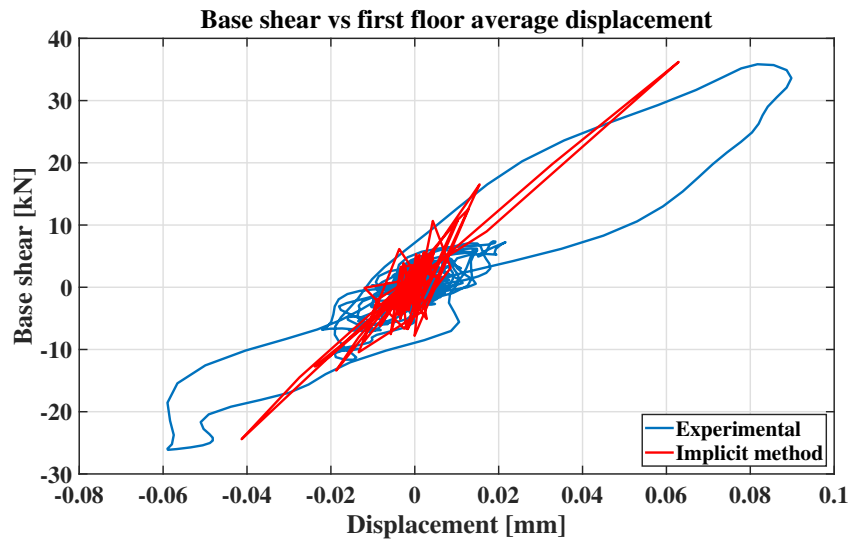
Figure A.4: Comparison of Base shear vs first floor average displacement

B | APPENDICES

Some typical positions of added mass elements in preliminary explicit analysis in Section 4.6.5 with explicit time step $\Delta t_{ex} = 5 \times 10^{-6}$ of original FE model, as described in Section 4.6, are given below, note these figures only show some typical elements which have added mass, not the all added mass elements in this model.

(a)

(b)   **(c)**
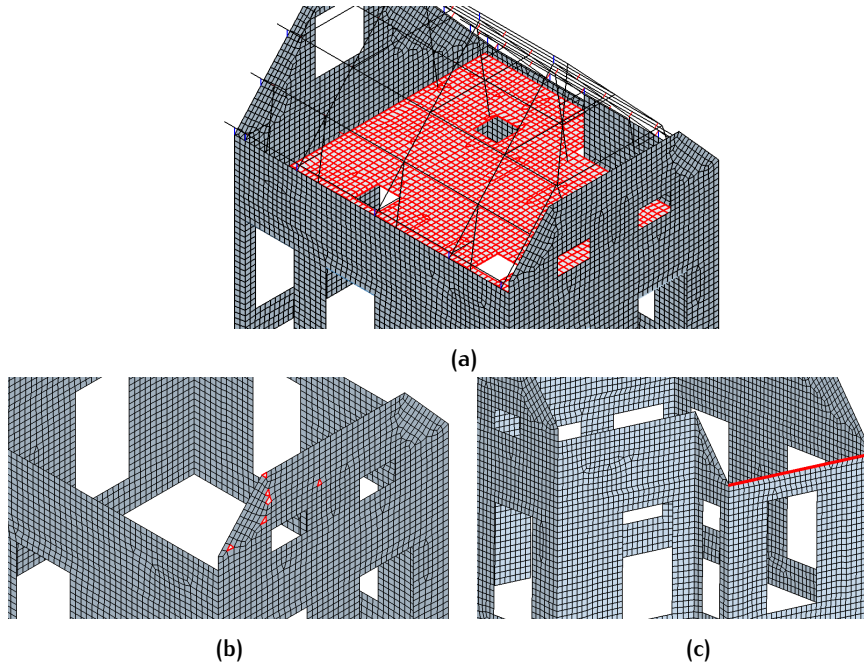
Figure B.1: Typical locations of added mass elements

All elements of timber floor structure have added mass. The reason is that compared to the masonry, the timber has much less density, therefore the elements of timber floor structure has relatively small natural periods. Then, some irregular shape elements and small volume have added mass, the reason is similar to above, i.e., small volume will cause small mass, and finally small natural period of the element.

C | APPENDICES

This appendix shows the additional analysis described in Section 5.5.4. This analysis is using the implicit method with a time step equaling to the explicit critical time step value. The analysis scheme is shown in Table C.1.

Implicit method	Newmark method
Time step Δt_{Im}	$4 \times 10^{-5}s$
Total steps N_{Im}	22500
Output time interval	$0.005s$

Table C.1: Analysis scheme for the additional implicit method

The solution of this additional analysis about relative displacement at top left node of the masonry wall is compared with the original implicit analysis solution and explicit analysis solution, as shown in Figure C.1 and Figure C.2.
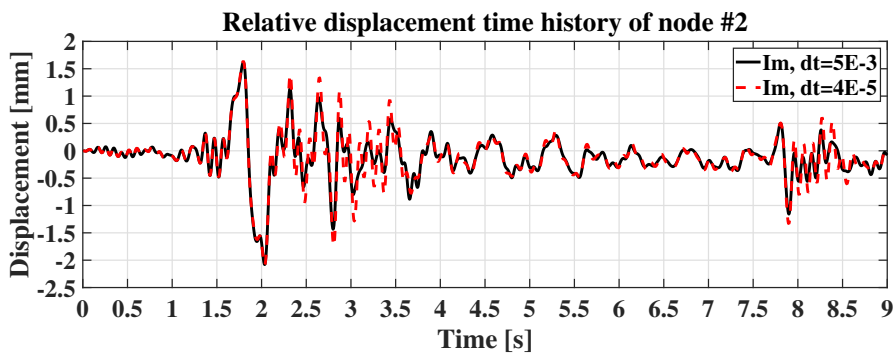
Figure C.1: Comparisons between additional implicit analysis and original implicit analysis
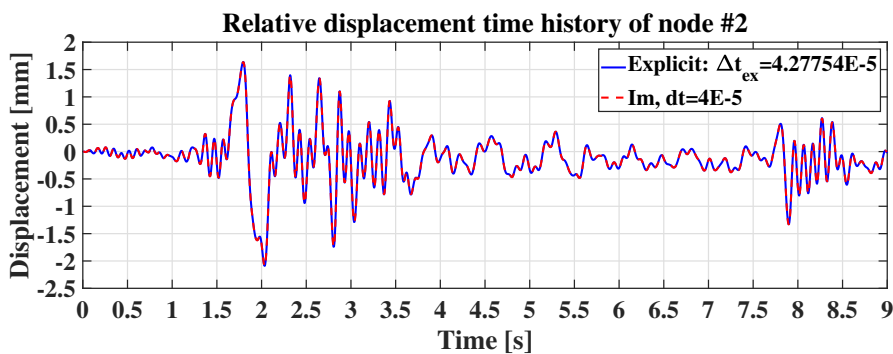
Figure C.2: Comparisons between additional implicit analysis with explicit analysis

It can be observed that once the implicit method is using a very small time step, e.g., critical time step for explicit method, the solution of implicit method will be exactly the same as explicit method solution. Compared with the original implicit analysis, which uses a large time step, it can conclude that extremely small time step could overcome the convergence problem in implicit method for nonlinear

behavior of the structure, and the fully converged solution completely agree with the explicit solution. However, using very small time step in implicit method is very expensive in computation, and also it abandoned the most important benefit of using implicit method, i.e., unconditional stability which allows using large time step to save computational effort. Above all, implicit method with very small time step is not recommended, since it is neither economic nor practical.